Design and Analysis of Fuzzy Logic Controller of Vector Controlled Doubly Fed Induction Generator in Wind Energy Conversion System for Maximum Power Transfer Capability

Melkamu Bekele Leza

A Thesis Submitted to

The Department of Electrical Power and Control Engineering

School of Electrical Engineering and Computing

Presented in Partial Fulfillment of the Requirement for the Degree of Master's in Electrical Power and Control Engineering (Specialization in Control Engineering)

Office of Graduate studies

Adama Science and Technology University

August, 2021

Adama, Ethiopia

Design and Analysis of Fuzzy Logic Controller of Vector Controlled Doubly Fed Induction Generator in Wind Energy Conversion System for Maximum Power Transfer Capability

Melkamu Bekele Leza

Advisor: Milkias Berhanu Tuka (Ph.D.)

A Thesis Submitted to
The Department of Electrical Power and Control Engineering
School of Electrical Engineering and Computing

Presented in Partial Fulfillment of the Requirement for the Degree of Master's in
Electrical Power and Control Engineering (Specialization in Control Engineering)

Office of Graduate Studies
Adama Science and Technology University

August, 2021
Adama, Ethiopia

DECLARATION

I hereby declare that this Master Thesis entitled "Design and Analysis of Fuzzy Logic Controller of Vector Controlled Doubly-Fed Induction Generator in Wind Energy Conversion System for Maximum Power Transfer Capability" is my original work. That is, it has not been submitted for the award of any academic degree, diploma, or certificate in any other university. All sources of materials that are used for this thesis have been duly acknowledged through citation.

Melkamu Bekele Leza	________________	________________
Name of the student	Signature	Date

RECOMMENDATION

I, the advisor of this thesis, hereby certify that I have read the revised version of the thesis entitled "Design and Analysis of Fuzzy Logic Controller of Vector Controlled Doubly Fed Induction Generator in Wind Energy Conversion System for Maximum Power Transfer Capability" prepared under my guidance by Melkamu Bekele submitted in partial fulfillment of the requirements for the degree of Masters of Science in Control Engineering. Therefore, I recommend the submission of revised version of the thesis to the department following the applicable procedures.

Milkias Berhanu (Ph.D.)	_______________	__________
Advisor	Signature	Date

APPROVAL SHEET

I, the advisor of the thesis entitled "Design and Analysis of Fuzzy Logic Controller of Vector Controlled Doubly Fed Induction Generator in Wind Energy Conversion System for Maximum Power Transfer Capability" by Melkamu Bekele, hereby certify that the recommendation and suggestions made by the board of examiners are appropriately incorporated into the final version of the thesis.

Dr. Milkias Berhanu	________________	___________
Advisor	Signature	Date

We, the undersigned, members of the Board of Examiners of the thesis by Melkamu Bekele have read and evaluated the thesis entitled "Design and Analysis of Fuzzy Logic Controller of Vector Controlled Doubly Fed Induction Generator in Wind Energy Conversion System for Maximum Power Transfer Capability" and examined the candidate during the open defense. This is, therefore, to certify that the thesis is accepted for partial fulfillment of the requirement of the degree of Master of Science in Electrical Power and Control Engineering (Control).

________________	________________	___________
Chairperson	Signature	Date
________________	________________	___________
Internal Examiner	Signature	Date
Dr Beteley Teka	________________	14/09/2021
External Examiner	Signature	Date

Finally, approval and acceptance of the thesis is contingent upon submission of its final copy to the Office of Postgraduate Studies (OPGS) through the Department Graduate Council (DGC) and School Graduate Committee (SGC).

________________	________________	___________
Department Head	Signature	Date
________________	________________	___________
School Dean	Signature	Date
________________	________________	___________
Office of Postgraduate Studies, Dean	Signature	Date

ACKNOWLEDGMENTS

First and foremost, I would like to thank my almighty God. Next, I would like to express my deepest gratitude to my supervisor, Dr. Milkias Berhanu for his supervision, friendly attitude, and sharing of many good ideas. Regardless of his often-high workload, he always makes time to answer questions as well as giving encouraging advice.

You are highly appreciated!

I also wish to express my sincere gratitude to Mr. Minyamer Gelaw Wase for lots of advice and providing me the necessary comments.

Finally, I would like to thank my whole family. Especially, words cannot express how grateful I am to my father and mother for their love, encouragement, and all of the sacrifices that they have made on my behalf.

TABLE OF CONTENTS

LIST OF TABLES

LIST OF FIGURES

LIST OF ACRONYMS

AC	Alternating current
DC	Direct current
DFIG	DFIG Doubly Fed Induction Generator
FLC	Fuzzy Logic Controller
GSC	Grid Side Converter
GVOVC	Grid Voltage Oriented Vector Control
IGBT	Insulated Gate Bipolar Transistor
IEEE	Institute of Electrical and Electronics Engineering
MPPT	Maximum power point tracking
MW	Mega Watt
NPC	Neutral Point Converter
PI	Proportional Integral controller
PWM	Pulse Width Modulation
SVPWM	Space Vector Pulse Width Modulation
THIPWM	Third Harmonics Injection Pulse Width Modulation
THD	Total Harmonic Distortion
TSR	Tip speed ratio
VSC	Voltage source converter
WECS	Wind Energy Conversion System

LIST OF SYMBOLS

C	Filter Capacitance
C_{dc}	DC Link Capacitor
C_p	Power coefficient
C_t	Torque coefficient
f_r	Rotor Frequency
fs	Rated Stator Frequency
f_{sw}	Switching Frequency
f_v	Damping coefficient
Ψ	Flux
G	Gear box ratio
i_d	d-axis current
i_q	q-axis current
i_s	Stator current
i_r	Rotor current
J	Moment of inertia
L_m	Mutual inductance
L_r	Rotor inductance
L_s	Stator inductance
ω_m	Mechanical rotational speed
P	Number of poles
P_s	Stator active power
Q_s	Stator reactive power
ρ	Air density
s	Slip
Sa−g, Sb−g, Sc− g	Switching Function of the Converter
V_{dc}	Dc link voltage
V_s	Three phase stator voltage
ω_r	Rotor speed of the generator
θ_r	Rotor angle
V_d	d-axis voltage
V_q	q- axis voltage

ABSTRACT

In recent times, the environmental pollution has added up a major concern in individual's lifestyle and a possible energy crisis has led them to create modern innovations for generating energy. Renewable energy assets have gained critical consideration of the industry and scholars, since it is ecologically friendly. Wind energy has gotten to be one of the foremost important and promising sources of renewable energy due to its cost effectiveness and availability. It has been recognized that, doubly fed induction generator (DFIG) based variable speed wind turbine technology is the foremost successful with less cost and high-power generation. Hence, this study has chosen a 2MW DFIG based wind turbine framework for complete study of modeling, analysis and control research. It consists of stator and rotor windings, where the stator part is directly connected to the electrical network, and the rotor is connected to the grid through AC/DC/AC voltage source converters. The AC/DC/AC voltage source converter includes both machine side converter and grid side converter with a common Dc-link capacitor. The main purpose of the generator side converter is to adjust the speed of the generator rotor and independently control the active and reactive power of the stator. The grid-side converter regulates the DC-link bus voltage to a constant value and maintains the reactive power exchange between the electrical grid and wind turbine generator with the unity power factor to produce the maximum active power output. In this thesis work, an artificial fuzzy logic control strategy is designed and developed for a vector controlled DFIG to regulate rotor speed. When compared with proportional integral control method, the proposed control strategy, which is applied to the speed loop reduces the settling time by 40% and eliminate the maximum overshoot to zero. Maximum power point tracking control strategy is designed by using an indirect speed control procedure in order to drive the aerodynamic torque to follow the maximum power curve proportional to wind speed change. Since, power electronic voltage source converters are connected with the rotor part of the generator, the grid faces voltage and current harmonic problems at the point of common coupling. In order to mitigate such harmonic disturbances, an LCL filter is introduced and three-phase multi-level voltage source converter is modeled and designed by applying space vector pulse width modulation (SVPWM) technique. The overall analysis, modeling and simulation have been developed by using MATLAB/Simulink software.

Key words: Back-to-Back converter, DFIG, Fuzzy Logic Controller, SVPWM

CHAPTER ONE

INTRODUCTION

1.1 Background

In recent times, the environmental pollution has added up a major concern in individual's lifestyle and a possible energy crisis has led them to create modern innovations for generating energy. Renewable energy assets have gained critical consideration of the industry and scholars because of their ecological friendliness [1]. In addition to solar energy, wind energy, hydro power and tidal energy are possible arrangements for environmentally friendly energy production. Among these renewable energy sources, wind power is growing rapidly in the energy industry [2]. Due to concerns about environmental pollution, many countries are building wind power generation through government-level methods. Today, wind power plants are increasingly becoming renewable energy sources alongside hydroelectric power generation in Ethiopia. This is due to the advancement and awareness of innovations aimed at reducing green gases or global warming. Therefore, wind power is one of the most effective, reliable, economical and fastest growing renewable energy sources and requires a well-designed control system.

Squirrel-cage asynchronous generator-based wind turbine is the first invented technology, which generates electricity at a fixed wind speed. Later, variable speed wind turbines were invented. Wind turbines usually operate at variable speeds to provide high-efficiency electricity, and the extracted electricity accounts for a large part of the customer's energy needs. With the increasing popularity of wind energy, wind farms are directly affecting the energy system [1].

Among the different classifications of wind turbine technology, the Type 3 wind turbine is the most widely used variable speed wind turbine concept today because it extracts more energy from the wind, smooth power fluctuations and reduces mechanical stress on the shaft and gear. Due to their high energy efficiency and controllability, doubly fed induction generators (DFIGs) are the most popular among various variable speed wind turbine generators currently on the market [3]. The wind energy conversion system based on DFIG has several advantages. The main advantages of using wind turbines for variable-speed operation include [4]:

- possibility of reducing mechanical structural stress.
- independent control of active and reactive power.
- reduction of power loss and cost.

The general form of a DFIG is that its stator part is directly connected to the network, while the rotor part is connected to the network through two converters connected to a DC-link capacitor to allow power exchange between the network and generator. The electronic power converter connected between the rotor circuit of the DFIG and the grid effectively decouples the grid frequency from the rotor frequency [4]. Figure 1.1 illustrates the general structure of DFIG for wind turbine application with AC/DC/AC voltage source converter.

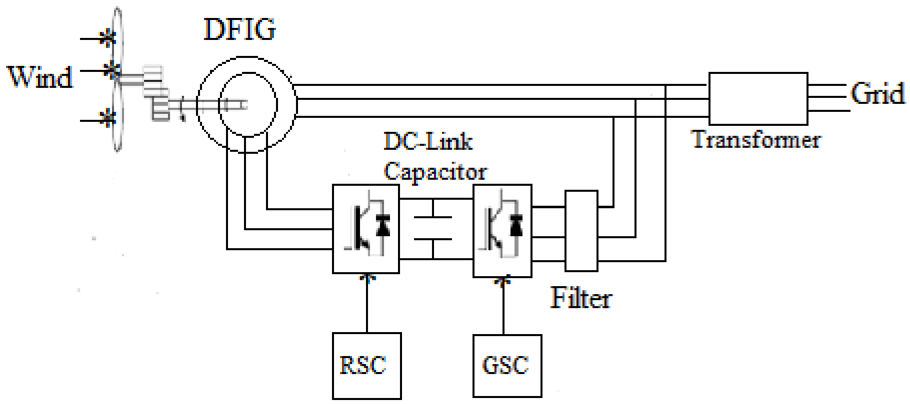

Figure 1.1 General structure of DFIG with back-to-back converter [5]

Know days technology is becoming more and more advanced, and several different power converter technologies have been developed to integrate wind turbines with the grid or network. The use of electronic power converters allows variable speed wind turbine operation and better energy extraction. In variable speed operation, a control strategy is needed to extract maximum power from the turbine while providing a constant grid voltage and frequency. All control schemes integrated with electronic power converters are designed to maximize power output at all possible wind speeds in which the speeds vary from cut-in to cut-out speed [1].

Since DFIG is widely used in the operation of variable speed wind turbines, its dynamic characteristics require the creation of high-performance control schemes. However, the dynamic features of such generators are mainly dependent on certain non-linear parameters, such as stator flux, stator current, and rotor current, which makes the whole system more complicated. Therefore, it is necessary to design a robust controller in this type of system to support the dynamic frequency of wind energy in order to maintain the stability and good performance of the system.

Generally speaking, conventional control design, such as proportional integral (PI) controller, results in many shortcomings, such as difficulty in setting parameters, and reduced robustness. In this thesis work fuzzy logic controller is applied to regulate the rotor speed of DFIG whereas PI controller is applied to regulate the rotor current loop of DFIG in the rotor side voltage source converter. The grid side inverter is controlled by using proportional integral control strategy to adjust the DC-bus voltage and to maintain the reactive power exchange between the generator and the grid at unity power factor. By applying a vector control strategy, the rotor-side converter (RSC) is controlled to regulate the generator rotor speed (outer loop) and rotor currents (inner loop). In order to control grid side voltage source converter (GSC), grid voltage orientation technique is applied. The main purpose of GSC is to control and maintain the DC-link volage constant and the gride power factor unity.

The coupling of voltage source converters between rotor part of the generator and grid arises harmonic distortion, which affects the operation of grid and reduces output voltage levels. In this thesis work, different modulation strategies based two-level and three-level back-to-back VSCs are developed to improve the performance of grid connected inverters and to minimize the total harmonic disturbance (THD). In order to attain the THD value in IEEE 519-1992 standard (THD < 5%), it is necessary to use an LCL filter and SVPWM with diode clamped VSC.

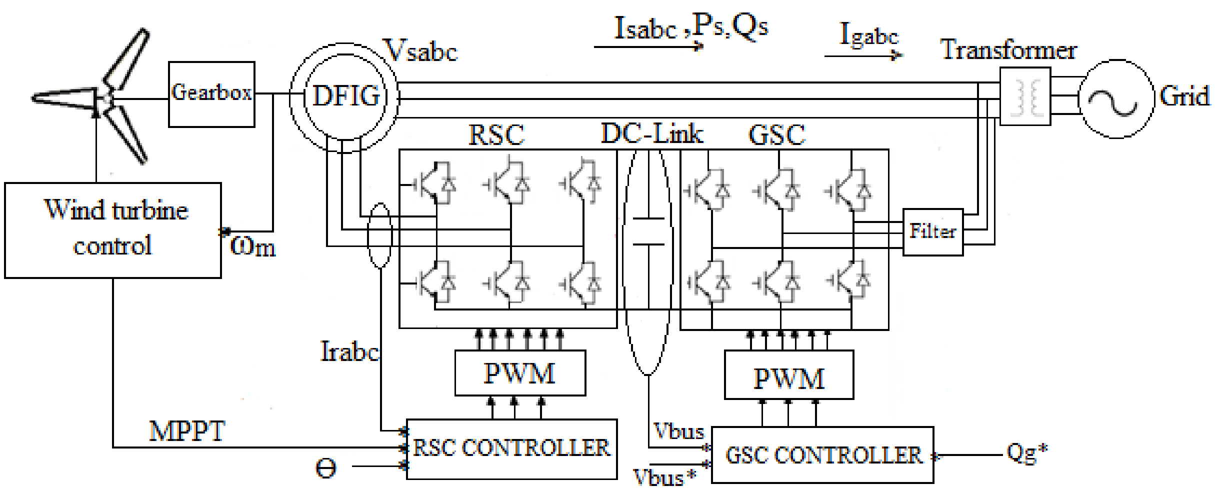

Figure 1.2 Proposed block diagram of DFIG Control [6]

1.2 Statement of the Problem

Currently, researchers compete to improve the energy efficiency of wind turbines to obtain the maximum generated electric power. Applying an efficient control mechanism in wind turbine design results in an enhanced and improved power extraction from wind energy. Even though many control mechanisms of DFIG has been studied, the widely used and appliable one in wind industry today is conventional PI controller, which requires adjustment for every change in reference pattern and also results in high overshoot and large settling time. Due to the frequent uncertainty of wind speed fluctuations, PI controllers cannot provide high-quality power generation and tracking references by extracting the maximum power. Hence, to ensure robustness of the system against external disturbances fuzzy logic controller is applied to the generator side converter in order to regulate the generator rotor speed.

In wind turbines of DFIG, the rotor winding is connected with the grid via the power electronic converter called back-to-back converter, which produces harmonics that could result in voltage distortions at point of common coupling to the grid. Due to this harmonics problem, eddy current losses can be produced in the generator and the grid faces the power quality problems, which also affect the operation and the reliability of the electrical grid. Therefore, multilevel neutral point clamped voltage source converters-based SVPWM strategy is applied to minimize the generated harmonics. In addition to this, LCL filter is developed and located in between the grid side converter and the grid in order to improve the total harmonic disturbance with in the standard of IEEE 519-1992.

1.3 Objective of Study

1.3.1 General Objective

The main objective of this thesis work is to develop an improved control strategy for the RSC and GSC of DFIG based wind turbine mainly by minimizing the total harmonic disturbance of grid connected voltage source converters to obtain adequate and effective power output.

1.3.2 Specific Objectives

The specific objectives of this thesis are to:

- Develop vector control strategy for the RSC and GSC.
- Develop the rotor current controller for active (Ps) and reactive power (Qs) control and hence for toque control.
- Design fuzzy logic controller for the RSC in order to control the rotor speed of the generator to reduce the peak overshoot due to conventional PI controller.
- Design the three-phase two-level and three-level grid connected VSCs based different modulations techniques in order to minimize the total harmonic disturbance.
- Model and simulate the overall system by using the MATLAB/Simulink software.

1.4 Significance of Study

Producing an efficient and improved energy is the most intention of the world nowadays, since the world is shifting the non-renewable energy source usage to the renewable energy source. Especially in the case of variable wind speed-based wind turbine plants, controlling wind turbine generator and reducing the total harmonic distortion is very important to increase the efficiency of the grid.

1.5 Scope of the Study

This thesis work focuses on the mathematical model and MATLAB simulation design of DFIG for the application of wind turbine technology. The artificial fuzzy logic control technique is applied to control the DFIG rotor speed and the inner current loop is controlled by PI controller using MATLAB/Simulink for wind turbine application. In order to reduce the total harmonic distortion, sinusoidal pulse width modulation, third harmonic injection based sinusoidal pulse width modulation and SVPWM techniques are developed and designed for three-phase two-level conventional AC/DC/AC converter and three-level NPC grid connected inverter.

1.6 Limitations of the Study

The thesis is limited to the simulation of the system using MATLAB/Simulink by showing how the different components of the system interact with each other. Implementing the real system is quite difficult because it takes an additional time and cost to make the actual prototype implementation.

1.7 Thesis Organization

This thesis work is organized into four chapters. The first chapter illustrates about introduction, statement of the problems, objectives, significance, scope, and limitations of the thesis work following the second chapter. The second chapter include literature review on the control mechanism of DFIG based wind turbine system and the system components briefly. The third chapter describes methodology and the overall modeling followed in this thesis work. Then after the fourth chapter presents the proposed results and discussions. At the end, the overall system is concluded and recommendations are made.

CHAPTER TWO

LITERATURE REVIEW

2.1 Components of Wind Energy Conversion System

The Figure 2.1 illustrates the main components of a typical wind power generation system, which comprises wind turbine blades, gearbox, generator, AC/DC/AC converter and step-up transformer [7]. The kinetic energy of the wind turns the blades of the wind turbine. The blade is linked to the shaft. The generator converts mechanical energy into electrical energy. Gearboxes and wind generators are used to convert low speed, high torque mechanical power into standard speed electrical power. To adjust the low speed of the wind turbine rotor to a higher speed, a gearbox is applied. Wind turbines convert mechanical energy into electricity and electrical energy is sent to the grid through electronic power converters and grid-connected transformers. In wind turbine technology, fiber optic sensor technology is applied to turbine blade monitoring, fatigue failure detection and optimization of wind turbine production [8].

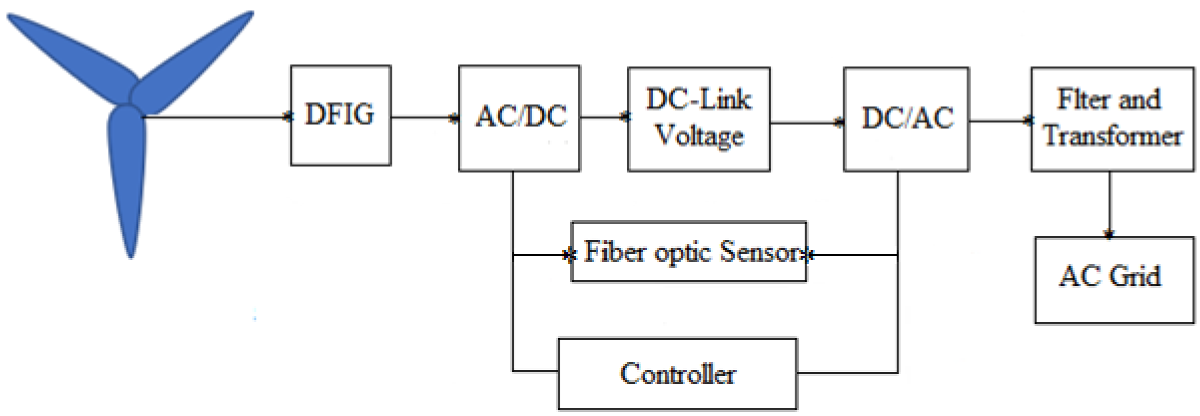

Figure 2. 1 Block diagram of typical wind power generation system [9]

2.1.1 Wind Turbine Topologies

Wind turbines have two distinct aspects, mechanical and electrical. The mechanical side corresponds to the turbine itself and the gearbox. The behavior on this side is basically controlled by the motion equation of the turbine and the pitch angle actuator. But during this thesis work the mechanical aspect is not mostly considered. On the contrary, the electrical aspects are related to DFIG and electronic power converters [10].

The designer of wind turbine can choose a large number of topologies. In any case, commercial plans for power generation have presently focused to horizontal axis, three-blade wind turbines which are appropriate in large power generating turbines [11].

According to their operating speed, wind turbines are usually divided into fixed speed wind turbines and variable speed wind turbines [12]. Fixed speed wind turbines can operate only at limited range of wind speeds and when the wind speed changes, the output power is fluctuated. Since the nature of wind will vary and not linear, there is power fluctuation problem and thus, affect the power quality of the grid. The squirrel cage induction generator is suitable for fixed speed wind turbines. Wind turbines based on variable speed can operate with maximum energy conversion efficiency over a wide range of wind speeds. In this case the power quality improves compared to fixed speed wind turbines. In solving the limitations of fixed speed wind turbines and alleviating their deficiencies, variable speed wind turbine technology has advantages. In general terms, generation of wind energy uses a fixed speed or a variable speed turbine, which can be classified into four main types. These are type 1, type 2, type 3 and type 4 wind turbines. DFIG concepts belong to type 3-based wind turbines, which are widely used technologies for variable speed wind turbine plants. The wind turbines have to work at variable speed and trace the curve of maximum power extraction [13]. Therefore, the variable speed wind turbine uses the resources of wind energy used more efficiently than the fixed speed wind turbine, so there is no output power fluctuation in the case of variable speed wind turbine.

2.1.2 Operating Regions of a Wind Turbine-Generator System

The wind turbine operates with different dynamics, from minimum to maximum wind speed, and the operating regions of the wind turbine power versus wind speed curve is illustrated in figure 2.2. Wind speed regions are the cut-in, rated and cut-out speeds. The cut-in speed (point A) is the point at which the wind turbine blades begin to rotate and generate electricity. As the wind speed increases, more electricity is generated until it reaches the maximum limit (point C). This maximum limit point is the rated speed and occurs when the turbine produces maximum output power or rated power. Wind speeds between the cut-in speed and therefore the rated speed, is an MPPT zone (Zone 2) [14].

The maximum power tracking adjustment is achieved especially by controlling the converter on the generator side. In the case of high-speed wind, the wind turbine stops running and shuts down to prevent damage. The wind speed at which the shutdown operation occurs is the cut-off wind speed (Zone 3). When wind turbines experience high wind speeds, this may damage the its mechanical part, so to prevent such issue cut-off speed needed [7]. Figure 2.2 illustrates the operation regions of wind turbine generator system.

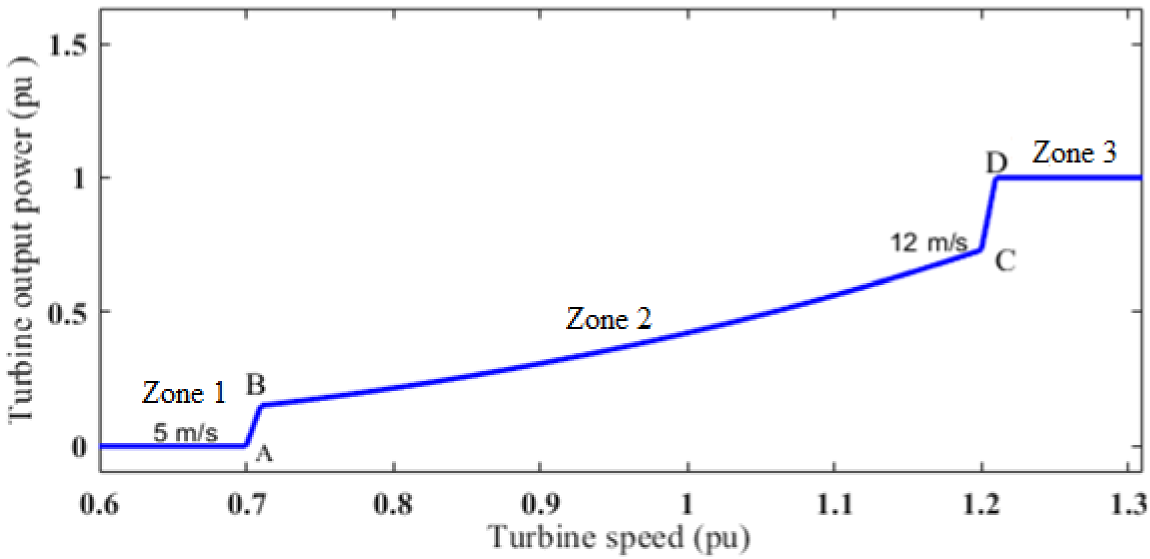

Figure 2.2 Turbine output power verse wind speed curve [15]

2.2 Doubly fed Induction generator (DFIG)

DFIG is also called an induction generator with wound rotor winding which consists of the stationary and rotating parts [16]. It is suitable for operation of wind turbines based on variable speed. In the DFIG-based wind energy conversion topology, the converter called AC/DC/AC is connected to the rotor part and stator part is directly connected to the network [15]. In DFIG independent control of active and reactive power, and a wide range of operating speed controlled by the RSC. These days, DFIG is most commonly utilized for large wind turbines in the wind turbine industry. DFIG based wind turbine consists of a wound rotor asynchronous generator and AC/DC/AC VSC with reduced cost and power rating of the converter.

2.2.1 Operating Principles of DFIG

Generally, high-power wind energy conversion system is based on doubly-fed asynchronous generator.

The stator winding of DFIG is directly connected to a three-phase 50 Hz frequency grid, whereas the rotor winding is connected to the network through back-to-back power electronic converters to allow the generator operation at variable speeds in response to changing wind speeds. The rotor power circuit is composed of two components, RSC and GSC, which are independently controlled. Between the two electronic power converters, DC-link capacitor is placed as energy storage to maintain a constant DC bus voltage [2]. RSC controls active and reactive power by controlling the rotor current, while GSC regulates the intermediate circuit voltage and the reactive power exchange with the grid [17]. The stator side always supplies active power to the grid, and according to the DFIG operating mode, active power is fed in or out of the rotor circuit.

2.3 Power Electronic Converter Topologies

Numerous sorts of wind turbines based on variable speed wind turbine technology utilize power electronic converters as an interfacing instrument. Since, the wind turbine works at variable speed, the frequency of the generator changes and must hence be decoupled from the grid. This may be accomplished by employing power electronic converter technology [18]. In DFIG, electronic power converter is connected to the rotor winding, allowing bi-directional power flow in the rotor circuit and increasing the speed range of the generator. The converter topology enhances overall power conversion efficiency, extends generator speed range and improves dynamic performance of wind turbine technology. In variable speed wind turbine systems, power electronic converters have an ability to regulate and decouple the active and reactive power conveyed to electrical network. These characteristics have made the DFIG based wind turbine system widely accepted in today's wind turbine market.

2.4 Back-to-Back Voltage Source Converter (VSC) Models

The AC/DC/AC converter model based on two-level voltage source converter topology is widely used in renewable energy systems. In DFIG based wind turbine generator system, the machine needs to be operated either in sub-synchronous speed mode or super-synchronous speed mode according to various wind speeds. Therefore, the back-to-back VSC configurations become necessary due to their bi-directional operation ability. The converter provides good abilities to transmit the generated power from wind turbine to grid effectively, respond quickly and accurately. Figure 2.3 shows a typical AC/DC/AC converter which consists an AC/DC and DC/AC converters with a common capacitor of DC-link [4]. IGBT device is used in electronic power converter for switching purpose.

Advantages of using IGBTs over other types of transistor devices are, it combines the benefits of both MOSFETs and bipolar transistors [19].

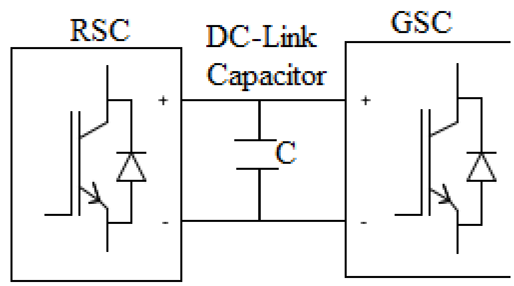

Figure 2. 3 AC/DC/AC voltage source converter [4]

2.4.1 Two-level Voltage Source Converter (VSC)

Two-level VSC has been the foremost broadly utilized power converter for three-phase drive applications in which the output wave form is created by utilizing PWM with two voltage levels. In the case of two-level VSC, the output voltage and current are distorted, which shows that there are more THD. Due to such limitations of two-level VSC, multilevel VSCs are developed in order to produce more sinusoidal output voltage and current to capture efficient and better energy by reducing the THD. Since two-level inverters have the disadvantage of achieving higher power levels, three level inverter configurations have been developed to meet high voltage level requirements. Therefore, multilevel inverters promised lower torque ripples and copper loses as compared to the two-level inverter [20]. In three-level VSC the voltage and current are much more sinusoidal and THD is reduced. Figure 2.4 illustrated a two-level back-to-back VSC.

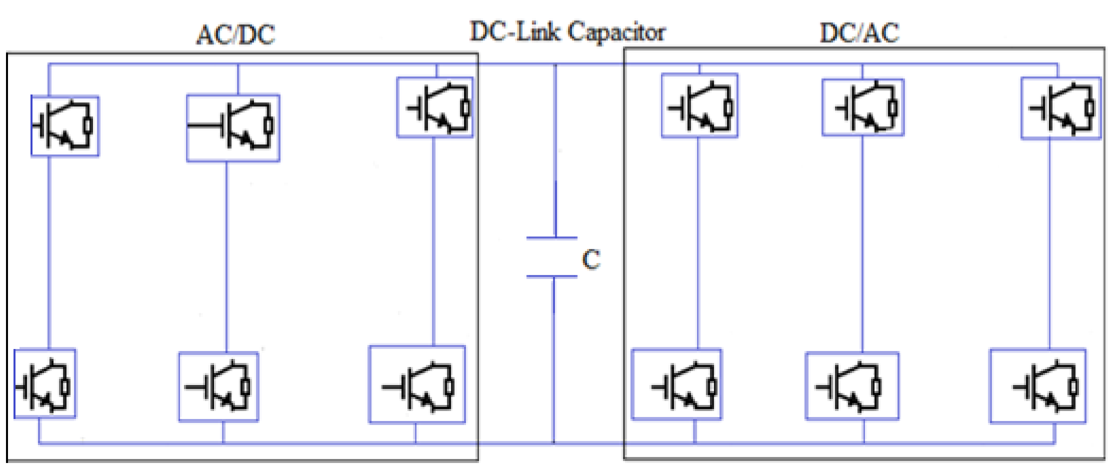

Figure 2. 4 Two level AC/DC/AC VSC [21]

2.4.2 Neutral-Point-Clamped (NPC) multi-level Converters

Multilevel voltage source converter topologies permit the handling of high power with standard components such as semiconductors, drivers and smaller filters, to empower the operation in higher voltage levels. To realize this, the switches are arranged in advance than within the classical two-level converters. The increased number of switching devices gives additional degree of flexibility, which improves the performance and quality of voltage and generated power. In general, multi-level VSCs can be divided into three categories [22]. These are:

- The NPC multi-level converters or diode-clamped converters
- Flying capacitor converters and
- Cascaded H-bridge converters

Multi-level NPC voltage source converter is more beneficial over the three-phase conventional VSI due to [23]:

- It generates more output line-to-line voltage levels, so the output voltage and current THD content can be reduced.
- Pure sinusoidal wave forms are generated and this shows that the harmonic distortion is decreased.
- It has high efficiency
- Since all phases share a common DC-bus, capacitor requirement is reduced.

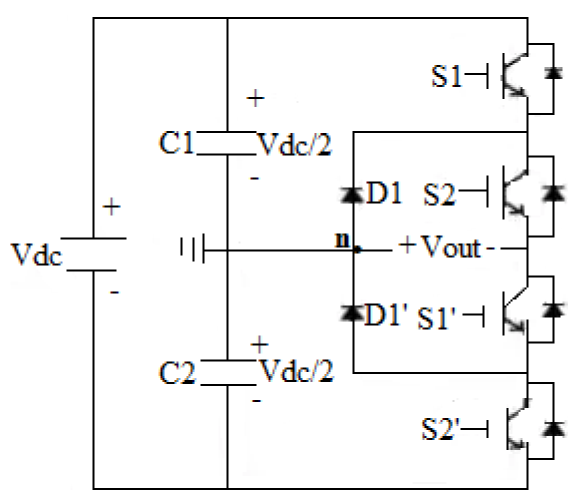

Figure 2. 5 Three-level diode clamped multilevel inverter [24]

2.5 Pulse width modulation (PWM)

The correct choice of PWM to generate rectangular switching signals from power electronic converters is the main factor affecting the performance and efficiency of wind power systems. Generating sinusoidal output voltage with minimum harmonic distortion in GSC is the main goal of PWM. Due to the following advantages, the PWM strategy is applicable:

- To control the voltage output waveform
- In order to achieve a good spectral performance by minimizing the THD.
- To achieve a good DC-bus utilization.

In power electronic converters, the electrical energy from one level of voltage or current is changed into another using semiconductor-based electronic switch.

The essential characteristic of these types of circuits is that the switches are operated only in one of two states, either ON or OFF states. The process of switching the electronic devices during a power converter from one state to different state is modulation. Modulation strategy plays a crucial role within the minimization of harmonics and switching losses in converters [4]. The modulation strategy is used to obtain a variable output with the largest fundamental component and the smallest harmonic. Modulation technology is used to switch and operate controlled voltage source converters to produce excellent output voltage and current for various types of loads. By using modulation techniques, the switching device can obtain precise amplitude and frequency with a specified quality. In this thesis work, the sinusoidal PWM, third-harmonic injection and SVPWM techniques are applied with the grid connected three-phase voltage source converters in order to reduce the THD.

2.5.1 Sinusoidal Pulse Width Modulation (SPWM)

In recent decades, SPWM has been broadly applied in control application of AC drive. In this modulation technique, the three-phase reference modulation signal is compared to the carrier signal to give a high or low state. This traditional SPWM technology is the most widely used technology because it is easy to implement and control, and it is compatible with almost all modern digital applications. But it has some disadvantages that can reduce its flexibility in some applications. Still, this strategy cannot make full utilize of the inverter voltage [25].

2.5.2 Third Harmonic Injection PWM (THIPWM)

Applying third harmonic injection to a three-phase sinusoidal signal improves the output voltage without causing overmodulation. The third harmonic signal is added to the reference signal and causes the amplitude to increase without loss of quality. The peak fundamental wave component may be higher than the peak value of the triangular carrier wave that increases the fundamental wave voltage [26]. Adding third harmonic signal with conventional SPWM improves the fundamental output voltage and reduces the THD.

2.5.3 Space Vector Pulse Width Modulation (SVPWM)

The concept of space vector was initially determined from the turning field of an asynchronous drive and was utilized in PWM applications. Compared with SPWM technology, SVPWM has better dynamic performance and higher modulation even the computational complexity is relatively increased. In this thesis work three level grid connected NPC inverter topology based on SVPWM strategy is addressed to reduce the THD. In this type of modulation technique, eight switching patterns are used to approximate the reference voltage vector. Within the execution of SVPWM, determination of the reference voltage, duration of the switching time, and the switching time of each switch are crucial steps, and the switching sequence should provide less switching loss [26]. Compared with traditional SPWM technology, SVPWM has the following advantages:

- Better spectral performance.
- Enhanced DC-bus utilization.
- Generates less harmonics distortions in the output voltage or currents.

Therefore, SVPWM techniques are applied to grid connected inverter topology in order to eliminate or reduce the THD [25]. By applying SVPWM, the drawbacks of SPWM are reduced.

2.6 Related Works

In this scenario, related works of DFIG-based wind turbine control strategies are introduced. More specifically, related works on modeling, designing and control strategies of DFIG and analysis of THD for voltage source inverters are illustrated.

In [27] the controller design of a DFIG driven by a variable speed wind turbine using particle swarm optimization technology is described.

DFIG's mathematical model, its power converter and its controller have been explained. Simple low-level DFIG diagrams have been used in the design of PID controllers using the numerical differentiation of the Simulink model. The DFIG-based WECS design and its fitness function using PSO technology are presented. With a PSO-based controller, the DFIG system has slightly improved response in terms of terminal voltage, current, active and reactive power, DC-Link voltage, and generator speed. The controller based on PSO technology not only improves system response, but also reduces percentage overshoot to zero. The results obtained show that the system using the PSO-based controller stabilizes in a shorter time than the system based on the monitoring PID controller, but the THD problem is not considered or analyzed.

Author in reference [28] describes the dynamic modeling and DFIG control based on the wind turbine systems. The Active and reactive power is controlled by the using feedback technique in the converter on the rotor side and reduces oscillation of the turbine generator.

Even if feedback control technique improves better power flow, the GSC is not controlled and also THD analysis is not considered.

Author in reference [29] presents an improved direct vector command (DVC) based on three-level SVPWM. The essential disadvantage that is usually associated with DVC is the high harmonic current and power ripples. To overcome this harmonics and ripple issue, a SVPWM technique is proposed based on neural networks technique. The neural network regulator is applied to reduce the stator reactive and active power ripples and to improve performance of the DVC command. The THD analysis is considered and reduced by applying three-level inverter based SVPWM technique by using Matlab/Simulink, but the generator side converter is not regulated.

Author in reference [30] describes direct power and vector control in combined manner based on direct current regulatory approach for RSC of DFIG. The system gained benefits of both control strategies in a compacted control system. Its benefit compared to vector control include a rapid dynamic response and robustness against changes in machine parameters. On the other hand, it benefits compared to direct power control including less disturbance and ripple. Since, two-level grid connected VSC is used, the THD becomes more.

Author in reference [31] presents the control strategy of the RSC of DFIG by utilizing vector control with FLC to regulate the rotor currents. But GSC and THD analysis are not considered.

Author in reference [32] describes the help of battery energy storage systems to reduce DFIG power fluctuations. By applying a field-oriented control strategy, active and reactive power generated by the generator are decoupled. The overall system is tested and modelled by using Matlab/Simulink software. But THD analysis is not considered.

In reference [33], the author describes DFIG control strategy by using direct torque control approach. But in conventional DTC technique there are high-current harmonics and noise that will reduce the control performance.

In [34], the modeling and control of a wind turbine converter system based on a doubly-fed asynchronous generator is proposed to adjust the active and reactive power of the stator using MPPT control strategy. But the outer did not consider harmonics issue at all.

In [35] RSC and GSC of DFIG are controlled by utilizing improved control method considering harmonic distortion. Even if both RSC and GSC are controlled and harmonic disturbance is analyzed, the grid connected VSC used is a conventional two-level inverter. Still THD analysis is required and an advanced LCL filter circuit must have to be designed to get more sinusoidal current and voltage signals with small THD value.

In [36] synchronous power generation and harmonic current suppression using DFIG based WECS are described. In addition to harmonic isolation, the active and reactive power control strategy is applied. The GSC control analysis is not considered.

In [37] direct AC to AC matrix converter with SVPWM is utilized and MPPT control strategy is applied for speed regulation. But matrix converter can’t utilize DC voltage fully.

The above listed related literature reviews show the control strategy and modelling of DFIG based wind turbine technology with some limitations and drawbacks. In order to extract maximum power by using DFIG based wind turbine technology, the RSC and GSC must have to be controlled. In addition to this, THD in point of common coupling must be mitigated. In order to obtain pure sinusoidal signals of grid voltage and current, multilevel inverter and filter type of LCL. To improve the output fundamental voltage levels, the SVPWM technique is applied with grid connected multilevel voltage source converters. Therefore, the listed literature reviews did not consider such control strategy to extract maximum power. In this thesis work, this all-control scheme is applied and maximum power transfer capability is ensured while the voltage output waveform is increased by minimizing the THD content.

CHAPTER THREE

MATERIALS, METHODS AND SYSTEM DESCRIPTION

3.1 Introduction

This chapter mainly focuses on the methodology that has been followed to accomplish this thesis work. The materials, analysis techniques, mathematical modeling of DFIG for both generator and grid side converter, vector control algorithm, and design of fuzzy logic controller. In addition to this, two-level back-to-back converter and three-level grid connected NPC multilevel inverter design and pulse generation techniques are presented.

3.2 Materials

In this thesis, MATLAB/2019b is used to develop the Simulink block and Math Type 6.0 is used to develop the overall system mathematical design.

3.3 Methods

To achieve the general and specific objectives of the study stated in the previous chapter, the following methods will be followed.

- Gathering and reviewing of closely related papers and literatures from different books, related journals and google scholars.
- Modelling of DFIG based wind turbine using Clark and Park transformation.
- Designing of fuzzy logic control technique for vector controlled DFIG based wind turbine.
- Model and design three-phase grid connected voltage source converter and simulating using different PWM techniques.
- The overall system is simulated using MATLAB/Simulink and the results are analyzed.
- Finally, the proposed system is concluded and recommendation is made for future.

The method used in this thesis to accomplish the required task is shown in Figure 3.1.

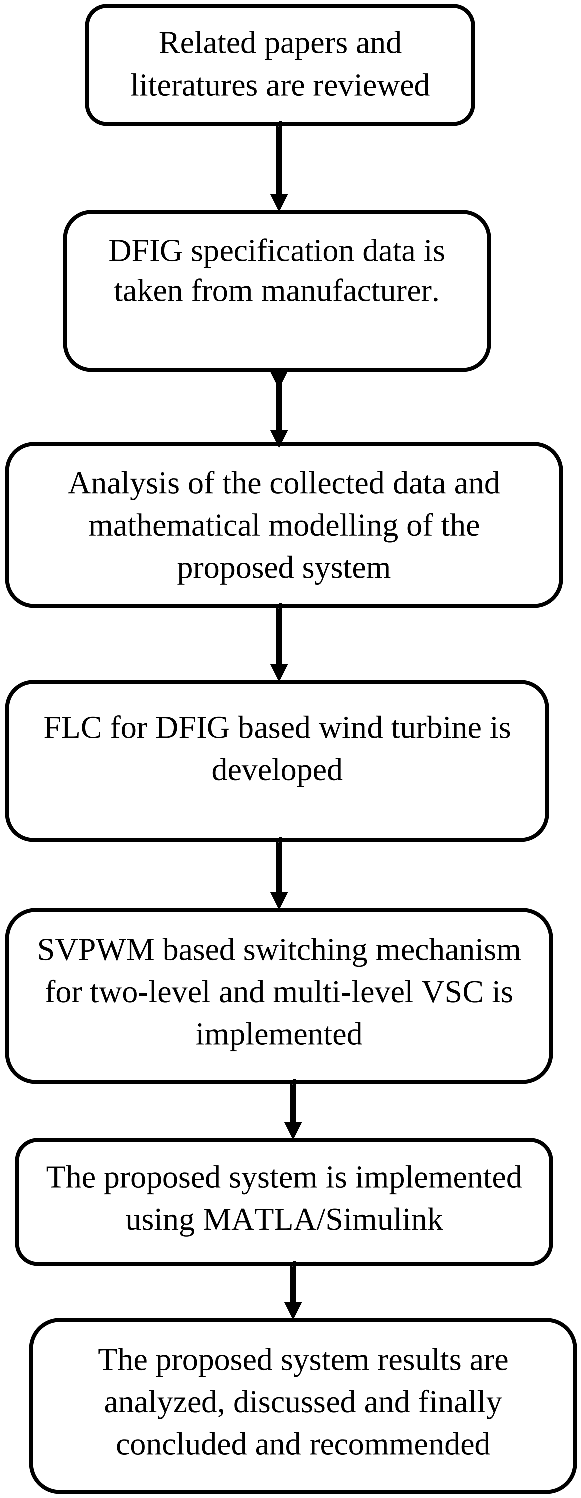

Figure 3.1 Block diagram of research methodology

3.4 Wind Turbine Aerodynamic Model

Innovative wind turbine technology converts the kinetic energy of the wind into mechanical energy by generating torque. The aerodynamic model represents the power drown from the rotor and calculates the generated torque depending on the air flow on the blades. The power due to a wind speed V_{wi} and a surface area A_1 is given by [38]:

$$P_{vw} = \frac{1}{2}\rho A_1 V_{wi}{}^3 \tag{3.1}$$

Turbine power is expressed by the maximum power coefficient, which is given by [39]:

$$P_t = P_{vw} c_p = \frac{1}{2}\rho\pi R^2 V_{wi}{}^3 c_p \tag{3.2}$$

where: R is the radius of the turbine rotor or length of the blades, c_p is the power coefficient.

The power coefficient c_p is a dimensionless parameter that represents the effectiveness of the wind turbine in converting the kinetic energy of the wind into mechanical energy. It is a function of the wind speed, rotational speed Ω_t, and pitch angle β [4]. In addition, the power coefficient c_p and TSR are expressed as:

$$\lambda = \frac{R\Omega_t}{V_{wi}} \tag{3.3}$$

where: Ω_t is mechanical rotational speed of rotor

Power coefficient c_p is given by [40]:

$$\begin{cases} \dfrac{1}{\lambda_i} = \dfrac{1}{\lambda + 0.02\beta} - \dfrac{0.003}{\beta^3 + 1} \\ c_p = c_p(\lambda,\beta) = 0.46(\dfrac{151}{\lambda_i} - 0.58\beta - 0.002\beta^{2.14} - 13.2)(e^{\frac{-18.4}{\lambda_i}}) \end{cases} \tag{3.4}$$

The mechanical power extracted by the turbine based on the turbine torque is given by [41]:

$$P_m = T_t\Omega_t \tag{3.5}$$

Figure 3.2 describes a relationship between the power coefficient c_p and lambda. It can be seen that for a specific TSR value, the C_P value becomes the highest.

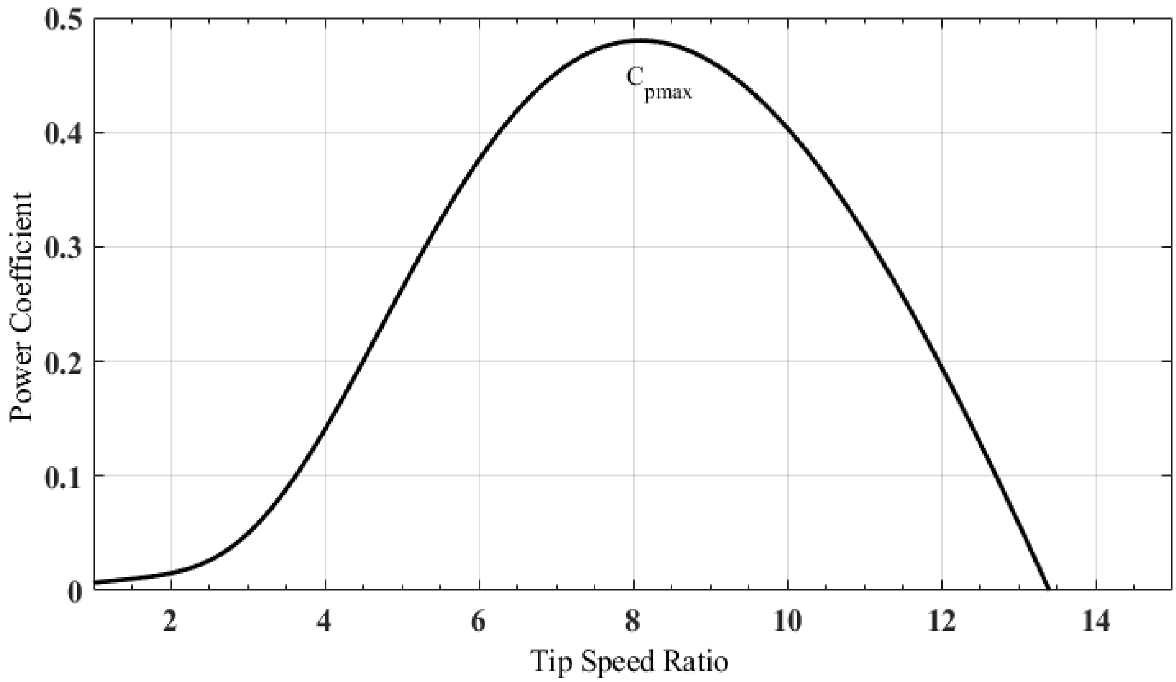

Figure 3.2 Power coefficient vs tip speed ratio (Lambda) graph [4]

The turbine torque is expressed according to the angular speed of the rotor and the mechanical power of the turbine by the following relation [4].

$$T_t = \frac{P_m}{\Omega_t} = \frac{1}{2}\rho\pi R^3 C_t V_w{}^2 \tag{3.6}$$

where:

$C_t = \frac{C_p(\lambda)}{\lambda}$ which is the coefficient of the torque.

The turbine gearbox ratio (N) is required between the speed of the turbine shaft (low speed shaft) and the speed of the generator shaft (high speed shaft).

$$\omega_m T_m = \omega_t T_t \tag{3.7}$$

$$N = \frac{\omega_m}{\omega_t} = \frac{T_t}{T_m} \tag{3.8}$$

where: ω_m , ω_t are rated speeds of generator and turbine in rpm, T_t and T_m indicates the torque of turbine (on low-speed shaft) and generator (on high-speed shaft) respectively.

3.4.1 Maximum Power Point Tracking (MPPT) Control Strategy

MPPT control strategy controls the electromagnetic torque to adjust the mechanical speed and maximize the generated electrical output. When the turbine operates at maximum power, the tip speed ratio and the maximum power coefficient becomes in optimal state [40] .The torque reference is adjusted by the following values:

$$T_{em\text{-}ref} = \frac{T_t}{N} = k^{op}\Omega_m \tag{3.9}$$

where: $k^{op} = \frac{1}{2}\rho\pi R^3 \frac{C_p{}^{op}}{\lambda_p{}^{op} N^3}$

To obtain the mechanical speed, the mechanical model equation of the DFIG is considered and given by:

$$T_{em} - T_{mech} = J\frac{d\Omega_m}{dt} + f_v\Omega_m \tag{3.10}$$

where: J is inertia, f_v is the damping coefficient, Ω_m is mechanical rotational speed.

It is also possible to derive the electric rotational speed ω_m and the angle θ_m from the mechanical model equation of the DFIG. By applying Laplace transform, mechanical rotational speed is given by:

$$\Omega_m = \frac{T_{em} - T_{mech}}{J_s + f_v} \tag{3.11}$$

3.5 Steady State Model of DFIG

The induction generator steady state model is very useful for testing steady state generator performance. Then the dynamic behavior of the machine will be developed based on this knowledge. In a steady state, the stator is fueled by a constant symmetrical signal of AC from the network. The generator rotor winding is also powered by a constant balanced three-phase AC signal via back-to-back VSC independent of the stator. The frequency ω_s, ω_r and the electric speed of rotor ω_m are given by [4]:

$$\omega_s = \omega_r + \omega_m \tag{3.12}$$

$$\omega_m = p.\Omega_m \tag{3.13}$$

where: p is pole pairs and Ω_m is mechanical rotational speed at the rotor in rad/s.

The slip s of the generator is defined as follows:

$$s=\frac{\omega_s-\omega_m}{\omega_s}=\frac{\omega_r}{\omega_s} \tag{3.14}$$

As illustrated in previous sections, the stator part of DFIG is directly connected to the grid. So, the frequency of grid and stator becomes constant. Depending on the slip sign and rotor speed, doubly fed generators operate in different operating modes [42].These include:

- $\omega_m < \omega_s \Rightarrow \omega_r > 0 \Rightarrow s > 0 \Rightarrow$ Sub synchronous operation
- $\omega_m > \omega_s \Rightarrow \omega_r < 0 \Rightarrow s < 0 \Rightarrow$ Hypersynchronous operation
- $\omega_m = \omega_s \Rightarrow \omega_r = 0 \Rightarrow s = 0 \Rightarrow$ Synchronous mode of operation

3.5.1 Sub-Synchronous Speed Mode

When the operating speed of the generator is less than synchronous speed ω_s, DFIG operates in the sub synchronous speed mode. In this case, the rotor winding rotates at a speed lower than its synchronous speed. Here mechanical and rotor power will be sent to the network through the stator. In this mode of operation, the generator slips and electromechanical torque developed has a positive value. The Figure 3.3 shows the sub-synchronous operation of DFIG [42].

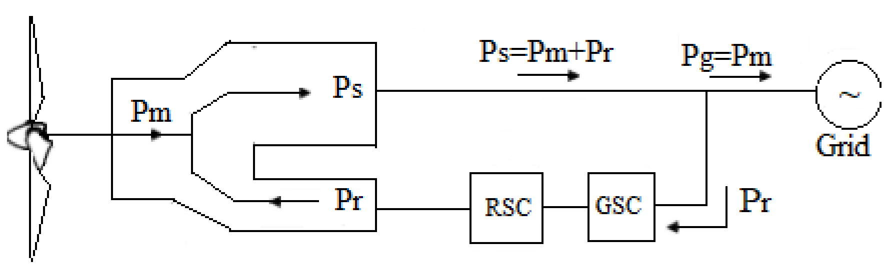

Figure 3.3 Sub-synchronous operating mode of DFIG [42]

3.5.1 Super-synchronous Speed Mode

In this mode of operation, the generator rotor increases above synchronous speed and the rotor's magnetic field rotates counterclockwise. The mechanical power of the shaft is transmitted to the network through the stator and rotor circuits. The rotor power is transmitted to the network through the power converter in the rotor circuit and the stator power is transmitted directly to the network. In this operating mode, the electromechanical torque generated is negative. This scenario is shown in Figure 3.4.

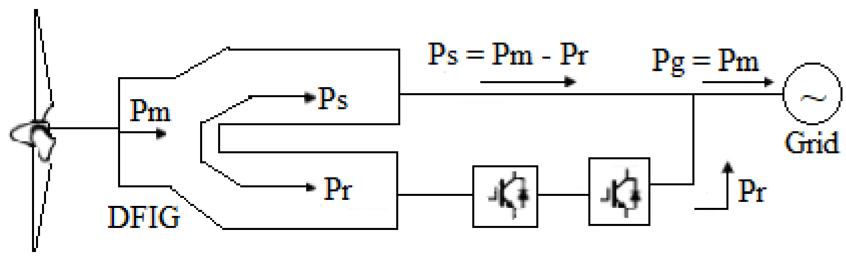

Figure 3. 4 Super-synchronous operating mode [42]

3.5.3 Synchronous Speed Mode

In this operating mode, the generator operates as a synchronous motor because RSC provides DC excitation for the rotor windings. Since the rotor winding does not provide any current or power, the rotor power is zero, but the stator winding provides a large amount of reactive power to the network. The generated nominal speed is equal to operating speed of the generator and the slip is zero. Figure 3.5 illustrates the torque and slip characteristics of the three DFIG modes of operation.

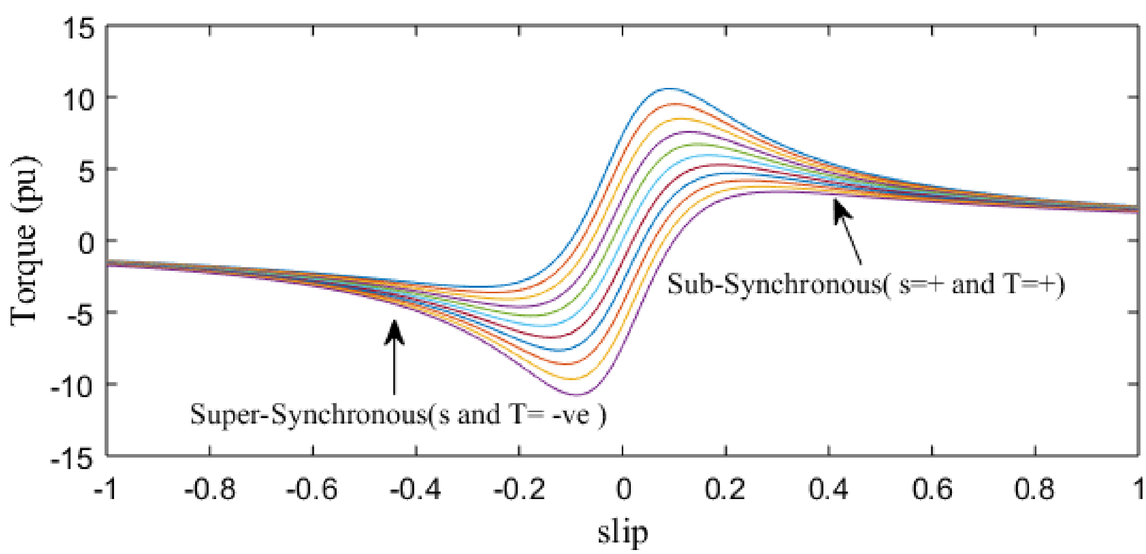

Figure 3. 5 Torque slip characteristics for DFIG modes of operation [43]

3.6 Dynamic Modelling of DFIG

In order to study the actual behavior of DFIG, it is necessary to consider dynamic equations to obtain a more reasonable perception. Before controlling and analyzing the performance of the machine, it is very important to use Clark and Park to transform the machine model in the form of space vector to facilitate the simulation and implementation of the control scheme. The space vector model of induction generator is generally composed of three sets of equations, including voltage equation, magnetic flux equation and motion equation. The general voltage equation is given by [4]:

$$V = I.R + \frac{d|\psi|}{dt} \tag{3.15}$$

where, ψ is the flux of the generator.

In dynamic DFIG modeling in space vector theory, three different rotating reference frames are usually used. They are:

- Stator reference frame (αβ), also known as stationary reference frame.
- Rotor reference frame (DQ) rotates at ω_m, and
- Synchronous reference frame (d-q) rotates at ω_s.

3.6.1 αβ Model

The αβ components of voltage and currents from the measured values are calculated with the Clarke transformation. The purpose of a Clarke transformation is to transform a-b-c reference frame to α β [4]:

$$x_{\alpha\beta} = T_c x_{abcs} \tag{3.16}$$

where, T_c is the transformation matrix of Clarke transformation

$$T_c = \frac{2}{3}\begin{bmatrix} 1 & -1/2 & -1/2 \\ 0 & \sqrt{3}/2 & -\sqrt{3}/2 \end{bmatrix} \tag{3.17}$$

$$\begin{bmatrix} i^s{}_{\alpha r} \\ i^s{}_{\beta r} \end{bmatrix} = T_r \begin{bmatrix} i_{\alpha r} \\ i_{\beta r} \end{bmatrix} \tag{3.18}$$

where, T_r is expressed as follows

$$T_r = \begin{bmatrix} \cos\theta & -\sin\theta \\ \sin\theta & \cos\theta \end{bmatrix} \quad (3.19)$$

3.6.2 d-q Model

To make the computation simpler, three-phase system is transformed in to d-q axis which is applied to decouple d and q axis currents of rotor independently. Transformation of αβ frame to an orthogonal rotating reference frame (d-q) is known as Park transformation.

$$\begin{bmatrix} i_{ds} \\ i_{qs} \end{bmatrix} = T_p(\theta) \begin{bmatrix} i_{\alpha s} \\ i_{\beta s} \end{bmatrix} \quad (3.20)$$

where, T_p is the transformation matrix and θ is the angle between d-axis and α-axis.

$$T_p(\theta) = \begin{bmatrix} \cos\theta & -\sin\theta \\ \sin\theta & \cos\theta \end{bmatrix} \quad (3.21)$$

Stator voltage equation is shown in Equation (3.22) and rotor voltage equation is represented in Equation (3.23) in stationary axis [19]:

$$\begin{cases} V_{\alpha s} = R_s I_{\alpha s} + \dfrac{d\psi_{\alpha s}}{dt} \\ V_{\beta s} = R_s I_{\beta s} + \dfrac{d\psi_{\beta s}}{dt} \end{cases} \quad (3.22)$$

$$\begin{cases} V_{\alpha r} = R_r I_{\alpha r} + \dfrac{d\psi_{\alpha r}}{dt} + \omega_m \psi_{\beta r} \\ V_{\beta r} = R_r I_{\beta r} + \dfrac{d\psi_{\beta r}}{dt} + \omega_m \psi_{\alpha r} \end{cases} \quad (3.23)$$

The flux in αβ axis is given by:

$$\begin{cases} \psi_{\alpha s} = L_s i_{\alpha s} + L_m i_{\alpha r} \\ \psi_{\beta s} = L_s i_{\beta s} + L_m i_{\beta r} \end{cases} \quad (3.24)$$

$$\begin{cases} \psi_{\alpha r} = L_m i_{\alpha s} + L_r i_{\alpha r} \\ \psi_{\beta r} = L_m i_{\beta s} + L_r i_{\beta r} \end{cases} \tag{3.25}$$

where: L_s and L_r are inductances of the stator and rotor, L_m is the magnetizing inductance L_s and L_r are related to leakage inductance of the stator and rotor ($L_{\sigma s}$, $L_{\sigma r}$), and given by:

$$\begin{cases} L_s = L_{\sigma s} + L_m \\ L_r = L_{\sigma r} + L_m \end{cases} \tag{3.26}$$

The active power of stator and rotor side becomes:

$$P_s = \frac{3}{2}(v_{\alpha s} i_{\alpha s} + v_{\beta s} i_{\beta s}) \tag{3.27}$$

$$P_r = \frac{3}{2}(v_{\alpha r} i_{\alpha r} + v_{\beta r} i_{\beta r}) \tag{3.28}$$

The rotor and stator side reactive power are given by:

$$Q_s = \frac{3}{2}(v_{\beta s} i_{\alpha r} - v_{\alpha s} i_{\beta r}) \tag{3.29}$$

$$Q_r = \frac{3}{2}(v_{\beta r} i_{\alpha r} - v_{\alpha r} i_{\beta r}) \tag{3.30}$$

The generated electromagnetic torque of DFIG is given by:

$$T_{em} = \frac{3}{2} p(\psi_{\beta r} i_{\alpha r} - \psi_{\alpha r} i_{\beta r}) \tag{3.31}$$

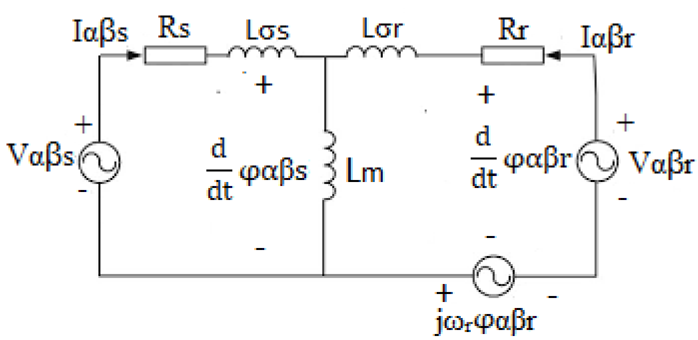

Figure 3. 6 Equivalent circuit of the DFIG in stator coordinates [19]

By applying park transformation matrix to Equations (3.22) and (3.23), the voltage equation in rotating frame of refence is given by:

$$\begin{cases} v_{ds} = R_s i_{ds} + \frac{d\psi_{ds}}{dt} - \omega_s \psi_{qs} \\ v_{qs} = R_s i_{qs} + \frac{d\psi_{qs}}{dt} - \omega_s \psi_{ds} \end{cases} \tag{3.32}$$

$$\begin{cases} v_{dr} = R_r i_{dr} + \frac{d\psi_{dr}}{dt} - \omega_r \psi_{qr} \\ v_{qr} = R_r i_{qr} + \frac{d\psi_{qr}}{dt} - \omega_r \psi_{dr} \end{cases} \tag{3.33}$$

Also, the stator and rotor flux equations in d-q axis is given by:

$$\begin{cases} \psi_{ds} = L_s I_{ds} + L_m I_{dr} \\ \psi_{qs} = L_s I_{qs} + L_m I_{qr} \end{cases} \tag{3.34}$$

$$\begin{cases} \psi_{dr} = L_r I_{dr} + L_m I_{ds} \\ \psi_{qr} = L_s I_{qr} + L_m I_{qs} \end{cases} \tag{3.35}$$

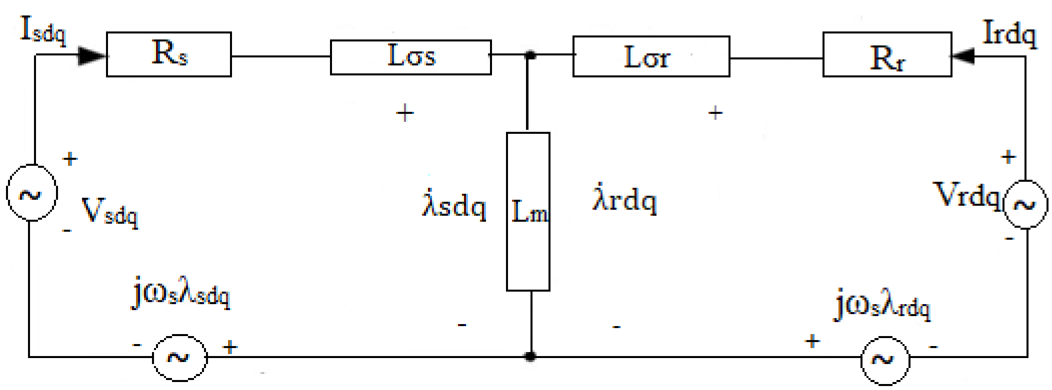

Figure 3. 7 Equivalent circuit of the DFIG in the rotating d-q coordinates [19]

The electromagnetic torque equation in the rotating d-q reference frame is given by:

$$T_{em} = \frac{3}{2} P \frac{L_m}{L_s} (\psi_{qs} i_{dr} - \psi_{ds} i_{qr}) \tag{3.36}$$

3.7 Vector Control Strategy of DFIG for RSC

The control strategy of AC motor can be roughly categorized into scalar and vector control. The former one is easy to design, and despite its slow dynamics, it still provides relatively stable state response. These limitations result in innovation of control system called vector, which is applied to solve the slow response caused by scalar control.

In the vector control of DFIG, the d-axis and q-axis components of the rotor currents are adjusted. In order to be able to easily control the generator, stator flux orientation frame is used to realize independent control of active and reactive power by means of the quadrature and the direct current, respectively. The principle is to align the flux of stator in d-axis [44]. In this case the stator fluxes in d and q axis are assumed as:

$$\begin{cases} \psi_{ds} = \psi_s \\ \psi_{qs} = 0 \end{cases} \tag{3.37}$$

Since the stator winding of DFIG is directly connected with the stable grid, the stator resistance is assumed as neglected. Consider the assumptions for the stator voltages in d-q axis [44]:

$$\begin{cases} V_{ds} = 0 \\ V_{qs} = V_s = \omega_s \psi_s \end{cases} \tag{3.38}$$

From the Equations (3.27) and (3.29), and (3.35) the rotor current in the direct and quadrature axis is calculated:

$$\begin{cases} L_s I_{ds} + L_m I_{dr} = \psi_s \\ L_s I_{qs} + L_m I_{qr} = 0 \end{cases} \tag{3.39}$$

The direct and quadrature axis stator current is given by:

$$\begin{cases} I_{ds} = \dfrac{\psi_s}{L_s} - \dfrac{L_m}{L_s} I_{dr} \\ I_{qs} = -\dfrac{L_m}{L_s} I_{qr} \end{cases} \tag{3.40}$$

$$\begin{cases} P_s = \dfrac{3}{2} V_{qs} I_{qs} = -\dfrac{3}{2} V_s \dfrac{L_m}{L_s} I_{qr} \\ Q_s = \dfrac{3}{2} V_{qs} I_{ds} = \dfrac{3}{2} \dfrac{V_s^2}{L_s \omega_s} - \dfrac{3}{2} \dfrac{L_m}{L_s} I_{dr} \end{cases} \tag{3.41}$$

Equation (3.41) shows, under the direction of stator flux, P_s and Q_s are decoupled and controlled independently. T_{em} depends on q axis current and stator flux.

$$
\begin{cases}
T_{em} = \frac{3}{2} P \frac{L_m}{L_s} (-\psi_{ds} i_{qr}) \\
T_{em} = -\frac{3}{2} P \frac{L_m}{L_s} |\vec{\psi}_s| i_{qr} = K_T i_{qr} \\
K_T = -\frac{3}{2} P \frac{L_m}{L_s} |\vec{\psi}_s|
\end{cases}
\tag{3.42}
$$

The voltage expression of rotor in d-q axis depends on the stator flux. To obtain the expression of rotor voltage, Equations (3.33) and (3.35) are considered.

$$
\begin{cases}
\psi_{dr} = \left(L_r - \frac{L_m^{\ 2}}{L_s} \right) I_{dr} + \frac{L_m}{L_s} \psi_{ds} \\
\psi_{qr} = \left(L_r - \frac{L_m^{\ 2}}{L_s} \right) I_{qr}
\end{cases}
\tag{3.43}
$$

As clarified in previous chapters, since the rotor part of DFIG is connected with power electronic VSCs, the rotor is supplied by voltages of different frequencies and amplitudes. The voltage equation in d-q coordinate, which is aligned with the stator flux space vector is given by [44]:

$$
\begin{cases}
V_{dr} = R_r i_{dr} - \omega_r \sigma L_r i_{qr} + \sigma L_r \frac{d}{dt} i_{dr} + \frac{L_m}{L_s} \frac{d}{dt} \psi_{ds} \\
V_{qr} = R_r i_{qr} + \omega_r \sigma L_r i_{dr} + \sigma L_r \frac{d}{dt} i_{qr} + \omega_r \frac{L_m}{L_s} \psi_{ds}
\end{cases}
\tag{3.44}
$$

During the regular operation of DFIG, the grid voltage is constant in altitude and frequency because the stator winding of DFIG is connected directly to the grid at constant AC voltage. Therefore, the stator flux is constant and hence, the derivative of flux is zero. The term $\omega_r \frac{L_m}{L_s} \psi_{ds}$ is a perturbation, since it depends on the stator flux or the and voltage, which is an external variable independent of the inner loop.

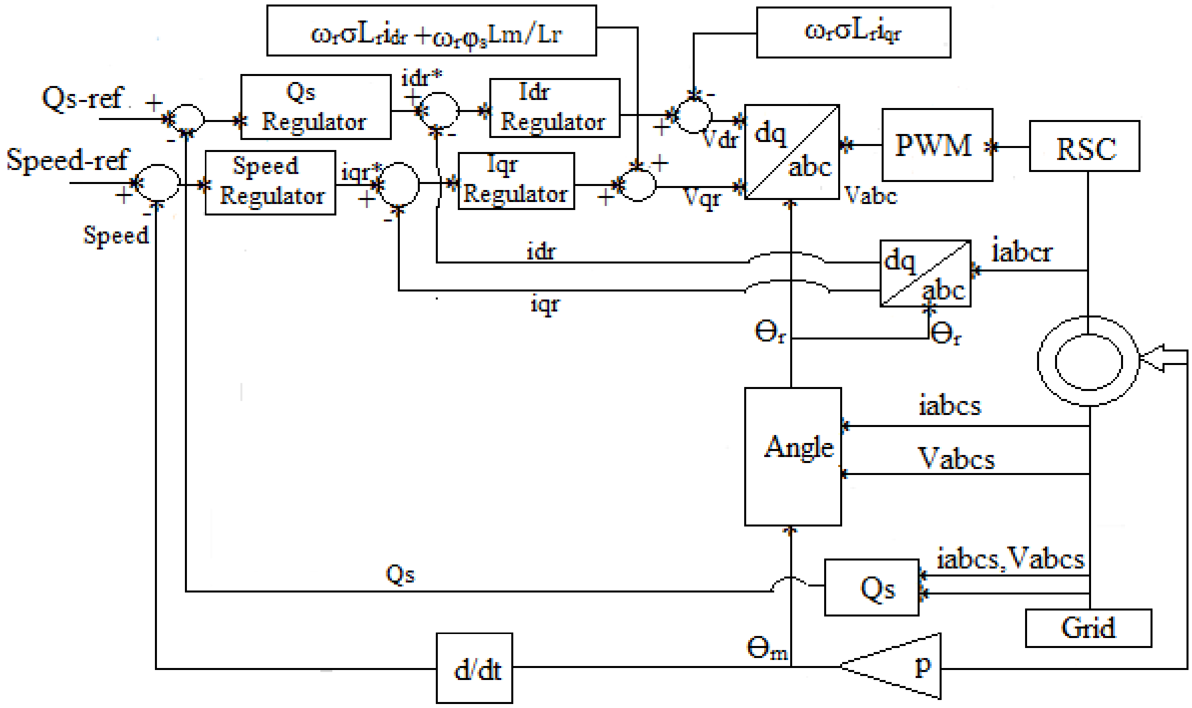

Figure 3. 8 Generator-side converter control block diagrams

Figure 3.8 illustrates vector control structure for RSC of DFIG to regulate the rotor speed and current loop. PWM technique is applied to control the switching signals of the power electronic converters. The outer loop is the rotor speed control loop and the inner one is control loop of rotor current.

3.7.1 Current Loop Transfer Function of RSC

In vector control strategy of DFIG in RSC, the regulator is the conventional PI controller. In the case of tuning the PI gain parameters, the coupling terms are cancelled. The regulator gains are tuned by using transfer function of current loop.

3.7.2 Proportional Integral Regulator Design

Proportional plus Integral (PI) controller is used to calculate and reduce error deviation due to the difference between a measured variable and set point for the current loop as well as for the speed loop. A simple block diagram of PI controller is illustrated in Figure 3.9.

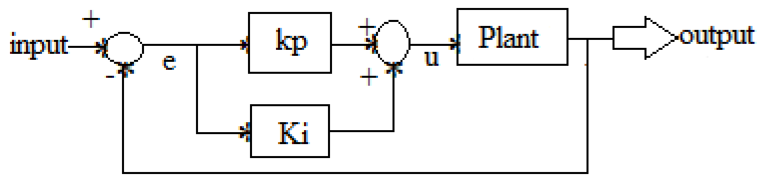

Figure 3. 9 Block Diagram of PI Controller [45]

The coupling terms are disappeared from the final transfer function by means of the control. The current loop transfer function for both d and q components are given by [19]:

$$\frac{i_{dr}(s)}{i_{dr}^*(s)} = \frac{i_{qr}(s)}{i_{qr}^*(s)} = \frac{\left(K_p s + K_i\right)/\sigma L_r}{s^2 + \left(\frac{K_p + R_r}{\sigma L_r}\right)s + \frac{K_i}{\sigma L_r}} \tag{3.45}$$

$$\frac{i(s)}{i^*(s)} = \frac{\left(K_p s + K_i\right)/\sigma L_r}{s^2 + 2\xi\omega_n s + \omega_n^2} \tag{3.46}$$

By choosing the damping ratio of 1, which means that the system is critically damped. Then, the current loop transfer function is given by:

$$\frac{i(s)}{i^*(s)} = \frac{\left(K_p s + K_i\right)/L}{\left(s + \omega_n\right)^2} \tag{3.47}$$

The current loop PI controller gains are tuned and the values are directly related with generator parameters.

$$\begin{cases} K_p = 2\omega_n \sigma L_r - R_r \\ K_i = \omega_n^2 \sigma L_r \end{cases} \tag{3.48}$$

3.8 Dynamic Modeling and Control of Grid Side System

The grid side system comprises of inverter, filter and the grid voltage. The main goal of grid side converter is to regulate the DC-link capacitor voltage and the grid currents of d and q axis. Controlling the DC-bus voltage is required, since the DC link is mainly formed by a capacitor [4]. So, the active power flow through the rotor must cross the DC link and then it must be transmitted to the grid. Therefore, by controlling the DC link voltage to a constant value it is possible to ensure flow the actual power through the converter. Figure 3.10 illustrates overall structure of the grid side system.

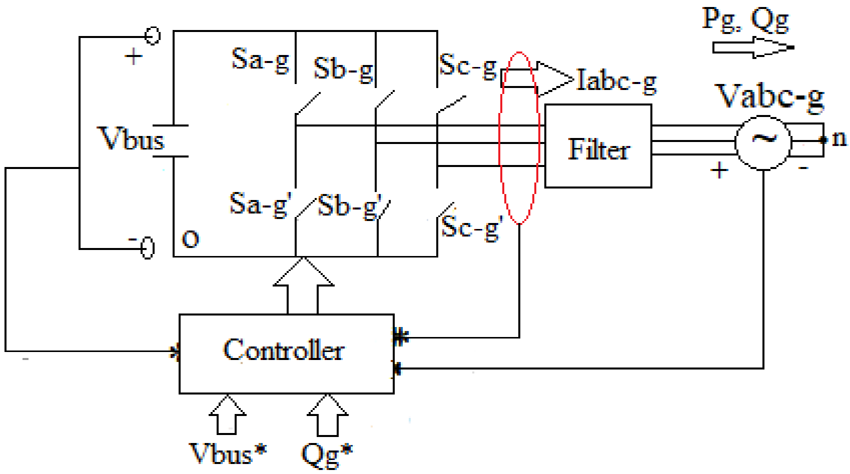

Figure 3. 10 Structure of GSC control system [20]

3.8.1 d-q Model of Grid side system

The dynamic modelling of grid side convertor of DFIG is analyzed in similar way to the RSC dynamic modelling [4]. The voltage equation for vector orientation is given by:

$$\begin{cases} V_{df} = R_f i_{dg} + L_f \dfrac{di_{dg}}{dt} + V_{dg} - \omega_a L_f i_{qg} \\ V_{qf} = R_f i_{qg} + L_f \dfrac{di_{qg}}{dt} + \omega_a L_f i_{dg} \end{cases} \tag{3.49}$$

The active and reactive powers exchanged with the grid becomes:

$$\begin{cases} P_g = \dfrac{3}{2}(V_{dg} i_{dg} + V_{qg} i_{qg}) \\ P_g = \dfrac{3}{2}(V_{qg} i_{dg} - V_{dg} i_{qg}) \end{cases} \tag{3.50}$$

3.8.2 Vector Control Strategy of the GSC

Vector control strategy for grid connected convertres provides good performance characteristics with reasonably simple implementation requirements. Figure 3.11 illustrates the grid voltage oriented control strategy**.** In order to get decoupled active and reactive power flow between the grid and GSC, vector control strategy is applied. The grid voltage of q axis is assumed to be zero and the grid voltage of d axis is the same as grid voltage [20].

$$\begin{cases} V_{qg} = 0 \\ V_{dg} = V_g \end{cases} \tag{3.51}$$

The active and reactive power is controlled independently by controlling the rotor currents of d and q axis respectively and given by:

$$\begin{cases} P_g = \frac{3}{2}(V_{dg} i_{dg}) \\ Q_g = -\frac{3}{2}(V_{dg} i_{qg}) \end{cases} \tag{3.52}$$

Equation (3.52) shows, P_g and Q_g are decoupled and regulated by grid currents. The set point for active power is created by the DC-link voltage regulator. The coupling term is considered from the voltage equation of the grid-side dynamic equation to obtain a better dynamic response. When the filter L is applied, the voltage equations of d and q-axis are given by [20]:

$$\begin{cases} V_{df} = R_f i_{dg} + L_f \frac{di_{dg}}{dt} + V_{dg} - \omega_s L_f i_{qg} \\ V_{qf} = R_f i_{qg} + L_f \frac{di_{qg}}{dt} + \omega_s L_f i_{dg} \end{cases} \tag{3.53}$$

The coupling term is given by:

$$\begin{cases} e_{df} = -\omega_s L_f i_{qg} \\ e_{qf} = \omega_s L_f i_{dg} \end{cases} \tag{3.54}$$

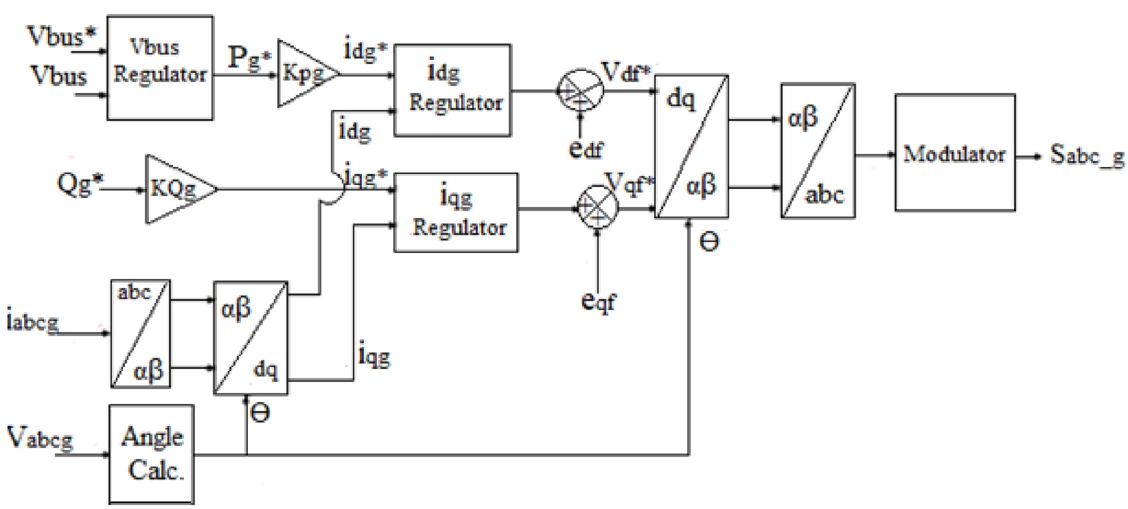

Figure 3. 11 Grid Voltage-oriented Vector Control Block Diagram

3.8.3 Phase Locked Loop (PLL)

For the transformation of voltage and current coordinates, angle of the grid voltage is required, which is estimated by the PLL. The simple PLL block estimates the grid voltage angle in a closed loop way. The closed loop PLL bock diagram is illustrated in Figure 3.12. The PI controller takes d component voltage from the d-q transformation block as error and modifies the estimated angular speed until this error equals to zero [4].

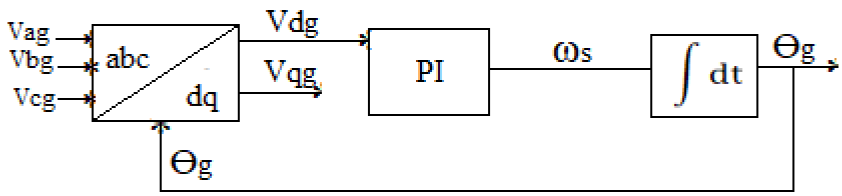

Figure 3. 12 PLL structure block diagram [4]

3.8.4 Tuning of Current Regulators

To tune the current loop regulator gains, transfer function is developed from the current loop by applying LaPlace transform to the above voltage equations.

$$\begin{cases} V_{df}(s) = R_f i_{dg}(s) + sL_f i_{dg}(s) \\ V_{qf}(s) = R_f i_{qg}(s) + sL_f i_{qg}(s) \end{cases} \tag{3.55}$$

The open loop transfer function for the current loop of grid side converter for L filter is given by:

$$\frac{i_{dg}(s)}{V_{df}(s)} = \frac{i_{qg}(s)}{V_{qf}(s)} = \frac{1}{L_f s + R_f} \tag{3.56}$$

The simplified structure for the current loop is shown in the Figure 3.13.

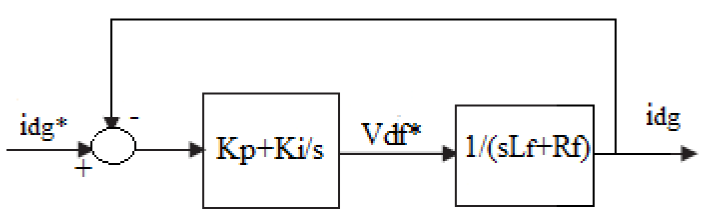

Figure 3.13 Current Loop structure for d component [20]

The closed loop transfer function is given by

$$\begin{cases} \dfrac{i_{dg}(s)}{V_{dg}(s)} = \dfrac{i_{qg}(s)}{V_{qg}(s)} = \dfrac{sk_p + k_i}{s^2(L_f) + s(R_f + k_p) + k_i} \\ \dfrac{i_{dg}(s)}{V_{dg}(s)} = \dfrac{i_{qg}(s)}{V_{qg}(s)} = \dfrac{\left(sk_p + k_i\right)/L_f}{s^2 + s(R_f + k_p)/L_f + k_i/L_f} \end{cases} \tag{3.57}$$

By equating with second order standard equation

$$s^2 + s(R_f + k_p)/L_f + k_i/L_f = s^2 + 2\xi\omega_n s + \omega_n{}^2 \tag{3.58}$$

Then, the required values of k_p and k_i are given by:

$$\begin{cases} k_i = L_f \omega_n{}^2 \\ k_p = 2L_f \xi\omega_n - R_f \end{cases} \tag{3.59}$$

When L filter circuit is replaced by LCL filter, the grid rotor voltage in d-q axis is given by:

$$\begin{cases} V_{df} = R_f i_{df} + L_f \dfrac{di_{df}}{dt} + R_g i_{dg} + L_g \dfrac{di_{dg}}{dt} + V_{dg} - \omega_s L_f i_{qf} - \omega_s L_g i_{qg} \\ V_{qf} = R_f i_{qf} + L_f \dfrac{di_{qf}}{dt} + R_g i_{qg} + L_g \dfrac{di_{qg}}{dt} + \omega_s L_f i_{df} + \omega_s L_g i_{dg} \end{cases} \tag{3.60}$$

The coupling terms are canceled by the regulator and the voltage equation becomes a function of grid current.

$$\begin{cases} V_{df} = R_f i_{dg} + L_f \dfrac{di_{dg}}{dt} + R_g i_{dg} + L_g \dfrac{di_{dg}}{dt} \\ V_{qf} = R_f i_{qg} + L_f \dfrac{di_{qg}}{dt} + R_g i_{qg} + L_g \dfrac{di_{qg}}{dt} \end{cases} \tag{3.61}$$

Then, by applying Laplace transform, the open loop transfer function for the current loop of grid side converter for LCL filter is given by:

$$\frac{i_{dg}(s)}{V_{df}(s)} = \frac{i_{qg}(s)}{V_{qf}(s)} = \frac{1}{(L_f + L_g)s + R_f + R_g} \tag{3.62}$$

The closed loop transfer function for current loop when LCL filter is used become:

$$\frac{i_d(s)}{i_d^*(s)} = \frac{i_q(s)}{i_q^*(s)} = \frac{sk_p + k_i}{s^2(L_f + L_g) + s(R_f + R_g + k_p) + k_i} \tag{3.63}$$

Finally, the required k_p and k_i values are obtained:

$$\begin{cases} k_i = (L_f + L_f)\omega_n^{\ 2} \\ k_p = 2(L_f + L_f)\xi\omega_n - (R_f + R_g) \end{cases} \tag{3.64}$$

3.8.5 DC – Link Model

It is the linkage between the RSC and GSC. DC-link model consists of a capacitor which is used to minimize power fluctuation. The main objective of Dc-link capacitor is to keep a constant voltage of GSC. The Figure 3.14 presents a shortened block of a DC-link circuit.

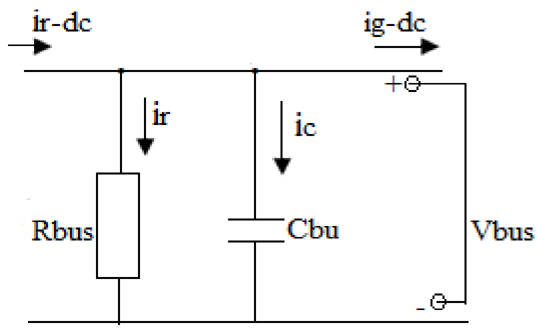

Figure 3. 14 DC- Link Power Converter [4]

The DC bus voltage can be calculated as [41]

$$V_{bus} = \frac{1}{C_{bus}} \int i_c dt \tag{3.65}$$

By applying the KCL to figure 3.14, the current through the capacitor can be found as

$$I = I_{r\_dc} - I_{g\_dc} - I_r \tag{3.66}$$

where; I_r is current through the resistance (A), I_{g_dc} is a DC current flow to the grid (A), I_{r_dc} is a DC current flow from the rotor (A).

The current through the resistance is:

$$I_r = \frac{V_{bus}}{R_{bus}} \tag{3.67}$$

3.9 Controller Design for RSC of DFIG

In DFIG controller is connected in order to regulate rotor speed, generated torque, active and reactive power exchange of the generator and the grid side inverter. In this thesis work, FLC is developed for the RSC of DFIG to control the rotor speed which provides a short transient time with zero overshoot, to increase efficiency of maximum power transfer capability. In this case maximum output power of the energy unit is ensured by reducing losses.

3.9.1 Fuzzy Logic controller Design

The PID controller is the standard control structure of classical control theory. However, due to non-linearity in the process plant, performance is greatly distorted and efficiency is reduced [46]. Fuzzy control is an intelligent control system based on analogous human fuzzy thinking, which uses fuzzy sets, fuzzy language variables, and knowledge of fuzzy logical inference to control complex systems. Fuzzy control has the advantages of good performance and robustness. This control strategy is applied for uncertain systems without computing mathematical model.

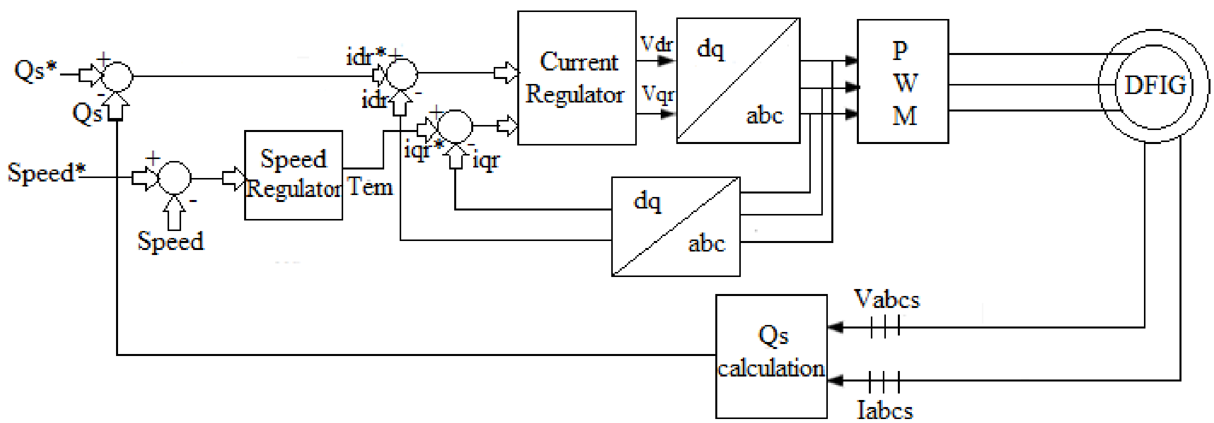

Figure 3.15 Proposed block diagram of Rotor side convertor control

Designing fuzzy logic controller includes fuzzification, inference rules and defuzzification. Fuzzification presents designing of membership functions and choosing the proper range. Inference rules consists of the rules that links the input to the output. The fuzzification process transforms the generated fuzzy functions in to crisp set. The general fuzzy logic block diagram is shown in Figure 3.16.

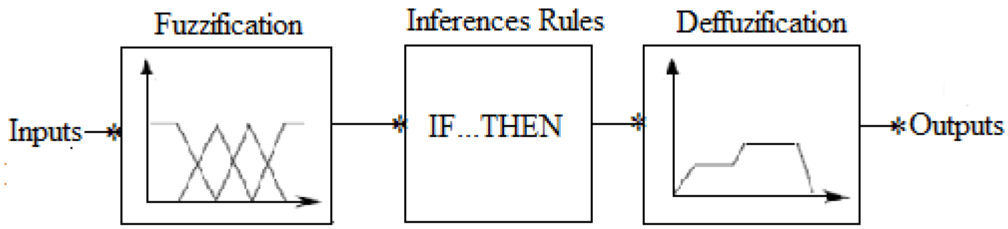

Figure 3.16 Structure of FLC [47]

The fuzzy logic controller (FLC) block is regulator for the outer loop called speed loop. The controller should provide a minimum difference of real rotor speed and the measured rotor speed of the DFIG. The Figure 3.17 shows the fuzzy logic controller block diagram for DFIG.

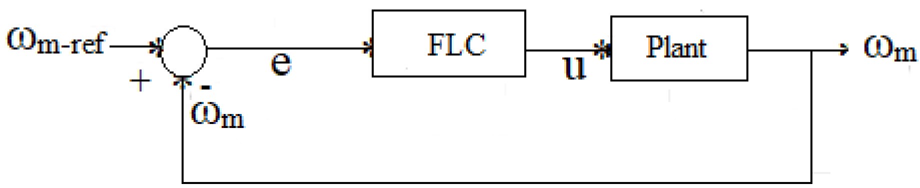

Figure 3.17 Speed Loop control block diagram

FLC is easily implemented in systems which doesn't need the mathematical model. In this thesis, the fuzzy logic controller chooses two inputs, namely rotor speed error and rotor speed variation error. The design consists of five triangular membership functions for Mamdani FIS type input and output. The membership function is expressed as, NB: negative big, NM: negative medium, Z: zero, PM: positive medium and PB: positive big. The appropriate rule set is established through trial and error. The appropriate rule set is constructed through trial and error. Table 3.1 illustrates the appropriate rules in which error e(t) is located in the row while change in error is in the column. The range of both inputs are chosen as [-80000 80000]. Table 3.1 describes fuzzy logic rule.

Table 3. 1 Fuzzy rules for speed control

$\frac{d}{dt}$	e(t)	NB	NM	Z	PM	PB
NB		NB	Z	NB	Z	Z
NM		Z	NM	NM	Z	Z
Z		NB	NM	Z	PM	PB
PM		Z	Z	PM	PM	PB
PB		Z	Z	PB	PB	PB

Figures 3.18 and 3.19 presents membership functions of both the input and output respectively for speed control using fuzzy logic control strategy. The output control signals are generated based on trial-and-error mechanism. The output range is chosen as [-8000 8000].

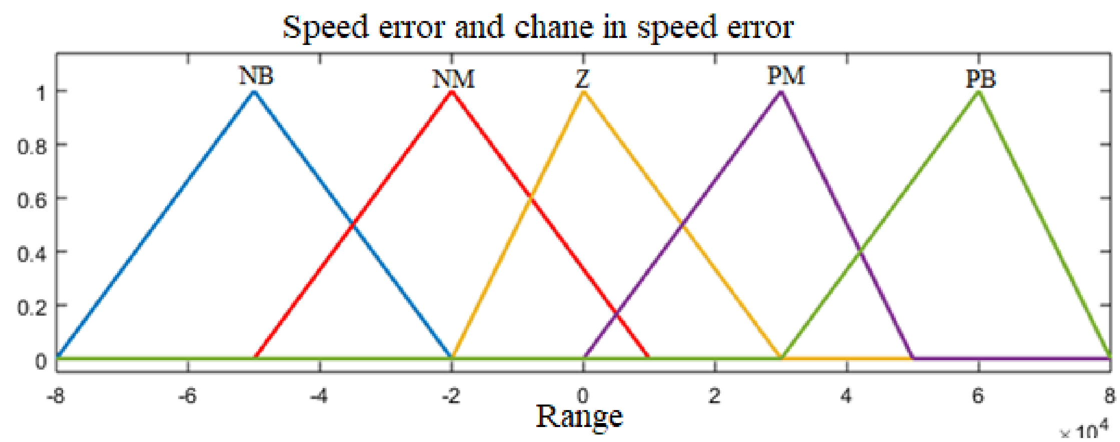

Figure 3.18 Input fuzzy membership function

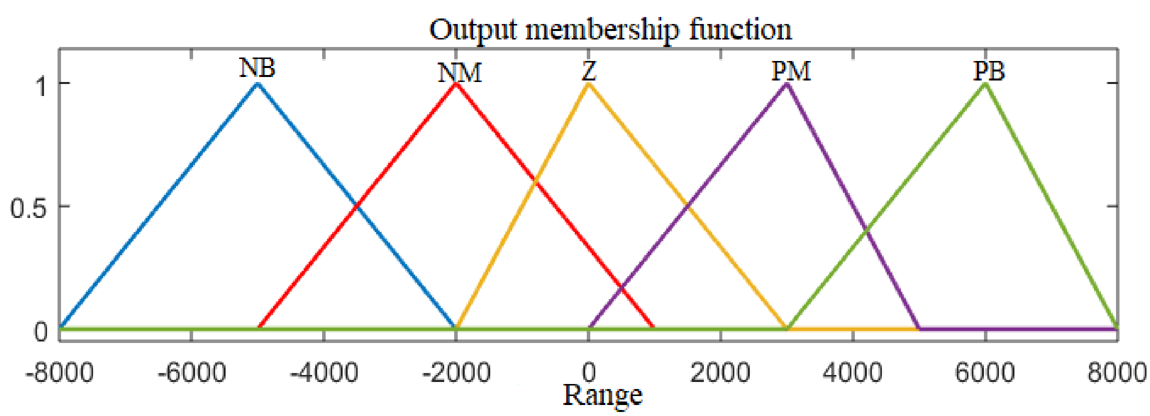

Figure 3.19 Output fuzzy membership function

3.10 Modelling of Grid Connected Filter and VSCs

In this section the grid connected filter and voltage source converters are analyzed. The voltage source converters are three-phase two-level and three-level diode clamped converters.

3.10.1 LCL Filter Analysis and Design

The PWM voltage output of grid-connected inverter comprises a large number of switching harmonic, due to this harmonic current is fed into the network. So, the objective of the filter, which is interfaced between the grid side converter and the grid, is to minimize the current and voltage harmonics generated by the switches of VSCs. An AC-DC-AC converter, which is connected to the rotor side of DFIG, is interfaced to the grid through an AC filter (L or LCL).

The first step is designing of the filter inductance. However, the use of inductive filters will lead to many disadvantages, such as reduced dynamic performance of the converter and a smaller operating range.

To better reduce the current ripple, an LCL filter can be selected because, its filtering capacity is significantly higher than that of the simple L filter [48]. Therefore, by selecting the LCL filter the resulting THD becomes less than 5% and IEEE 519-1992 standard is achieved [35]. To design the LCL filter, the converter's rated power, the grid and the switching frequencies are assumed. Then the base impedance, capacitance and inductance (Z_b, C_b and L_b respectively) are calculated. The objective of the input filter L_1 is to reduce the high harmonics at the converter side [19].

$$\begin{cases} Z_b = \dfrac{V_n^{\ 2}}{P_n} \\ L_b = \dfrac{Z_b}{\omega_n} \\ C_b = \dfrac{1}{\omega_n Z_b} \end{cases} \tag{3.68}$$

where: $\omega_n = 2\pi * f$, V_n is nominal line to line converter voltage.

$$Z_b = \frac{690^2}{2*10^6} = 0.2380\Omega ,\ L_b = \frac{0.2380}{2\pi f} = 0.75\text{mH} ,\ C_b = \frac{1}{2\pi f * 0.2380} = 13.3811\text{mF}$$

After calculating the base values of impedance, inductance and capacitance, the converter side inductance L_1 is calculated. From the manufacturer manual, the rating of the Grid side converter is given as 365 kVA. Assuming unity power factor for the gride side converter and neglecting the losses for the converters, then the Nominal RMS converter phase current (I_n) can be calculated as:

$$I_n = \frac{P_g}{\sqrt{3} V_n} = \frac{365\text{x}10^3}{\sqrt{3}\text{x}690} = 305\text{A} \tag{3.69}$$

Based on the IEEE 519-1992 limitations and the assumption that peak ripples must not exceed 10% of the grid current [49].

$$I_{\text{P-P rip}} = \sqrt{2} \text{ x } 0.1 I_n = 43.1335 \tag{3.70}$$

Assume that, the RMS converter voltage is equivalent with the grid rms voltage and becomes:

$$\begin{cases} L_1 = \dfrac{m\,V_{dc}}{8\sqrt{3}\,f_{SW}\,I_{p\text{-}p,rip}} \\ m = \dfrac{2\sqrt{2}\,V_{n\_rms}}{V_{dc}} \end{cases} \tag{3.71}$$

where, f_{SW} is a switching frequency

$$L_1 = \frac{2\sqrt{2}\,V_{n\_rms}}{8\sqrt{3}\,f_{SW}\,I_{p\text{-}p,rip}} \tag{3.72}$$

$$L_1 = \frac{2\sqrt{2}V \text{ x } 690/\sqrt{3}}{8\sqrt{3} \text{ x } 5000 \text{ x } 0.1 \text{ x} \sqrt{2} \text{ x } 305} = 0.21769\text{mH}$$

Now, the maximum ripple current $I_{max,rip}$ can be chosen in between 10% and 25% of the nominal phase current I_n and the limit of L_1 that has to be fulfilled is given by:

$$L_c \geq \frac{V_{dc}}{6\,f_{SW}\,I_{max\,,\,rip}} \geq \frac{V_g\sqrt{2}}{6\,f_{SW}\,I_{max\,,\,rip}} \tag{3.73}$$

Then, the maximum converter side ripple current can be calculated as:

$$I_{max,rip} = \sqrt{2} \text{ x } 0.2 \text{ x } 305 = 86.27\text{A}$$

$$L_c \geq \frac{690 \text{ x } \sqrt{2}}{6 \text{ x } 5000 \text{ x } 86.27} = 0.21769\text{mH}$$, which is the so called L_1

To finalize the design procedure, lets calculate the filter capacitance and grid side inductance L_2. For the design of the filter capacitance, it's considered that the filter capacitance should be less than 5% of the base capacitance C_b. The assumption for the reference capacitor is 4% of the base capacitor and the filter capacitor becomes [48]:

$$C_{ref} = 0.04C_b \tag{3.74}$$

$$C = C_{ref}C_b \Rightarrow \frac{C_{ref}}{\omega_n Z_b} = \frac{0.04}{100 \text{ x } 3.14 \text{ x } 0.2380} = 535.24\mu\text{F} \tag{3.75}$$

Finally, L_2 is developed on the grid side L_2. The main purpose of L_2 is to suppress the current harmonics injected into the network.

To attenuate the current ripples, L_1 is greater L_2 [19]. In this case, the division factor r_a is given by:

$$r_a = \frac{L_2}{L_1} \tag{3.76}$$

$$L_2 = r_a L_1 \tag{3.77}$$

$$r_a = \left| \frac{1 - H_A}{H_A (1 - L_1 C \omega^2_{sw})} \right| \tag{3.78}$$

$$\frac{L_2}{L_1} = \left| \frac{1 - H_A}{H_A (1 - L_1 C \omega^2_{sw})} \right| \tag{3.79}$$

Then, the grid side inductance is given by

$$\begin{cases} L_2 = L_1 \left| \dfrac{1 - H_A}{H_A (1 - L_1 C \omega^2_{sw})} \right| \\ \omega^2_{sw} = \left(2\pi f_{sw} \right)^2 \end{cases} \tag{3.80}$$

where: H_A is the harmonics attenuation of the phase current which chosen as 0.05 and f_{sw} is the switching frequency According to IEEE 519-1992 the THD factor is given by [50]:

$$THD_{IEEE} = \sqrt{\sum_{h=2}^{50} I^2(h)} * 100\% \tag{3.81}$$

$$L_2 = 0.2177 * \left| \frac{1 - 0.05}{0.05(1 - 0.000377 * 401 * 10^{-6} * \left[2\pi * 5000 \right]^2)} \right| = 0.0279 mH$$

3.10.2 Two-Level Three-Phase GSC Model

Figure 3.20 shows a two-level GSC with six IGBTs antiparallel freewheeling diodes, which inverts a DC power input into a controlled three phase AC power output based on the control signals applied on the gate circuits of IGBTs. The control signals are generated through different types of PWM technique. For the modelling purpose, GSC consists of an ideal switch and effects of the transformer or grid impedances are neglected [20].

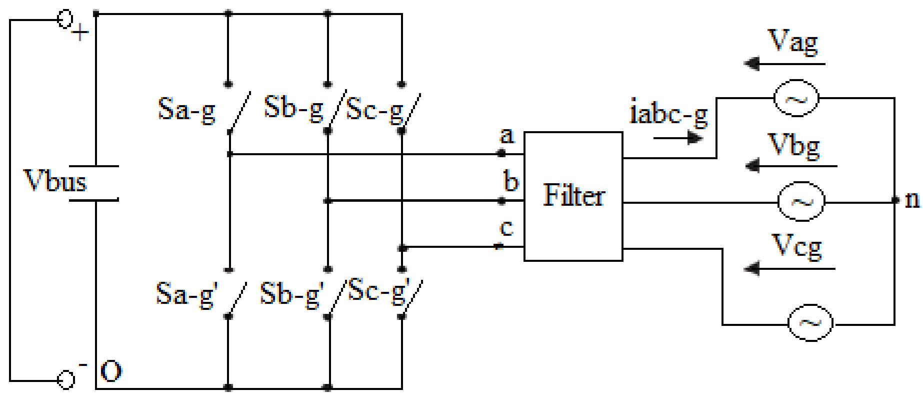

Figure 3.20 Grid connected three-phase two-level converter with filter [51]

The output voltages of the converter are synthesized by commanding the appropriate switching orders of the IGBTs: $S_{a\text{-}g}$, $S_{b\text{-}g}$, $S_{c\text{-}g}$. Both of the switches in the same leg can't be turned ON at the same time, as it would short the input voltage. Accordingly, the nature of the two switches in the same leg is complementary [20].

$$\begin{cases} S_{a\_g} + S'_{a\_g} = 1 \\ S_{b\_g} + S'_{b\_g} = 1 \\ S_{c\_g} + S'_{c\_g} = 1 \end{cases} \tag{3.82}$$

The output voltages referred to the neutral point of the DC bus is expressed as:

$$v_{j0} = V_{bus} S_{jg} \tag{3.83}$$

where: $S_{jg} \in \{0,1\}$ and $j = a, b, c$

According to Figure 3.21 voltage relationship is given by:

$$v_{jn} = v_{jo} - v_{no} \tag{3.84}$$

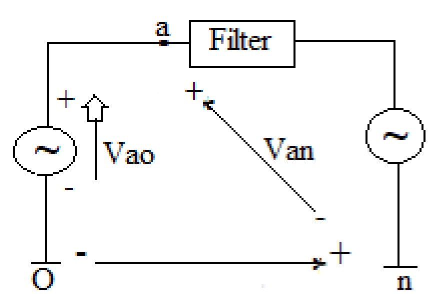

Figure 3.21 Equivalent grid circuit model [4]

Then, the output voltages of grid connected two-level inverter is given by [20]:

$$\begin{cases} v_{an} = \frac{v_{bus}}{3}\left(2S_{a\_g} - S_{b\_g} - S_{c\_g}\right) \\ v_{bn} = -\frac{v_{bus}}{3}\left(2S_{b\_g} - S_{a\_g} - S_{c\_g}\right) \\ v_{cn} = \frac{v_{bus}}{3}\left(2S_{c\_g} - S_{a\_g} - S_{b\_g}\right) \end{cases} \tag{3.85}$$

For two-level grid connected VSC, there are eight different combinations of output voltages. The output voltages are V_{ao}, V_{bo} and V_{co}. For two-level VSC, the output voltage takes only two voltage levels and which are V_{bus} and 0. The different Output Voltage Combinations are stated at Table 3.2.

Table 3. 2 Different Output Voltage Combinations of 2L-VSC [20]

S_{a_g}	S_{b_g}	S_{c_g}	v_{ao}	v_{bo}	v_{co}	v_{an}	v_{bn}	v_{cn}
0	0	0	0	0	0	0	0	0
0	0	1	0	0	V_{bus}	$-\frac{V_{bus}}{3}$	$-\frac{V_{bus}}{3}$	$\frac{V_{bus}}{3}$
0	1	0	0	V_{bus}	0	$-\frac{V_{bus}}{3}$	$2\frac{V_{bus}}{3}$	$-\frac{V_{bus}}{3}$
0	1	1	0	V_{bus}	V_{bus}	$-2\frac{V_{bus}}{3}$	$\frac{V_{bus}}{3}$	$\frac{V_{bus}}{3}$
1	0	0	V_{bus}	0	0	$2\frac{V_{bus}}{3}$	$-\frac{V_{bus}}{3}$	$-\frac{V_{bus}}{3}$
1	0	1	V_{bus}	0	V_{bus}	$\frac{V_{bus}}{3}$	$-2\frac{V_{bus}}{3}$	$\frac{V_{bus}}{3}$
1	1	0	V_{bus}	V_{bus}	0	$\frac{V_{bus}}{3}$	$\frac{V_{bus}}{3}$	$-2\frac{V_{bus}}{3}$
1	1	1	V_{bus}	V_{bus}	V_{bus}	0	0	0

3.10.3 Modelling of Grid Connected Three-Level NPC VSC

Three-level NPC inverter is diode clamped multilevel converter family which generates output phase voltage waveforms V_{ao}, V_{bo} and V_{co} with three switching levels of amplitude (0, $\frac{V_{bus}}{2}$ and V_{bus}). The voltages are created on the AC side by switching the controlled switches (S_{a1}, S_{a1}', S_{a2}, S_{a2}', S_{b1}, S_{b1}', S_{b2}, S_{b2}', S_{c1}, S_{c1}', S_{c2}, S_{c2}'), connecting the DC bus to the AC output. The DC bus is created by two DC sources providing a ground point z. The clamping diodes are associated from the neutral point to each arm (a, b, c) to achieve the medium voltage level $\frac{V_{bus}}{2}$ as shown in Figure 3.22. To perform a bidirectional flow of the current through the converter, each controlled switch is accompanied by one diode in antiparallel manner. Compared to the two-level grid connected inverters, this multilevel converter topology is suitable to achieve higher ranges of power and voltage. In this circuit, the DC-bus voltage is divided into three levels by two series-connected bulk capacitors, C_1 and C_2. The capacitors are identical and the middle point of the two capacitors, is defined as a neutral point.

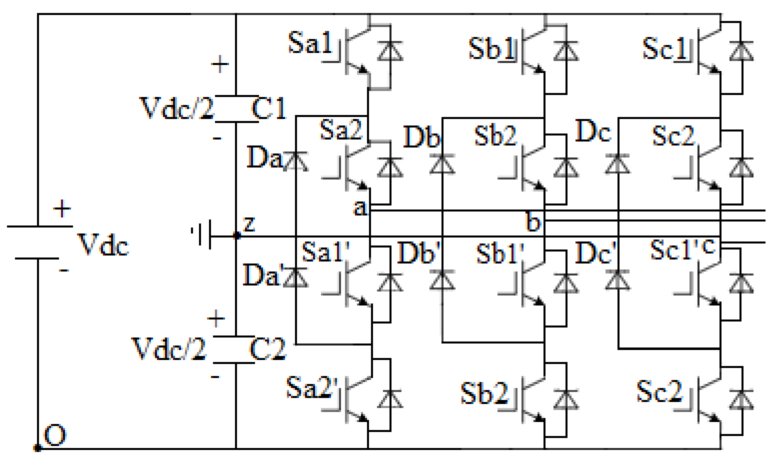

Figure 3.22 3L-NPC VSC Converter [20]

The switching states of the converter at each phase are restricted in such a way that each switch presents its complementary switch. In order to avoid non-permitted states, which results in improper operation, the following switching status is compulsory.

$$S_{ki} + S_{ki}' = 1 \tag{3.86}$$

where: k=a, b, c and i=1, 2

The output voltage of the three-level multilevel inverter is given by:

$$\begin{cases} V_{ao} = S_{a1}V_{C1} + S_{a2}V_{C2} \\ V_{bo} = S_{b1}V_{C1} + S_{b2}V_{C2} \\ V_{co} = S_{c1}V_{C1} + S_{c2}V_{C2} \end{cases} \quad (3.87)$$

From the expression of two-level converter

$$V_{an} = \frac{2}{3}V_{a0} - \frac{1}{3}(V_{b0} + V_{c0}) \quad (3.88)$$

Then, by substituting the output voltage equations of three-level multilevel inverter, the output AC voltage expressions are calculated depending on the order commands:

$$V_{an} = \frac{2}{3}(S_{a1}V_{C1} + S_{a2}V_{C2}) - \frac{1}{3}(S_{b1}V_{C1} + S_{b2}V_{C2} + S_{c1}V_{C1} + S_{c2}V_{C2}) \quad (3.89)$$

Then, by rearranging, the expressions for the output voltage becomes:

$$\begin{cases} V_{an} = \frac{V_{C1}}{3}(2S_{a1} - S_{b1} - S_{c1}) + \frac{V_{C2}}{3}(2S_{a2} - S_{b2} - S_{c2}) \\ V_{bn} = \frac{V_{C1}}{3}(2S_{b1} - S_{a1} - S_{c1}) + \frac{V_{C2}}{3}(2S_{b2} - S_{a2} - S_{c2}) \\ V_{cn} = \frac{V_{C1}}{3}(2S_{c1} - S_{b1} - S_{a1}) + \frac{V_{C2}}{3}(2S_{c2} - S_{b2} - S_{a2}) \end{cases} \quad (3.90)$$

The voltages of the capacitors in general are not necessarily exactly equal. The currents flowing through the DC bus capacitors can be calculated first by deducing the currents and becomes:

$$i_1 = S_{a1}i_a + S_{b1}i_b + S_{c1}i_c \quad (3.91)$$

By applying the KCL at node z and O of Figure 3.22 the currents are related as:

$$\begin{cases} i_1 = -i_{c1} \\ i_{c1} = i_{c2} + i_z \\ i_2 = i_{c2} = -(i_1 + i_Z) \end{cases} \quad (3.92)$$

The simplified currents at node z and O becomes:

$$\begin{cases} i_Z = (S_{a2} - S_{a1})i_a + (S_{b2} - S_{b1})i_b + (S_{c2} - S_{c1})i_c \\ i_2 = -(S_{a1}i_a + S_{b1}i_b + S_{c1}i_c) \end{cases} \quad (3.93)$$

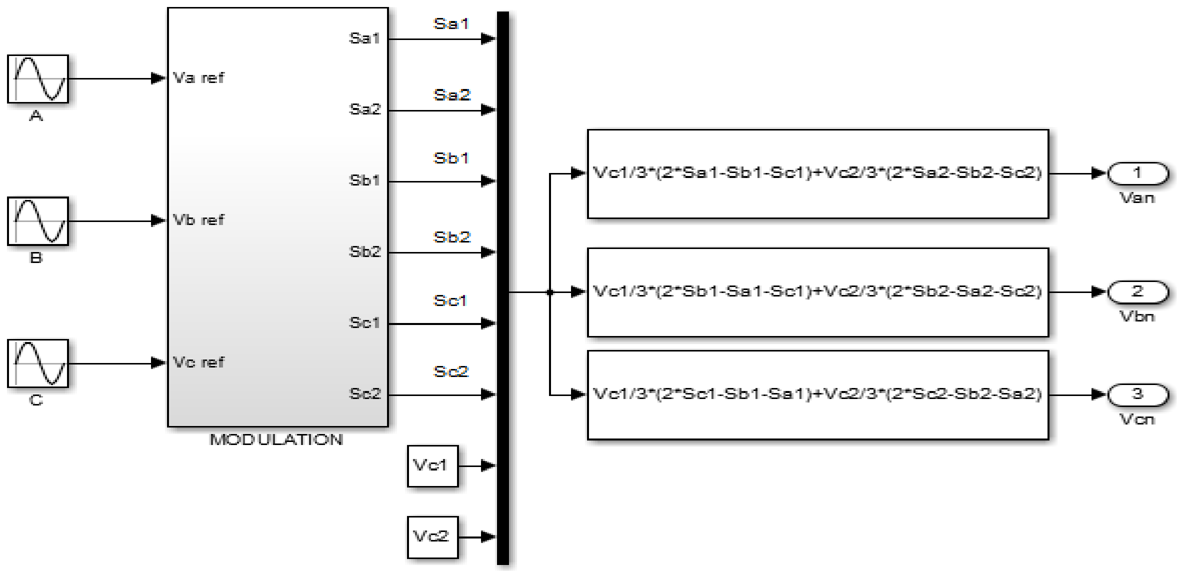

Figure 3.23 SIMULNK model of 3L-NPC VSC

3.11 Pulse Generation of the Controlled Switches

Pulse generators are applied for power electronic converters in order to generate rectangular pulses. The pulse generation techniques are:

- Sinusoidal pulse width modulation
- Sinusoidal pulse width modulation technique with third harmonics injection
- Space vector pulse width modulation technique

3.11.1 Sinusoidal Pulse Width Modulation (SPWM)

SPWM strategy is broadly expanded modulation technique among voltage sourced converters. From the set point values of DC bus voltage and the grid reactive power, this modulation techniques creates a-b-c voltage references V_{af}, V_{bf}, and V_{cf} references. Output voltage is created by using a triangular signal and comparing it with the reference signal to create pulses Sa−g, Sb−g, Sc−g and the resulting switching signals from each comparator are used to drive the inverter switches of the corresponding leg. In the case of sinusoidal pulse width modulation, the output voltage is created according to:

$$S_j = 1 \text{ if } V_j^* > V_{tri}, \quad j = a, b, c$$

where: V_j^* = reference signal, V_{tri} = triangular signal

Figure 3.24 presents the schematic block diagram of SPWM. Maximum output voltage without over-modulation (ma ≤1) is $Vbus/2$. In ideal conditions, the amplitude obtained between the fundamental voltage output and the DC bus voltage is given by the amplitude modulation index and is expressed as:

$$\langle v_{an} \rangle = m_a . \frac{Vbus}{2} \quad \text{if } m_a \leq 1 \tag{3.94}$$

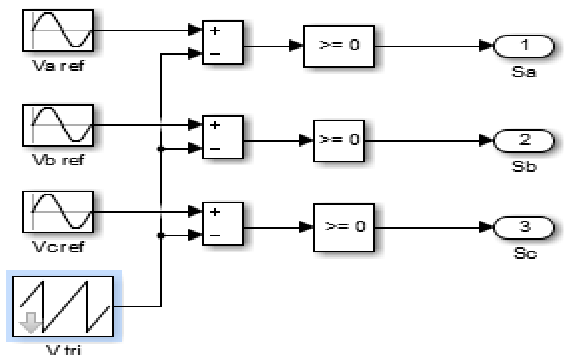

Figure 3.24 SIMULNK model of SPWM

3.11.2 Sinusoidal PWM With Third Harmonic Injection

Although sine pulse width modulation is simple to understand and design, full utilization of DC voltage is not achieved. Therefore, due to this weakness of SPWM and in order to increase the maximum achievable output voltage, SPWM involves the third harmonic. This technique improves the output voltage. Using sinusoidal PWM technology will not be too close to the maximum achievable output voltage. Therefore, only by adding the 3rd harmonic signal to each reference signal, a significant increase in the output voltage waveform can be obtained. At the output, the amplitude obtained from the harmonic wave (V_1) is equal to the amplitude of the reference fundamental wave. The reference signal occupies two maximum values at $\theta_1 = \pi/3$ and $\theta_1 = 2\pi/3$ equal to 1. The first and third harmonic equation is expressed as:

$$\begin{cases} V_1 = V_{1\,max} \sin\theta \\ V_3 = V_{3\,max} \sin(3\theta) \end{cases} \tag{3.95}$$

When $\theta_1 = \pi/3$, the output voltage becomes $\frac{V_{bus}}{2}$.

$$\begin{cases} \frac{V_{bus}}{2} = V_{1\max} \sin\left(\pi/3\right) \\ V_{1\max} = \frac{V_{bus}}{\sqrt{3}} \end{cases} \tag{3.96}$$

After third harmonic injection is added, the maximum achievable output voltage amplitude is 1.15 times greater than the SPWM. The output voltage waveform for each phase with third harmonic content is stated as:

$$\begin{cases} V_{1max} \sin(\omega t) + V_{3max} \sin(3\omega t) \\ V_{1max} \sin(\omega t - \frac{2\pi}{3}) + V_{3max} \sin(3\omega t) \\ V_{1max} \sin(\omega t + \frac{2\pi}{3}) + V_{3max} \sin(3\omega t) \end{cases} \tag{3.97}$$

3.11.3 Space Vector Pulse Width Modulation (SVPWM)

By using the space vector illustration principle, the SVPWM generates AC output voltage for the inverter. The SVPWM based voltage source converter utilizes DC-link voltage more and results in low harmonic distortion with high output voltage levels compared to the conventional sinusoidal PWM inverter. In this modulation technique, vectors are used as a reference point. As a result, it becomes better and takes an advantage. As discussed in the previous scenario the conventional VSC provides eight different output voltage combinations on the AC side (V0 to V7) that can be represented in a space vector diagram in Figure 3.25. The region in the plane covered by the voltage vector disposition is a hexagon divided into six different [29]. The three-phase output AC voltage reference $\vec{V}^*$ is also represented in the plane.

To implement the SVPWM technique, the voltage equation in the a-b-c axis is transformed in to the stationary D-Q reference frame. Figure 3.25 shows the hexagon of vector identification of each and every sector for SVPWM. The SVPWM has some advantages over SPWM in which it utilizes the DC source voltage more effectively and creates a higher voltage output.

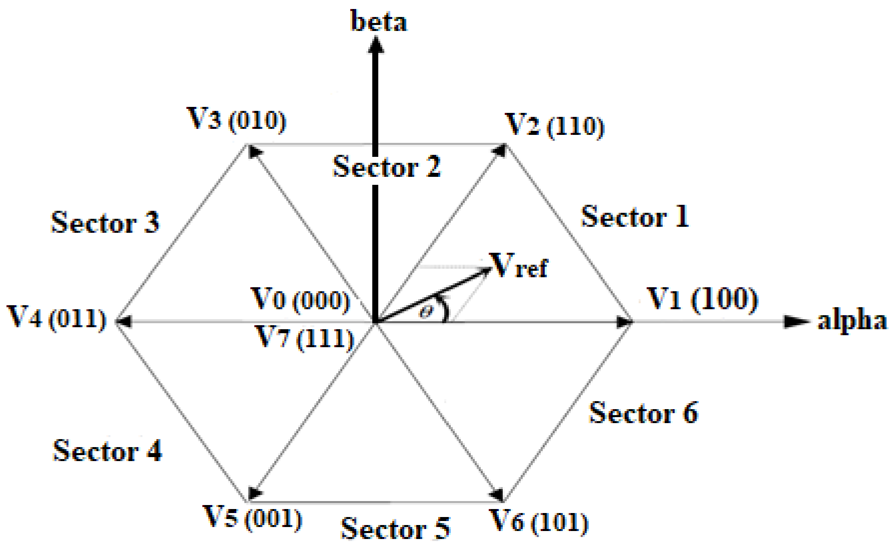

Figure 3.25 Space vector representation for SVM [29]

The maximum possible peak phase voltage that can be obtained using the space vector modulation strategy is given by the following formula:

$$V_{svpwm} = \frac{V_{dc}}{2}$$

To design the implementation of SVPWM techniques consider the following steps:

a. By applying Clarke transformaton techniques the three-phase system is transformed in to α-β frame.

$$\begin{bmatrix} V_\alpha \\ V_\beta \end{bmatrix} = \frac{2}{3}\begin{bmatrix} 1 & -\frac{1}{2} & -\frac{1}{2} \\ 0 & \frac{\sqrt{3}}{2} & -\frac{\sqrt{3}}{2} \end{bmatrix}\begin{bmatrix} V_{an} \\ V_{bn} \\ V_{cn} \end{bmatrix} \tag{3.98}$$

$$V_\alpha = \frac{2}{3}(V_a - \frac{1}{2}V_b - \frac{1}{2}V_c)$$

$$V_\beta = \frac{2}{3}(\frac{\sqrt{3}}{2}Vb - \frac{\sqrt{3}}{2}Vc)$$

When three-phase voltages are applied to an AC machine, a rotating magnetic flux is produced and this magnetic flow is represented as one of the rotary voltage vectors. After applying the Clark's transformation technique, the magnitude $|\bar{V}_{ref}|$ and angle α of this vector is given as follows:

$$\left|\bar{V}_{ref}\right| = \frac{2}{3}a\sqrt{V_\alpha^2 + V_\beta^2} \tag{3.99}$$

$$\alpha = \tan^{-1}\left(\frac{V_\beta}{V_\alpha}\right) = \omega t$$

$$= 2\pi f t$$

where:

f = fundamental frequency

b. Ones having the calculated values of Vα, Vβ and the magnitude of the reference vector $\bar{V}_{ref}$ then calculate the switching time duration for each sector V1−V6. For each sector $\bar{V}_{ref}$ can be found with two active and one zero vector. For sector 1(0 to $\pi/3$), the reference vector can be located with V0, V1 and V2. The time durations T_0 , T_1 and T_2 are the switching times and given by:

$$\int_0^{T_c} \bar{V}_{ref} = \int_0^{T_1} \bar{V}_1 dt + \int_{T_1}^{T_1+T_2} \bar{V}_2 dt + \int_{T_1+T_2}^{T_1+T_2+T_0} \bar{V}_0 dt \tag{3.100}$$

$$\bar{V}_{ref} T_c = \bar{V}_1 T_1 + \bar{V}_2 T_2 + \bar{V}_0 T_0 \tag{3.101}$$

where, T_c is the total cycle is given by:

$$T_C = T_1 + T_2 + T_0 \tag{3.102}$$

Then, dividing both sides of the above equation by T_c and expressed by the duty cycle as:

$$\bar{V}_{ref} = \bar{V}_1 D_1 + \bar{V}_2 D_2 + \bar{V}_0 D_0 \tag{3.103}$$

Then the average voltage for the sector 1 and the switching times can be given as:

$$T_c.\left|\bar{V}_{ref}\right|.\begin{bmatrix}\cos(\alpha)\\ \sin(\beta)\end{bmatrix} = T_1.\frac{2}{3}.V_{dc}.\begin{bmatrix}1\\ 0\end{bmatrix} + T_2.\frac{2}{3}.V_{dc}.\begin{bmatrix}\cos(\pi/3)\\ \sin(\pi/3)\end{bmatrix} \tag{3.104}$$

$$T_c.V_{ref}.\sin\alpha = 2/3.V_s.\sin(\pi/3).T_2 \tag{3.105}$$

The time duration T_1 and T_2 is given as follows:

$$\begin{cases} T_1 = T_c.a.\dfrac{\sin(\frac{\pi}{3}-\alpha)}{\sin(\frac{\pi}{3})} \\ T_1 = T_c.a.\dfrac{\sin(\alpha)}{\sin(\frac{\pi}{3})} \end{cases} \tag{3.106}$$

$$T_0 = T_c - (T_1 + T_2) \tag{3.107}$$

where: $T_c = \frac{1}{f_c}$ and $a = \frac{|\bar{V}_{ref}|}{\frac{2}{3}V_{dc}}$, which is a modulation index.

When generalizing the equation, T_1 and T_2 is given by:

$$T_1 = \begin{cases} \dfrac{\sqrt{3}.T_c.|\bar{V}_{ref}|}{V_{dc}}\left(\sin\left(\dfrac{\pi}{3} - \alpha + \dfrac{n-1}{3}\pi\right)\right) \\ \dfrac{\sqrt{3}.T_c.|\bar{V}_{ref}|}{V_{dc}}\sin\left(\dfrac{n\pi}{3} - \alpha\right) \\ \dfrac{\sqrt{3}.T_c.|\bar{V}_{ref}|}{V_{dc}}\left(\sin\dfrac{n}{3}\pi\cos\alpha + \cos\dfrac{n}{3}\pi\sin\alpha\right) \end{cases} \tag{3.108}$$

$$T_2 = \begin{cases} \dfrac{\sqrt{3}.T_c.|\bar{V}_{ref}|}{V_{dc}}\left(\sin\left(\alpha - \dfrac{n-1}{3}\pi\right)\right) \\ \dfrac{\sqrt{3}.T_c.|\bar{V}_{ref}|}{V_{dc}}\left(-\cos\alpha\sin\dfrac{n-1}{3}\pi + \sin\alpha\cos\dfrac{n-1}{3}\pi\right) \end{cases} \tag{3.109}$$

$$T_0 = T_c - (T_1 + T_2) \tag{3.110}$$

where, n = 1 through 6 and $0 \le \alpha \le 60°$

3.11.4 SVPWM for Grid Connected Three-Level VSC

Three-level NPC inverter contains twelves switching devices and supplied with two capacitors connected in series in which both capacitors are charged with DC bus voltage. The middle point of the two capacitors is the DC-voltage neutral point.

Each leg of the converter consists of four series connected IGBTs and two clamping diodes. The diodes are applied to clamp the six middle switches potential to the DC-link point at Z. the combinations of the twelve switches gives the three-level output voltage [19]. Figure 3.26 shows three-level NPC inverter with 12 switching devices. Specific combinations of the twelve switches gives the three-level output voltage.

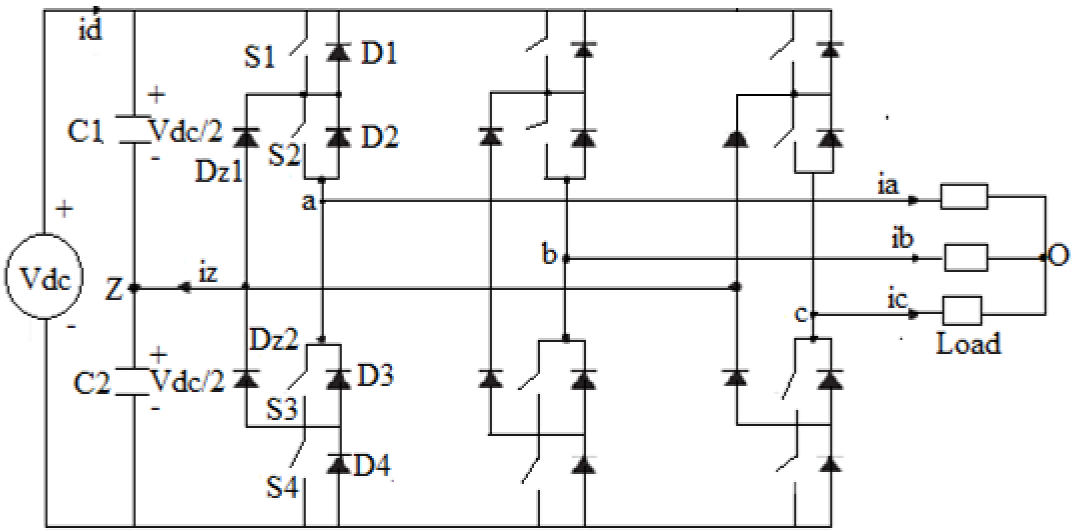

Figure 3.26 Three-level, three-phase neutral point clamped inverter topology [19]

The four switches in one phase leg can only be turned on two at a time and so be connected to the DC-link point's p, o, and n. These are represented with the switching states P, O and N. This means that three voltage levels can be created using O as the reference.

<u>Switching state</u>

The operating state of the switch in the NPC inverter can be expressed by the switch state, as shown in Table 3.3. The switch state "P" means that the upper two switches in branch A are turned on, and the inverter terminal voltage VAZ**,** that is the voltage at terminal Z relative to the neutral point Z, is +Vdc/2, whereas "N" means the lower two switches are conducting, resulting in to VAZ=−Vdc/2.

Table 3. 3 Switching states [52]

Switching states	Device Switching Status				Inverter terminal Voltage (VAZ)
	S1	S2	S3	S4	
P	ON	ON	OFF	OFF	+Vdc/2
O	OFF	ON	ON	OFF	0
N	OFF	OFF	ON	ON	-Vdc/2

The state of switch 0 means that the two internal switches S2 and S3 are on and the inverter terminal voltage is set to zero by the clamp diode. Depending on the direction of the load current Ia, one of the two clamping diodes conducts. For example, positive charge current (Ia> 0) forces DZ1 to turn on and terminal a is connected to neutral point Z through conduction of DZ1 and S2. As can be seen from the Table 3.3, switches S1 and S3 work in a complementary manner. One is open, the other must be closed. Similarly, S2 and S4 are also complementary pairs. These states represent connections to different DC-link points. The output phase voltage of the inverter generated, that is, the regulated voltage per line, is given by the following formula [52]:

$$\begin{cases} V_{AZ} = (2S_1 - S_1 - S_1) + (2S_2 - S_2 - S_2) \\ V_{BZ} = (2S_1 - S_1 - S_1) + (2S_2 - S_2 - S_2) \\ V_{CZ} = (2S_1 - S_1 - S_1) + (2S_2 - S_2 - S_2) \end{cases} \quad (3.111)$$

The line-to-line voltages are given by:

$$\begin{cases} V_{AB} = V_{AZ} - V_{BZ} \\ V_{BC} = V_{BZ} - V_{CZ} \\ V_{CA} = V_{CZ} - V_{AZ} \end{cases} \quad (3.112)$$

In the case of NPC inverter, three level output voltage is created. These are 2E, E, 0, −E and−2E.

CHAPTER FOUR

RESULTS AND DISCUSSIONS

4.1 Simulation of RSC using MATLAB/Simulink

The simulation of overall system is performed by using MATLAB/Simulink. The parameters of the generator used in this thesis work is shown in appendix part. As stated in the previous section, the DFIG operates in three operation modes. The simulated rotor speed of generator is illustrated in Figure 4.1. The running rotor speed is compared with the reference speed to operate the generator at synchronous, sub-synchronous and supper-synchronous conditions. As stated in Figure 4.1, from the initial to 3.63 seconds the generator is running at 90% of the rated speed and the measured speed tracks the reference signal with small overshoot. The set point is 142.8 rad/sec which is 90% of rated speed (1500rpm). In this case the generator is operating at speed less than the rated speed and hence in sub synchronous operation mode. At 3.63 second the rotor speed changes and the generator operates as a synchronous motor. The reference signal is 157rad/sec, which is the rated speed. From 3. 63 to 5 seconds, the measured signal is tracking set point smoothly at speed of 157 rad/sec. Since the rated speed and reference signal becomes the same, hence the generator is operating in synchronous mode of operation.

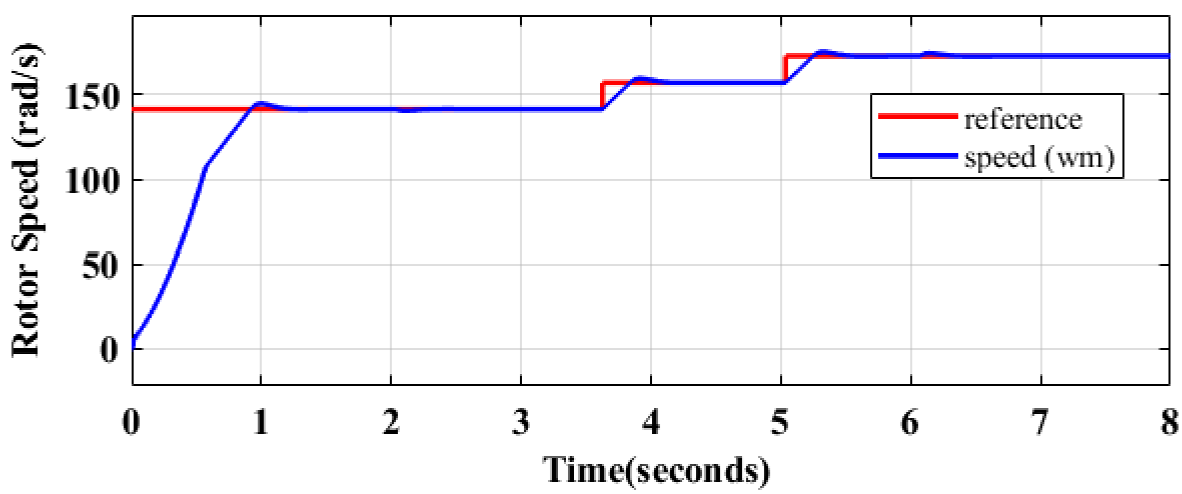

Figure 4.1 Simulated result of generator rotor speed

Finally, from 5 to 8 seconds the measured signal which is operating speed, is higher than the rated speed of the generator. The set point in this region is 172.7 rad/sec and the measured signal is smoothly tracking the reference signal and the generator is running at super-synchronous operation mode as shown in Figure 4.1.

Figure 4.2 illustrates generated electromechanical torque of the generator. If 1500 rpm is rated rotor speed of the generator, the reference signal is at 90% of the rated speed to present the generator operating mode at subsynchronous operation mode from the startup to 2 sec. In this case the torque reference is set as zero. After 2 sec, the generator is operating at 25% of the rated elechtromechanical torque until the generator operates at negative torque. At 2 sec the changed torque produces a pertubation for the rotor speed. After 6 sec, the torque becomes negative and the generator is working as a motor hence in super synchonous mode. So the variaon in rotor speed results in torque variation and hence the electromechanical torque is modified.

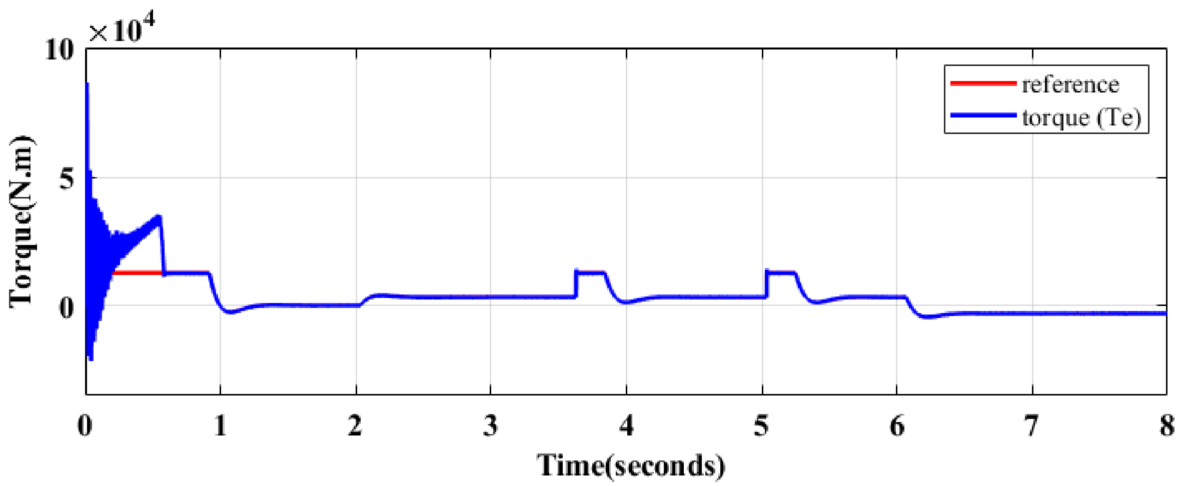

Figure 4.2 The electromechanical torque

The rotor current of the d component is maintained at 0 A in order to make the simulation easier and to control the current in q axis. Figure 4.3 presents the simulated rotor current in d axis and the measured signal is tracking the reference signal more or less perfectly.

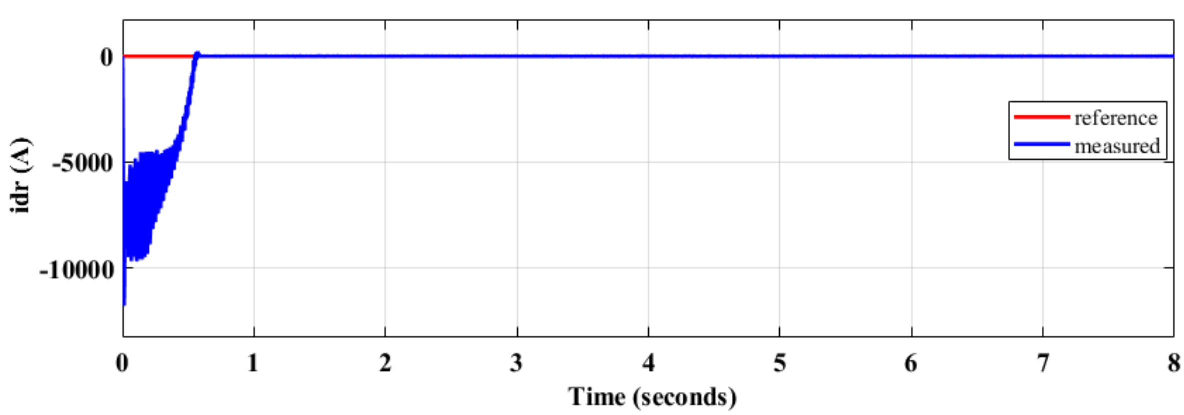

Figure 4.3 d axis rotor current

Figure 4.4 shows the simulated reference voltages in d-q axis. The voltage reference according to d axis rotor current is termed as d axis voltage and since id maintains in zero, hence the voltage reference called Vdr is more or less zero. The voltage reference according to q axis rotor current is Vq and results in variation due to the variation of i_q. The rotor speed variation results in the electromechanical torque modification and hence the rotor current in the q axis becomes modified. Therefore, the voltage reference of q axis shows modification accordingly with the rotor current of q component. As shown in Figure 4.4, the rotor voltage reference is tracking the setpoint signal very well.

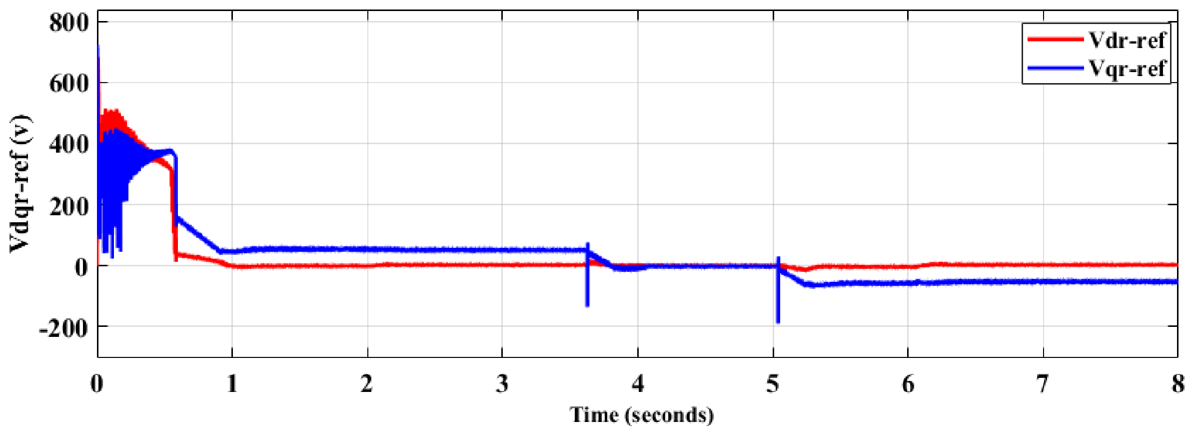

Figure 4.4 d-q axis reference voltages

From the principle of vector control, the rotor currents in d-q axis are decoupled and controlled independently. Therefore, the rotor current in q axis is directly related to T_{em} and d axis rotor current controls P_s.

Figure 4.5 shows the simulated result of rotor current in quadrature axis. The rotor current of q axis is modified accordingly to the torque.

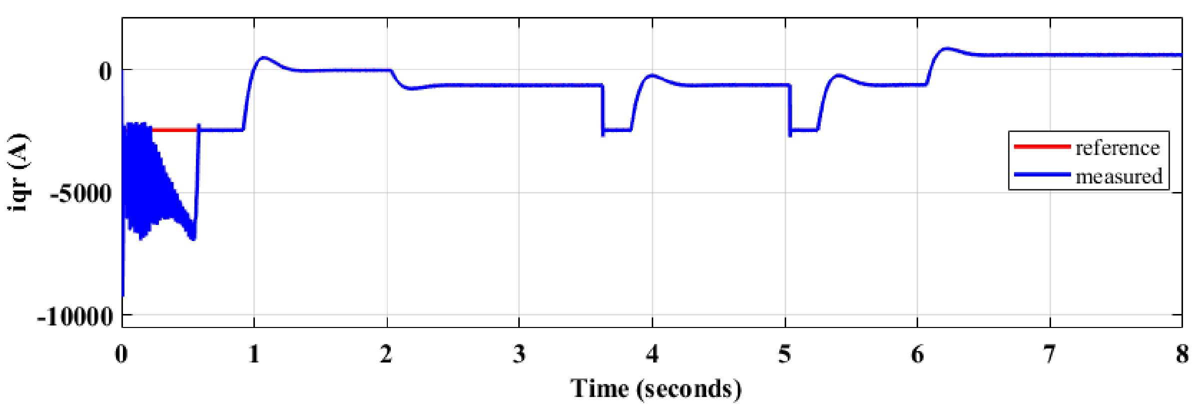

Figure 4.5 The simulated rotor current in quadrature axis

The Figures 4.6 and 4.7 illustrates the three phase stator currents and voltages respectively. The stator currents and voltages are purely sinusoidal with a frequency of 50 HZ.

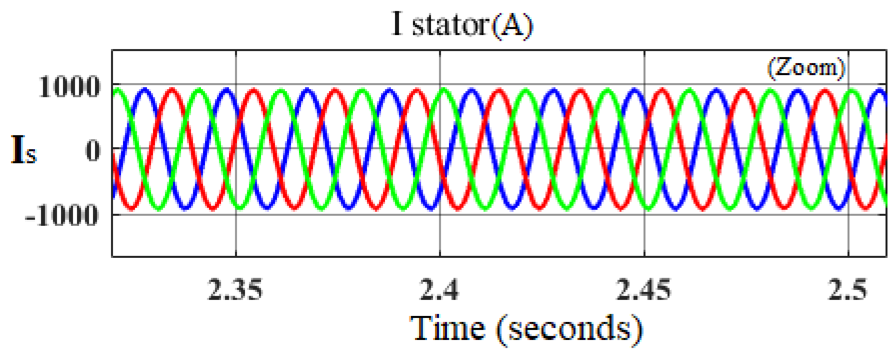

Figure 4.6 Stator Current

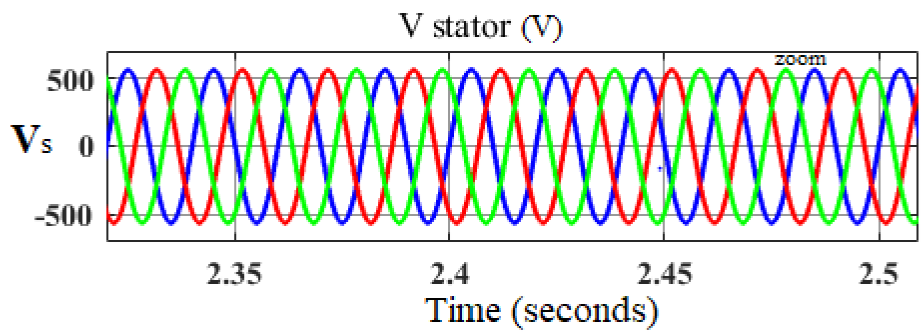

Figure 4.7 Stator voltage

Figure 4.8 illustrates the three-phase rotor currents. Since the rotor part of DFIG is connected with power electronic converters, the rotor current signal is not smoothly sinusoidal. So, the rotor current output is influenced. After 5 seconds, the sequence of rotor current is changed to a-c-b from a-b-c.

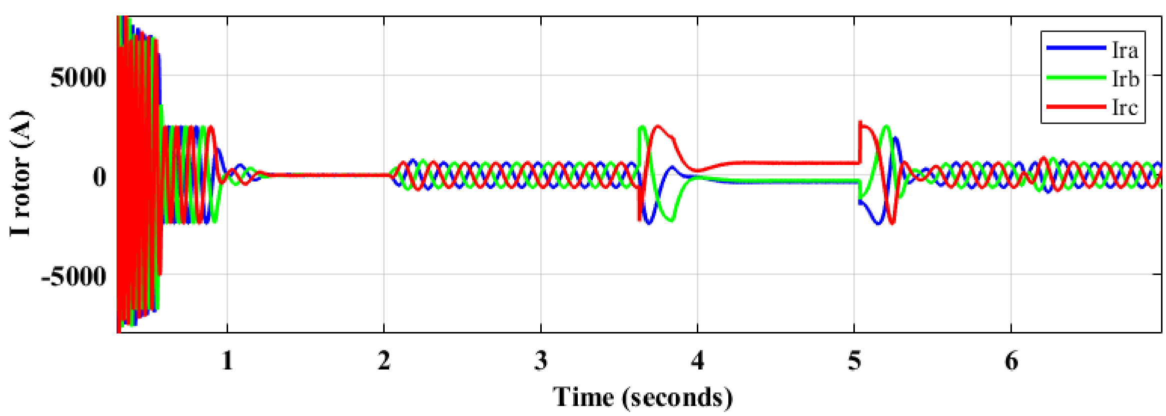

Figure 4.8 Rotor Current

Figure 4.9 illustrates the direct proportionality of speed of wind, speed of rotor and the generated output power. The generated output power becomes maximum at rated wind speed. Gradually, a 2MW output real power is generated after 5 second delay.

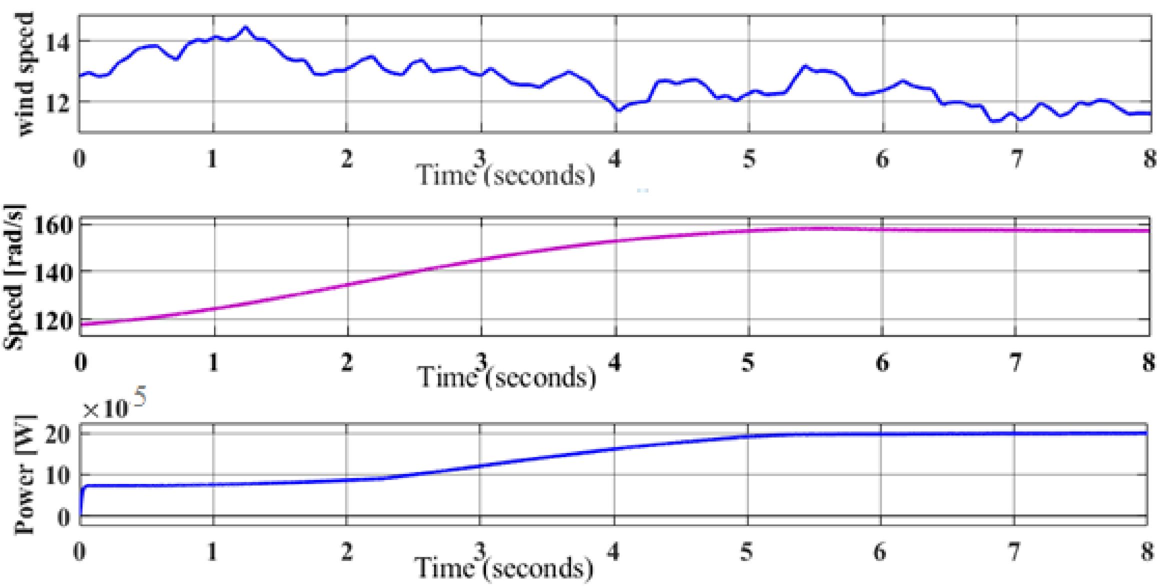

Figure 4.9 Wind speed, rotor speed and generated output power

Table 4. 1 Steady state analysis for rotor speed controller with PI controller

	Rotor speed of DFIG
Peak Overshoot	5 rad/sec
Settling time	1 sec

Table 4.1 illustrates the peak point and settling time for the rotor speed controlled by using PI from Figure 4.1.

4.2 Simulation of the RSC of DFIG for Different Wind Speed

Figure 4.10 illustrates the wind speed profile versus time. The initial wind speed is 12m/sec and at this speed the generator is at the rated condition. Then, the wind speed is reduced to 9m/s at 30sec and also declined to 6m/s at 60sec time.

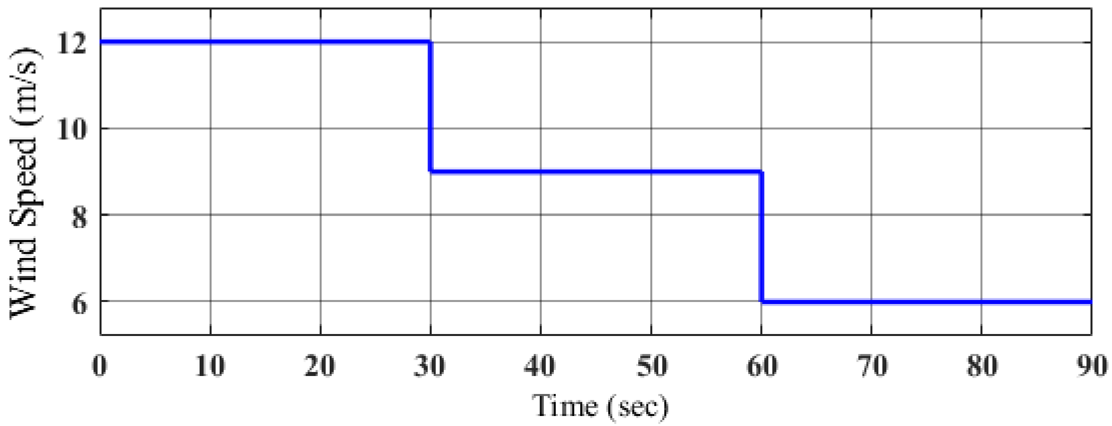

Figure 4.10 Wind Speed Versus Time

The Figure 4.11 presents simulated result of rotational speed of DFIG in reference to wind speed. The rotational speed of DFIG changes correspondingly as the wind speed changes. The rotational speed of the generator is directly related with the wind speed change and tracks the reference signal. When speed of wind decreases suddenly from 12 to 6m/s the rotor speed decrease gradually and then settles as per the control strategy made in the rotor side converter.

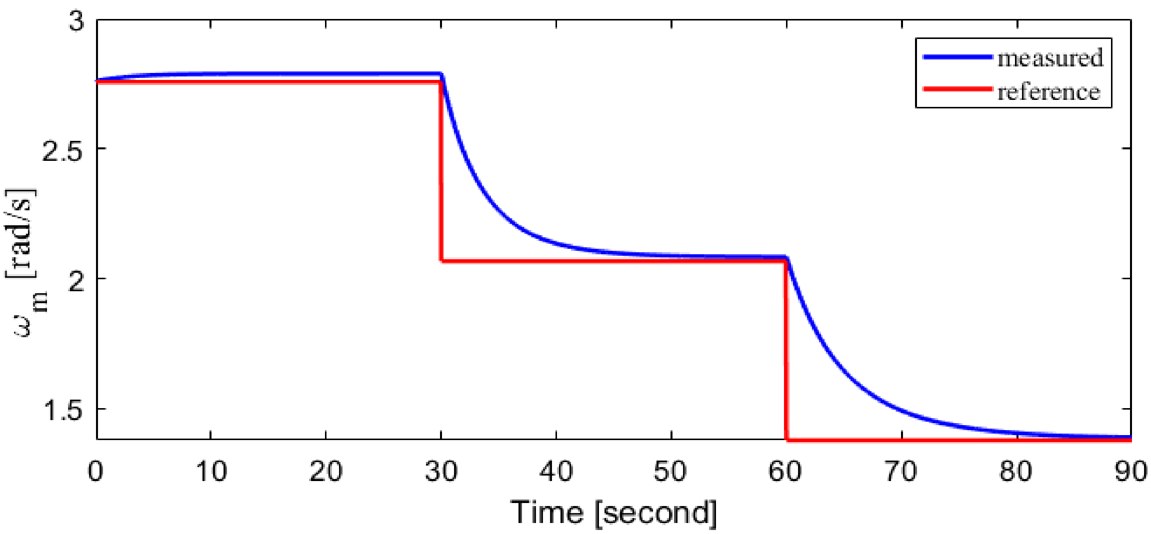

Figure 4.11 Rotational Speed of DFIG

As analyzed from the Figure 4.11, the controller regulates the rotational speed of the generator with respect to its optimal point as the wind speed changes. As stated in the literature review portion, the DFIG can operate under variable speed range so that the generator rotational speed is regulated even the wind speed is varying.

The Figure 4.12 presents the simulated electromechanical torque with respect to wind speed and the variation in wind speed results in variation in electromechanical torque. The measured signal is smoothly tracking the reference signal, so that the electromechanical torque of DFIG is regulated, and hence the active power is regulated. When speed of wind decreases the torque also declines, and indicates that, the change in wind speed will result in the electromechanical torque variation.

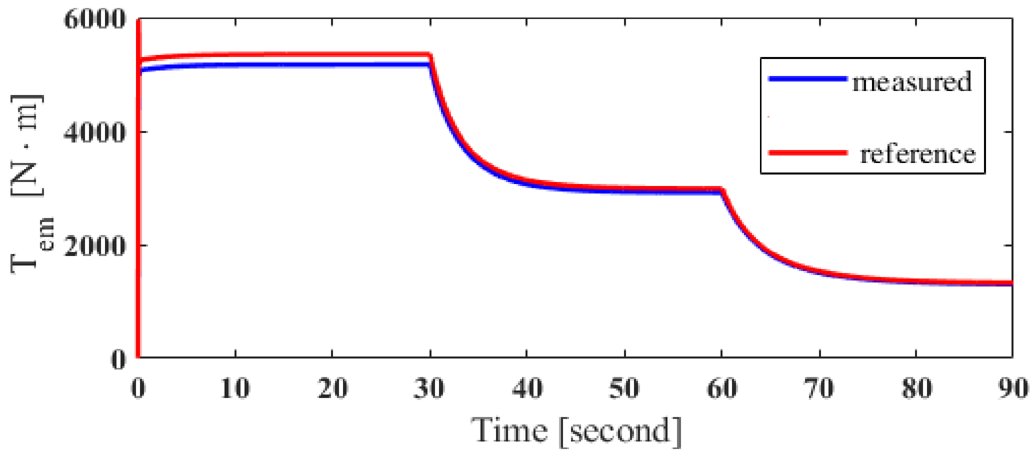

Figure 4.12 Electromechanical Torque

Figure 4.13 illustrates the output active power with respect to wind speed. The change in wind speed results in generator rotational speed to vary and, hence the generated torque and output active power changes accordingly with the wind speed.

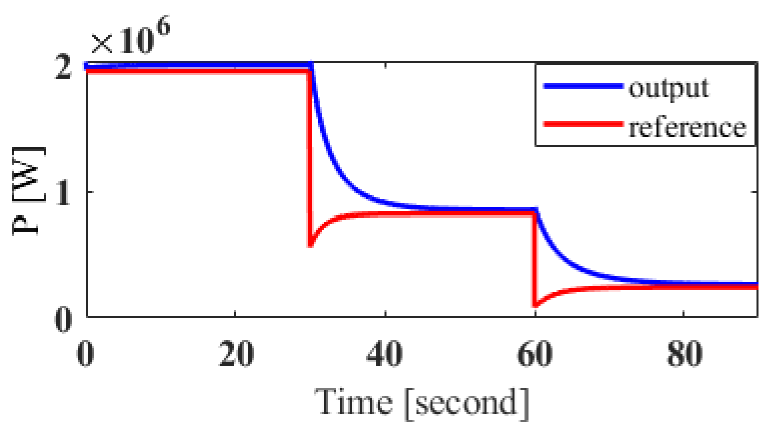

Figure 4.13 Active power

4.3 Simulation of Grid side Converter

Grid side converter control comprises the DC-link volatge at the outer loop and the rotor currents at the inner loop.

When controller block is aplied to GSC, voltage of DC-link capacitor becomes regulated and Q_g is maintained at a unity powerfactor. Figure 4.14 presents that, the DC-link voltage is fully constant at 1200v after the transien state is completed. From 0 to 1 sec, the simulated voltage shows some sinusoidal feature with overshoot and after 1 sec the system tracks the reference signal very well.

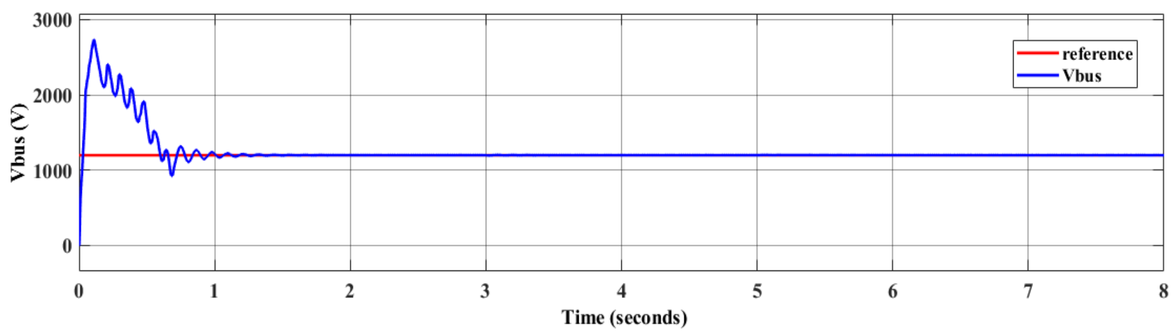

Figure 4.14 DC bus Voltage

Figure 4.15 illustrates the simulated grid side d axis grid current. The output is tracking the reference signal smoothly.

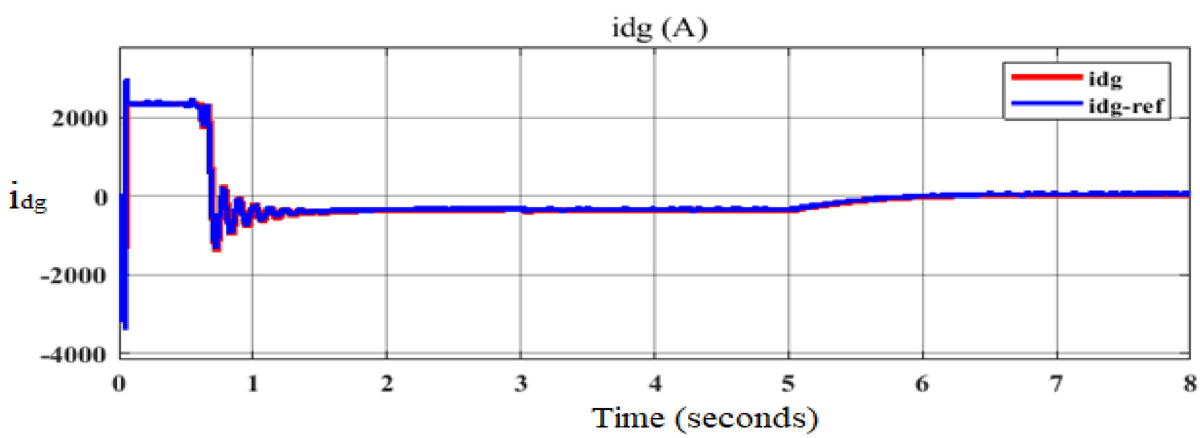

Figure 4.15 d axis grid current

The simulated q axis grid current is shown in Figure 4.16, which shows the objective of GSC is achieved since the grid current of q component is zero. This indicates the reactive power exchange is maintained at zero. Therefore, the grid has a unity power factor.

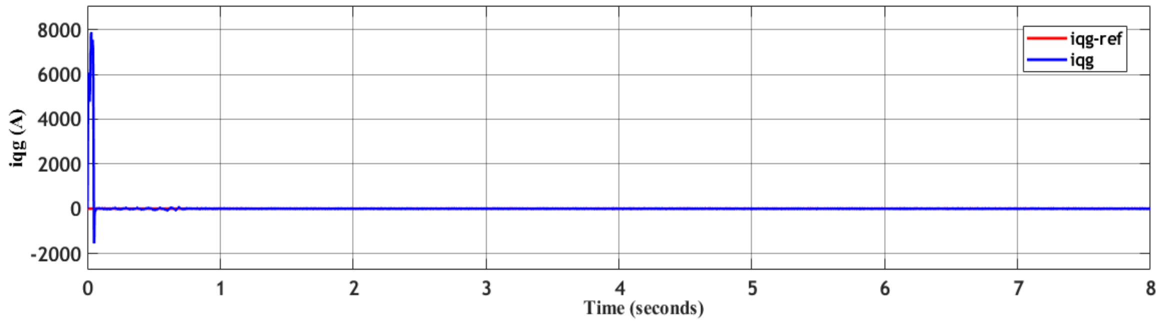

Figure 4.16 q axis grid current

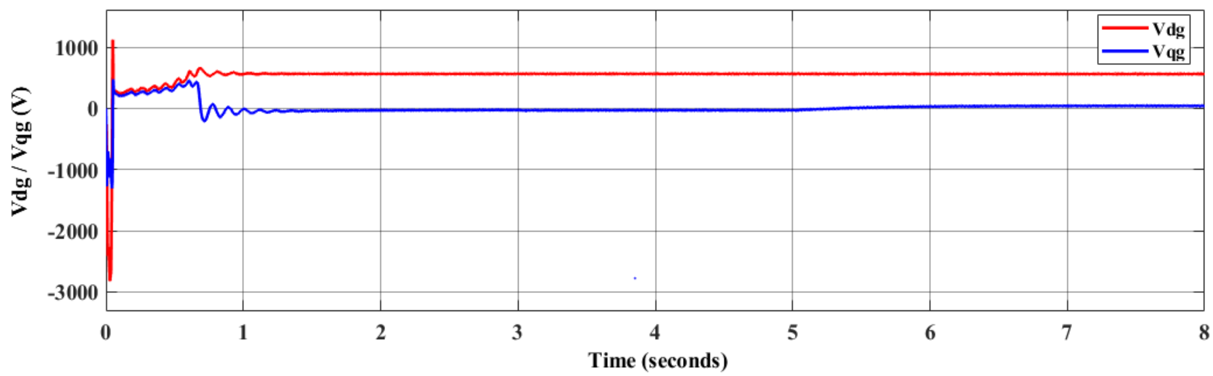

Figure 4.17 Grid voltage references

Since q axis grid current is maintained at zero, the resulting reference voltage V_{qg} settles at zero and V_{qg} changes accordingly with the direct axis grid current. Figure 4.17 represents grid reference voltages.

4.4 Speed Control Using Fuzzy Logic Controller

The Figure 4.18 below shows the simulated result of speed for the DFIG when fuzzy logic controller is applied to the outer loop or speed loop. In this case the simulated output is tracking the setpoint signal more smoothly and the settling time is reduced and the maximum overshoot is almost zero when compared with the conventional controller PI.

Table 4. 2 Steady state analysis for rotor speed controller with FLC controller

	Rotor speed of DFIG
Peak Overshoot	0
Settling time	0.6

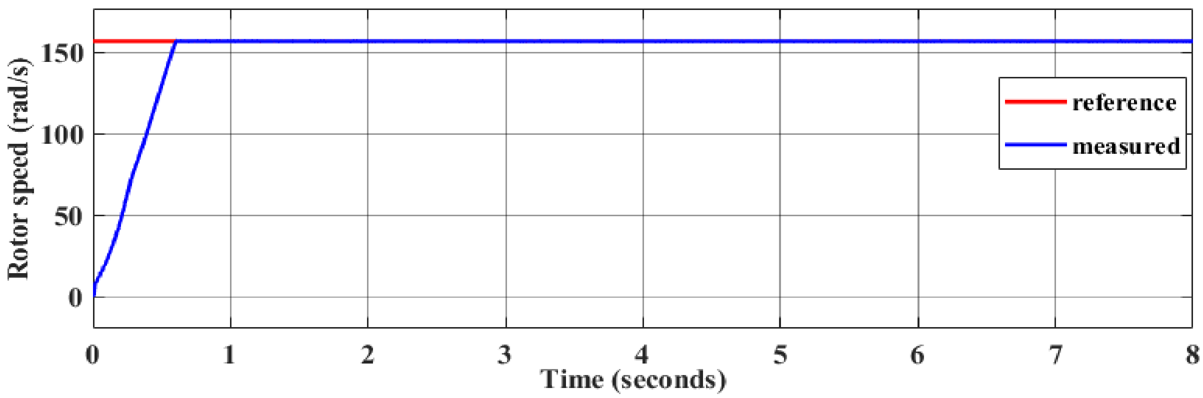

Figure 4.18 Rotor speed by using Fuzzy Logic Controller

The fuzzy logic-based rotor speed control is faster and more efficient than both indirect speed control and conventional PI speed control mechanism. The performance analysis of rotor speed using FLC is illustrated in Table 4.2.

4.5 Simulation of Two-Level Grid Connected Inverter using MATLAB

In this section a two-level grid connected voltage source converter is simulated by using pulse generation techniques such as SPWM, THIPWM, SVM.

4.5.1 Simulation of Two-Level VSC Based-SPWM Technique

Generating a PWM signal is very much familiar in the case of inverter topology and it is most efficient method of controlling the output voltage. In the case of PWM pulse signals are generated by using the triangular (as a carrier) signal and sinusoidal (as a reference) signal. The Figure 4.19 presents the generated PWM signal by using Matlab Simulink.

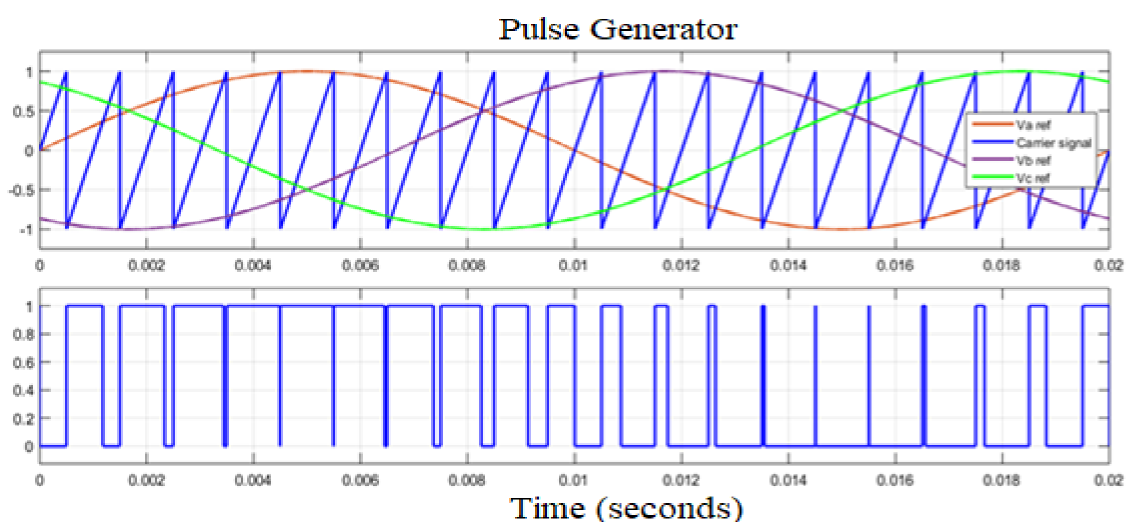

Figure 4.19 SPWM Generator

In this case three-phase voltage references are compared with a carrier signal and a rectangular pulse is generated. Figure 4.20 and 4.21 presents the output line to line and phase voltage profiles respectively. SPWM technique is applied to the grid connected three-phase two-level inverter and the gate pulse for each inverter leg is generated by comparing the sinusoidal signal with the carrier signal. The output phase and line voltages are generated based on the switching instant signal in the legs of the converter.

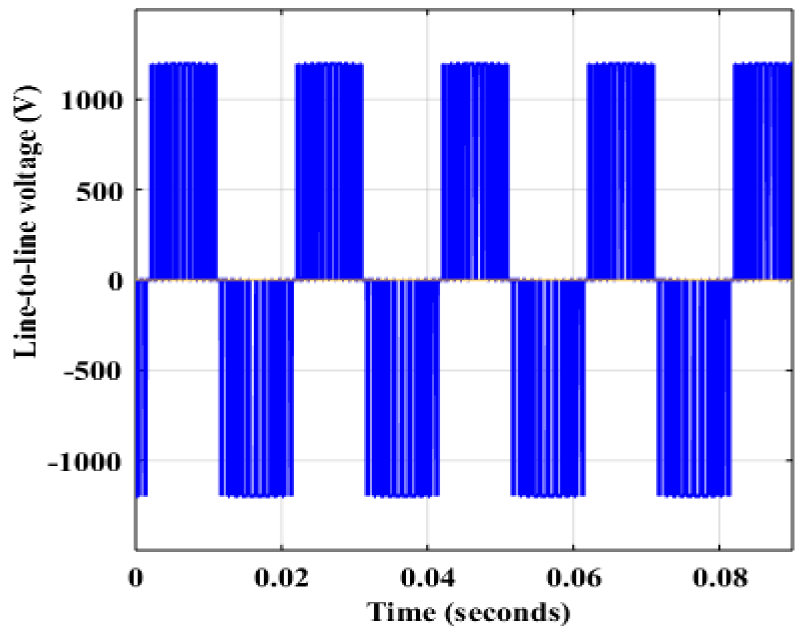

Figure 4.20 Line-to-Line Voltage profile of two-level converter with SPWM

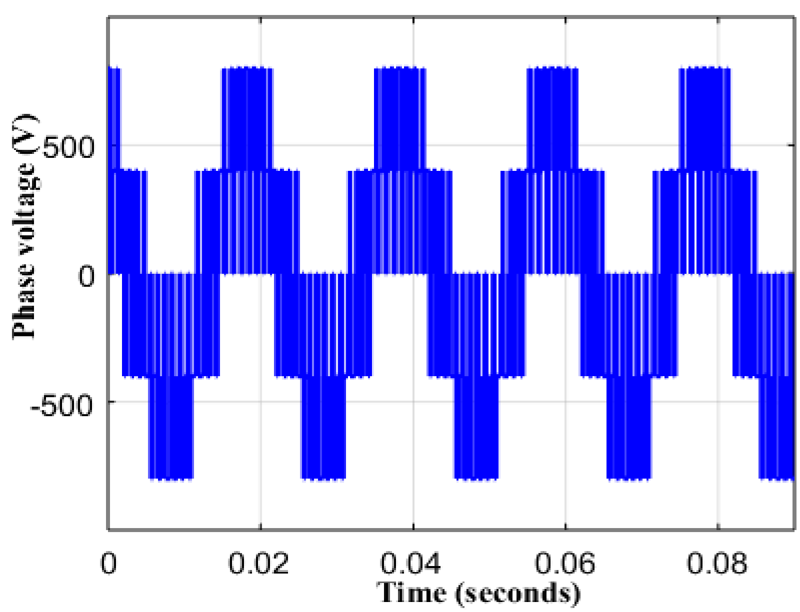

Figure 4.21 Phase voltage profile of two-level VSC using SPWM

From the FFT analysis of Matlab Simulink, THD content of conventional inverter is analyzed and presented in Figure 4.22. In this case the THD value is high with low voltage level.

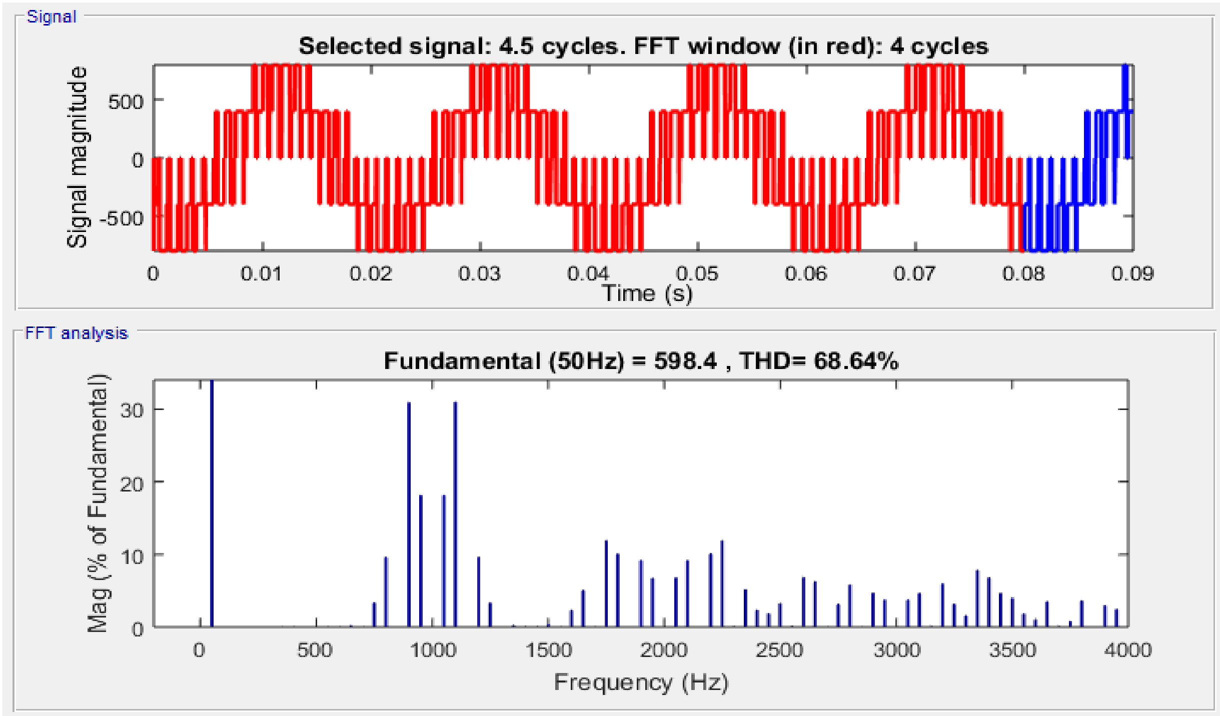

Figure 4.22 Harmonics spectrum and THD for two-level inverter based SPWM

4.5.2 Simulation of Two-Level VSC Based-THIPWM

In the case of inverter with SPWM as modulation index changes from 0 to 1, the peak of fundamental component of the phase voltage changes from 0 to 0.5Vdc. To enhance this range and increase DC voltage utilization THI is applied and the DC voltage is increased by 15% more than SPWM. As presented in the Figure, the SPWM based third harmonic technique is applied to two-level inverter and the switching signal is produced by comparing a reference waveform signal with the carrier signal. In compared to PWM based two-level inverter, the THI with PWM technique have higher utilization of DC bus voltage and the THD value is reduced as shown in Figure 4.24. By adding third harmonic signal to reference signal, third harmonic is injected with PWM and rectangular pulse is generated. This scenario is illustrated in Figure 4.23.

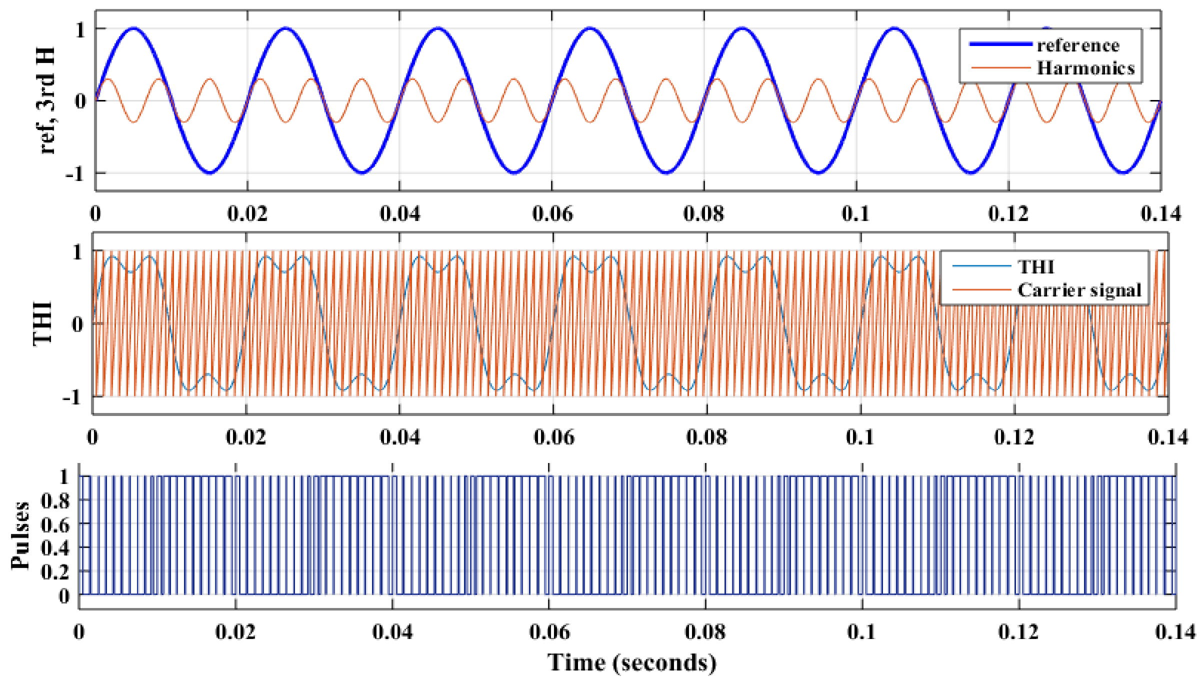

Figure 4.23 Third Harmonic injection with SPWM and the switching signal

Figures 4.24 presents the three-phase two-level line to line output voltage profiles using THIPWM technique. The output voltages are generated based on the switching signal in the legs of the converter. In the case of two-level inverters with SPWM the THD value is higher with the reduced fundamental output voltage, but when THIPWM is applied to two-level inverter the fundamental output voltage is increased by reducing the THD value. Figure 4.25 illustrate the harmonic spectrum and THD analysis for two-level inverter by using THIPWM strategy.

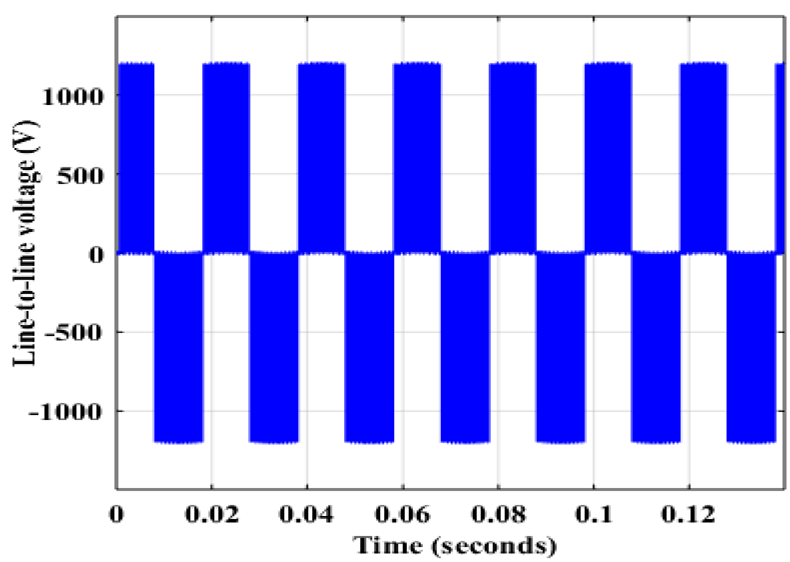

Figure 4.24 Line to line voltage of two-level VSC using THIPWM

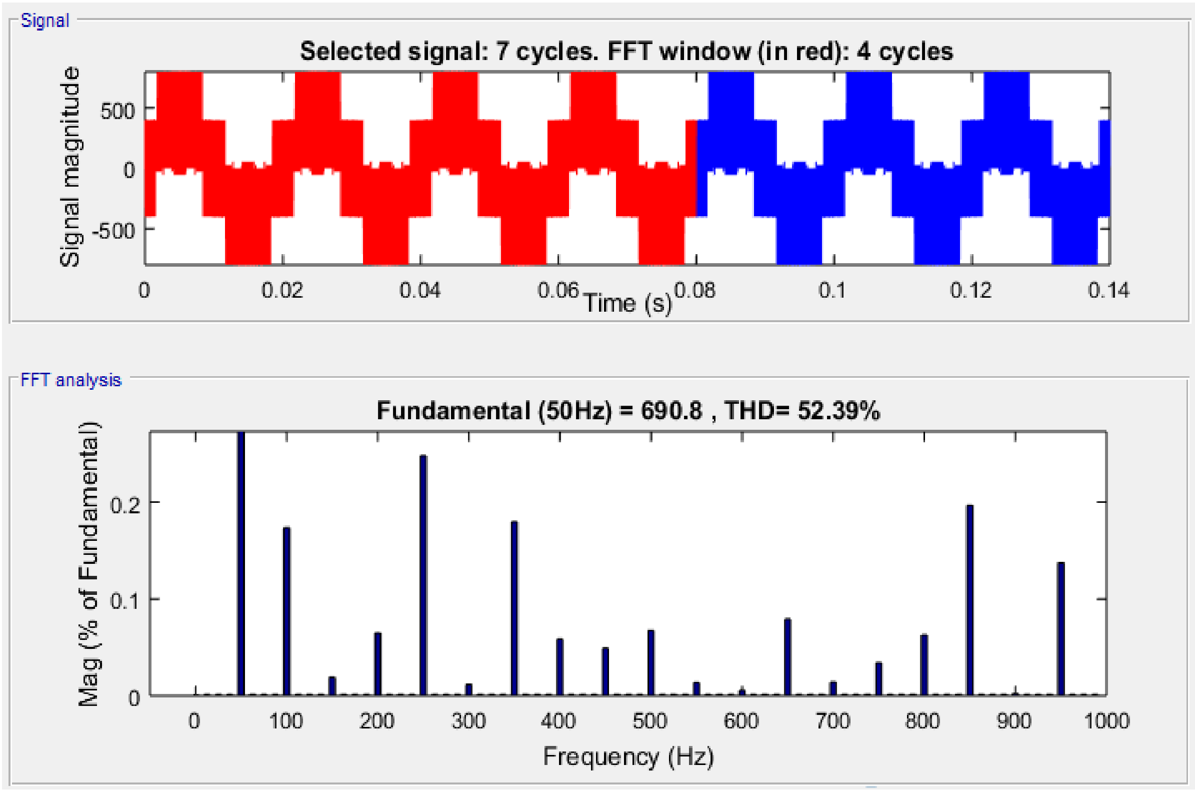

Figure 4.25 Harmonics spectrum and THD for two-level inverter with THIPWM

4.5.3 Simulation of Two-Level VSC Based- SVPWM Technique

Three-phase sinusoids are enclosing fixed 120 degrees phase shift and represented as vectors of different instantaneous magnitudes but fixed space angles. In the case of conventional VSC topology, it is composed of six switches in which each switch consists of a transistor with IGBTs and anti-parallel diode to provide a bidirectional conduction ability to the switch. If both switches get open and closed at the same time, there is no any useful output so this kind of state is ignored and forbidden respectively. Therefore, each phase of two-level inverter has only two useful states which are, either of the lower and upper switches are ON or OFF. The Figure 4.26 describes the three-phase reference signal and its equivalent alpha beta transformed signal with the angle value which goes from negative 180 degree to positive 180 degree.

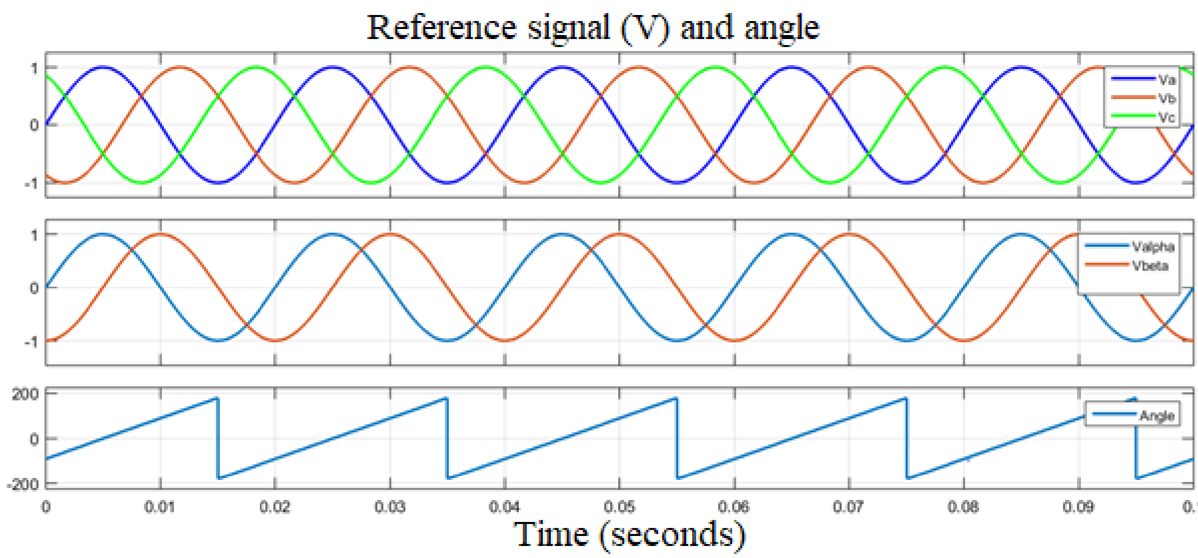

Figure 4.26 Reference Signal with Angle

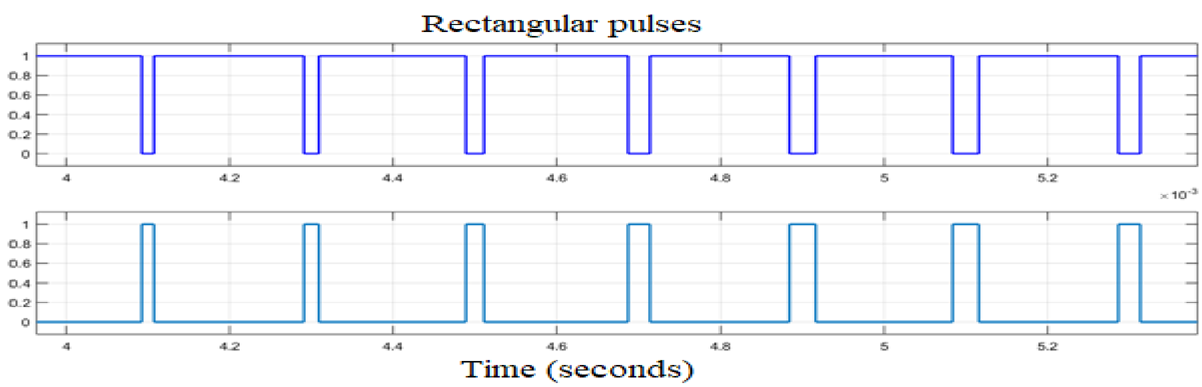

Figure 4.27 Rectangular Pulses

The rectangular pulses are generated when SVPWM technique based two level inverter is implemented. The output generated rectangular pulse is shown in Figure 2.28.

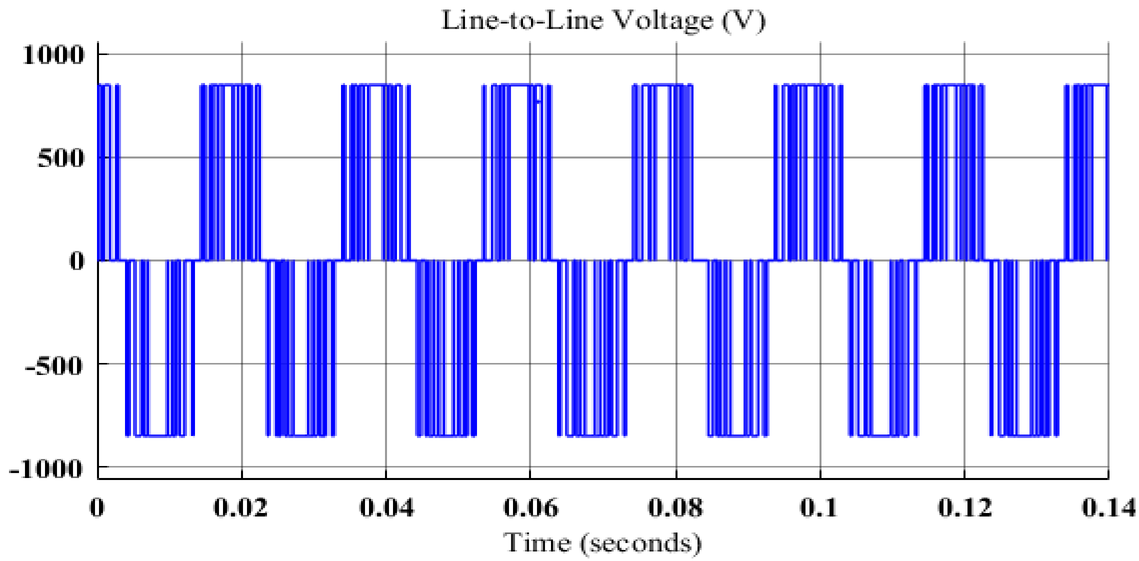

Figure 4.28 Output Voltage of two-level VSC using SVPWM

4.5.4 Simulation of Three-Level NPC VSC Based-SVPWM

Figure 4.29 illustrates output voltage levels for NPC converter. The switching signal is controlled by applying SVPWM instead of conventional PWM in order to reduce the THD and, hence the fundamental output voltage become improved.

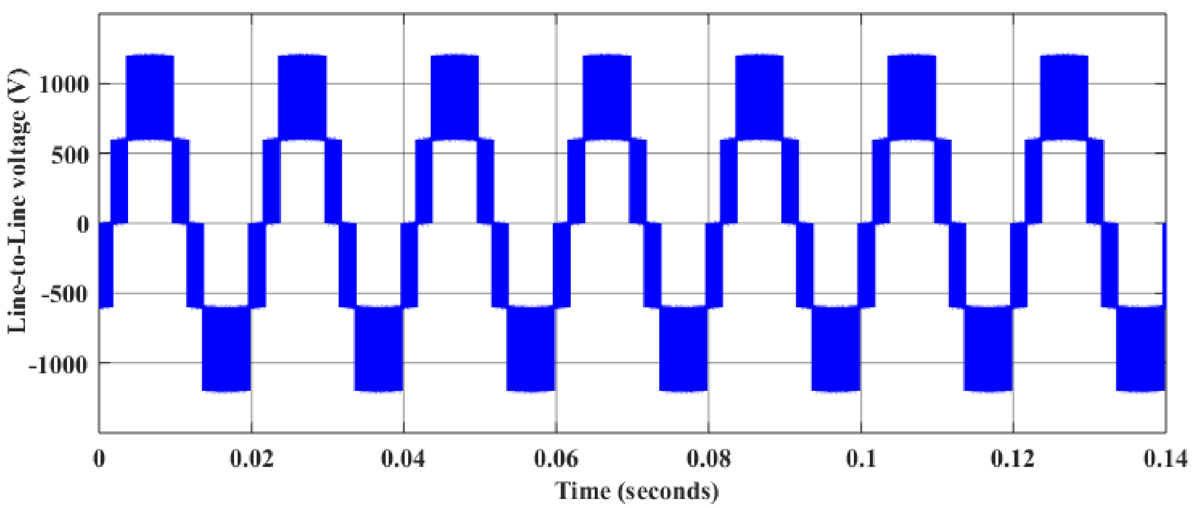

Figure 4.29 Output Voltage Level of NPC

As shown in Figure 4.30, by using NPC voltage source converter with SVPWM, the total harmonic distortion is reduced.

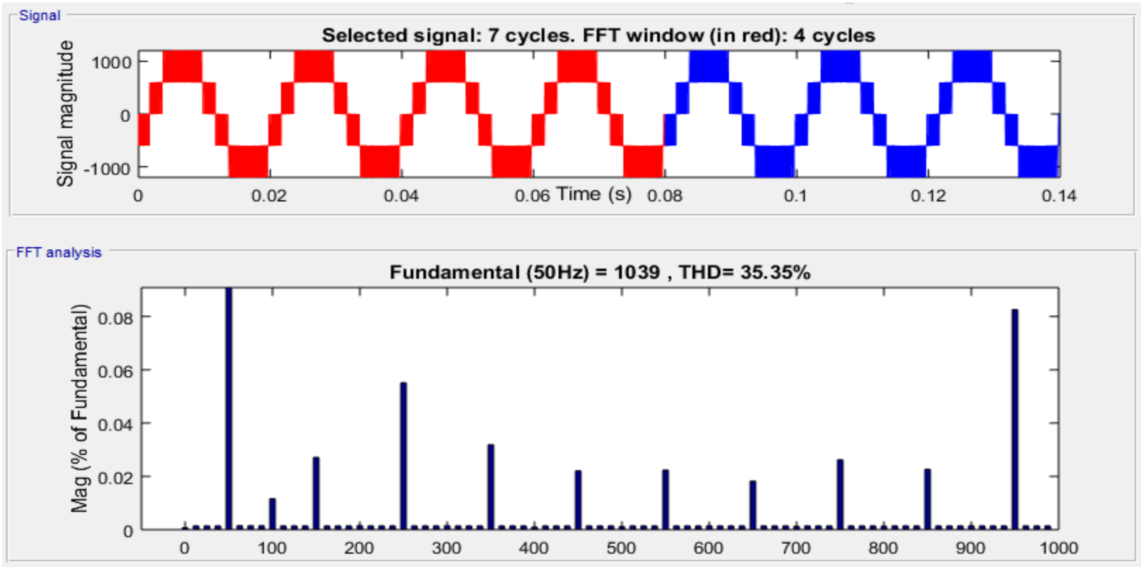

Figure 4.30 Harmonics spectrum and THD for NPC VSC with SVPWM

4.5.5 Simulation of Three-Level NPC VSC with LCL Filter and SVPWM

To improve the THD produced due to the grid connected voltage source converters, LCL filter is applied and located in between the power electronic converter and the grid in order to minimize harmonics with IEE standard. Figure 4.31 illustrates the simulation result when the NPC VSC is simulated with no filter.

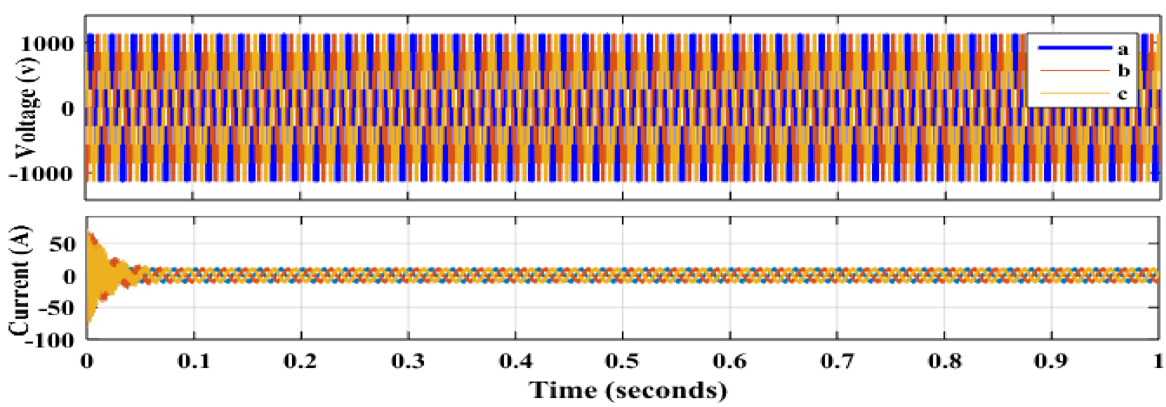

Figure 4.31 Simulated voltage and current signal without LCL filter

When LCL filter is added, the THD is below 5% and which is the correct range according to the IEE standard. Figure 4.32 shows the simulated voltage and current signals after the LCL filter is added and the signal is pure sinusoidal with improved harmonic issue. The THD value is with in permissible limit as indicated in Figure 4.33.

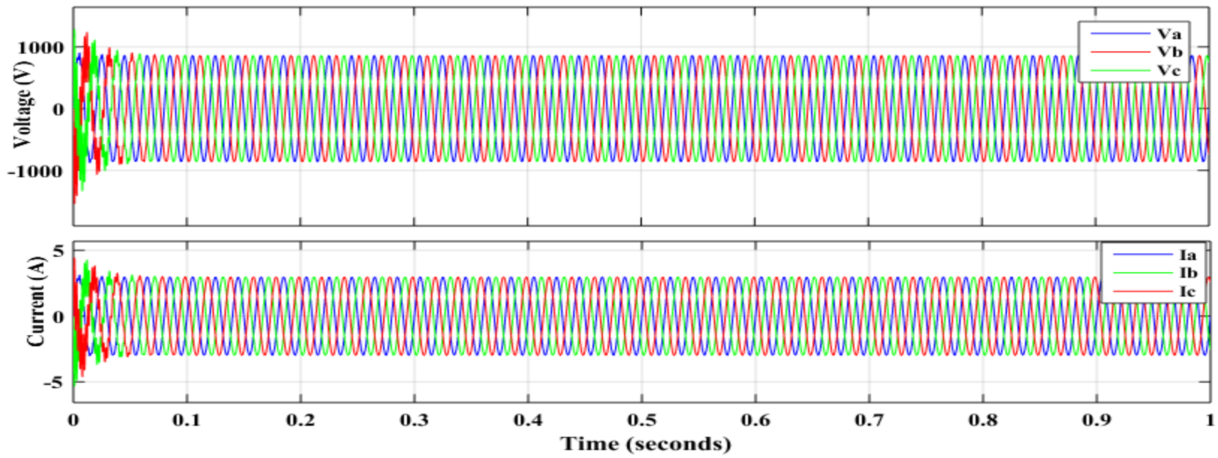

Figure 4.32 Simulated voltage and current signal with LCL

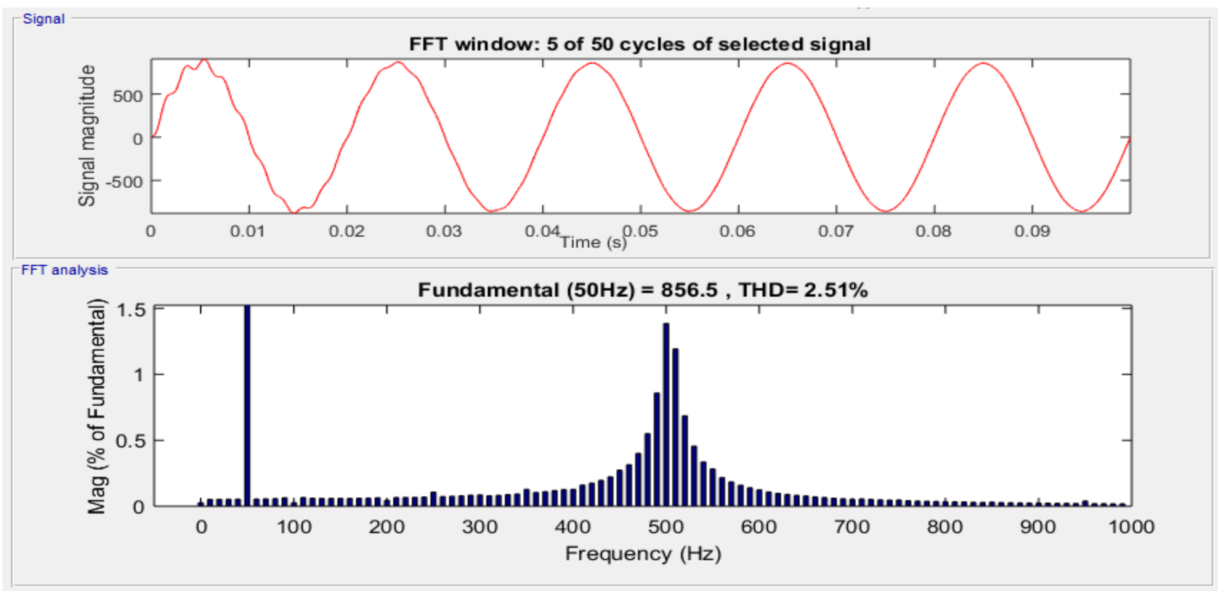

Figure 4.33 Harmonics Spectrum and THD for NPC VSC with SVPWM and LCL

Table 4. 3 Performance comparison of VSC based on modulation techniques

Modulation Techniques	2-L VSC		3-L NPC	
	Output V	THD%	Output V	THD%
SPWM	68.64	68.64		
THIPWM	690.8	52.39		
SVPWM			1039	35.35
SVPWM with LCL				2.51

CONCLUSION AND RECOMMENDATION

5.1 CONCLUSION

In this thesis work, design and analysis of fuzzy logic controller-based vector controlled DFIG in WECS for maximum power transfer capability has been studied. The overall system includes, modelling and control of rotor side converter, grid side converter and design of LCL filter. More specifically, the proposed controller called fuzzy logic controller is designed and analyzed to regulate the rotor speed for the rotor side converter. Different modulation strategy namely, SPWM, THIPWM, and SVPWM were presented and analyzed for both conventional two-level and three-level NPC voltage source converters. Controlling DFIG comprises control of the back-to-back power electronic converters, which are located between the rotor winding of the generator and the grid. The back-to-back converter consists of two voltage source converters, namely rotor side converter and grid side converter with a common DC-link capacitor. In this thesis work, the rotor side converter and grid side converter were controlled by vector control strategy. By controlling the rotor side converter, the generator rotor speed and rotor currents are controlled, hence active and reactive power were regulated according to the setpoint signal. So, the RSC control ensured the decoupling control of the stator active and reactive power by using vector control scheme. The behavior of the DFIG rotor speed, generated torque, active and reactive power were analyzed under different modes of operation the so called synchronous, sub-synchronous and super-synchronous modes. As analyzed from the simulated result, variation in rotor speed of the generator influences active and reactive power of stator winding. The MPPT control strategy based on the indirect speed control mechanism provides a reference value for the electromagnetic torque. In this way, the optimal tip speed ratio is maintained and maximum power output is achieved. The proposed fuzzy logic controller has been developed and applied to the outer loop of the rotor side converter. The proposed system result shows that, fuzzy logic controller has strong robustness against the external disturbances and the measured signal tracks the reference value smoothly with zero steady state error. In this case the settling time is reduced with almost no maximum overshoot. The vector control strategy is adopted to achieve the main goal of the grid-side converter. As analyzed from the simulated result of grid side converter, the DC-link voltage is regulated and maintained constant at 1200V, and the grid reactive power is regulated at zero so that, the grid has unity power factor.

In order to reduce the total harmonic disturbance due to the conventional two-level inverter, multi-level NPC voltage source converter has been studied and modeled by using SVPWM. For the power electronic converters, IGBT has been chosen as the switching device. According to the simulation and comparison result, the three-level NPC inverter has good performance with reduced total harmonic distortion. By adding the LCL filter, the THD been has been maintained at the IEEE standard. Finally, the objective of this thesis work has been achieved.

5.2 RECOMMENDATION

The future study will focus on the controller design in the case when fault or voltage dip happens. It is recommended that; the future study will conduct the hardware implementation with experiment in laboratory.

REFERENCE

[1] H. S. A. Eshaft, "Grid and Rotor Sides of Doubly-fed Induction Generator-based Wind Energy Conversion System Using Sliding Mode Control Approach," University of Sharjah, United Arab Emirates, 2017.

[2] X. Jing, "Modeling and Control of a Doubly-Fed Induction Generator for Wind Turbine-Generator Systems," Marquette University, 2012.

[3] W. X. L., "Torque and Reactive Power Control of a Doubly Fed Induction Generators," 2013.

[4] I. P. E. Board, Electrical System of a Variable Speed Wind Turbine, John Wiley & Sons, Inc., Hoboken, New Jersey, 2011, p. 22.

[5] "Model Reference Adaptive Control based on Fuzzy Logic for Doubly Fed Induction Generator used in a Chain of Wind Power Conversion," International Journal of Engineering Research And Management , vol. 03, no. 02, p. 1, 2016.

[6] A. B. R.-B. H. E. M. J. S. T. I. S. Yassir El Karkri, "Improved Control of Grid-connected DFIG-based Wind Turbine using Proportional-Resonant Regulators during Unbalanced Grid," Energies, p. 2, 2019.

[7] A. Abate, "Optimal Controller Design for WTS Using USING DYNAMIC PROGRAMMING," Addis Ababa Institute of Technology, Addis Ababa University, 2019.

[8] I. S. O. B. F. S. M. K. Lars Glavind, "Fiber-optical grating sensors for wind turbine blades," Optical Engineering, vol. Vol. 52(3), 2013.

[9] S. Sawalha, "Prospects of wind power generation in Jordan: the case of street lighting," International Conference on Renewable Energies and Power Quality, vol. 1, 2017.

[10] H. Pulgar-Painemal, "Basics of DFIG power generation," Universidad Tecnica Federico Santa Maria, Chile, 2013.

[11] S. Choudhury, "Performance Analysis of Doubly-fed Induction Generator in Wind Energy Conversion System," ODISHA, INDIA, 2011.

[12] M. T. Abdulfetah Shobole, "Fault Ride-through Capability of Wind Farm (Case Study of Adama Wind Farm Project, Dynamic Modeling and Simulation)," IEEE, Istanbul, Turkey, 2015 .

[13] B. o. I. P. W. P. C. S. D. W. Group, "Wind Turbine Generators for Wind Power Plants".

[14] P. P. J. Preeti Chakrawarti, "Complete Analysis of Doubly Fed Induction Generator Wind Turbine-Maximum Power Tracking Characteristics," International Journal of Electrical and Electronics Research, vol. Vol. 3, p. 14, 2015.

[15] T. TADESSE, "Study of Doubly Fed Induction Generator Control Under Grid Fault Conditions," Addis Ababa Institute Of Technology, 2016.

[16] M. ASHGLAF, "Development of Hybridization concept for horizontal axis wind / tidal systems using functional similarities and advanced real-time emulation methods," 2019.

[17] H. M. Marouane El Azzaoui, "Modeling and Control of A Doubly Fed Induction Generator Based Wind Turbine System Optimizition of The Power," Journal of Theoretical and Applied Information Technology, vol. Vol.80. No.2, p. 304, 2015.

[18] F. B. a. Z. Chen, "Power Electronics for ModernWind Turbines," Morgan & Claypool Publishers' series, 2006.

[19] Wiley, Power Electronics for Renewable Energy Systems, Transportation and industrial Applications, 2014.

[20] G. ABAD, Power Electronics and Electric Drives for Traction Applications, Mondragon University, Spain: John Wiley & Sons, Ltd., 2017.

[21] N. A. A. S. A. P. V. Rushikesh Mali, "Performance Comparison of Two Level Inverter with Classical Multilevel Inverter Topologies," IEEE, 2019.

[22] M. K. M. N. I. E. Mahrous Ahmed, "Performance Investigation of Multi-Level Inverter for DFIG during Grid Autoreclosure Operation," International Journal of Applied Engineering Research, vol. 13, p. 3655, 2018.

[23] M. M. H. C. Imane El Karaoui, "Contribution of improving the DFIG control using a multi-level inverter," International Journal of energy and power Engineering , vol. 13, p. 386, 2019.

[24] S. P. M. R. D. S. A. P. Kishan kumar Shukla, "A New Three-Level Diode Clamped Multilevel Inverter Topology," International Research Journal of Engineering and Technology, vol. 07, p. 3361, 2020.

[25] G. D. A. ,. J. a. S. P. V. Meenakshi, "Space Vector Modulation Technique Applied to Doubly Fed Induction Generator," Indian Journal of Science and Technology, vol. Vol 8(33), 2015.

[26] "Harmonic Analysis and Application of PWM Techniques for Three Phase Inverter," International Research Journal of Engineering and Technology, vol. 03, 2016.

[27] R. S. S. N. Om Prakash Bharti, "Controller design for doubly fed induction generator using particle swarm optimization technique," ELSEVIER, Vols. 114, part B, pp. 1394-1406, 2017.

[28] J. W. M. H. B. Ghulam Sarwar Kaloi, "Active and reactive power control of the doubly fed induction generator based on wind energy conversion system," ELSEVIER, vol. 2, p. 194–200, 2016.

[29] Z. B. A. B. Habib Benbuhenni, "DFIG-Based Wind Turbine System using Three-Level Neural Space Vector Modulation Technique," Majlesi Journal of Mechatronic Systems, Vols. Vol. 7, No. 2, 2018.

[30] e. d. S. V.-Z. Jafar Mohammadi, "A Combined Vector and Direct Power Control for DFIG-Based Wind Turbines," IEEE Transactions on Sustainable Energy, 2014.

[31] P. E. P. L. Sakina Elkhadiri, "Fuzzy logic control of DFIG-based wind turbine," IEEE, 2018 .

[32] V. V. A. J. Rahul Charles C Ma, "Field Oriented Control of DFIG Based Wind Energy System Using Battery Energy Storage System," ELSEVIER, p. 1203 – 1210, 2016.

[33] H. A. Ayrir Wiama, "Direct torque control-based power factor control of a DFIG," ELSEVIER, vol. 162, pp. 296-305, 2019.

[34] C. e. B. B. B. M. B. Yasmine Ihedrane, "Control of Power of a DFIG Generator with MPPT Technique for Wind Turbines Variable Speed," Springer Link, pp. 105-129, 2019.

[35] Y. Q. J. H. Heng Nian, "Improved control strategy of DFIG-based wind power generation systems connected to a harmonically polluted network," ELSEVIER, pp. 84-98, 2012.

[36] P. P. S. S. M. M. A. Gaillard, "Variable speed DFIG wind energy system for power generation and harmonic current mitigation," ELSEVIER, pp. 1545-1553, 2009.

[37] M. S. R. A. A. G. E. D. D. K. M. S. K. . G. Krishnan, "Control of A Doubly Fed Induction Generator for Wind Energy Conversion System Using Matrix Converter with SVPWM Technique," International Journal of Recent Technology and Engineering, vol. 8, no. 1S4, 2019.

[38] D. S. A. V. S. R. B Bhargava Reddy, "Modelling and Analysis of Wind Power Generation Using Pid Controller," International Journal for Scientific Research & Development|, vol. 1, no. 9, p. 2046, 2013.

[39] D. J. Saravanakumar Rajendran, "Control of Variable Speed Variable Pitch Wind Turbine at Above and Below Rated Wind Speed," Journal of Wind Energy , 2014.

[40] A. B. HADDAR Mabrouk, "The controlling of the DFIG Based Wind Energy Conversion System modeling and simulation," International Journal of Control, Energy and Electrical Engineering, vol. 7, 2019.

[41] P. D. I. R. L. D. M. M. Milkias Berhanu (PhD Scholar), "Analysis, Modeling and Simulation of a Doubly Fed Induction Generator in Wind Energy Conversion System," 2017.

[42] T. D.Srinivasa Rao, "Grid Connected DFIG With Efficient Rotor Power Flow Control Under Sub & Super Synchronous Modes of Operation," International Journal of Engineering Research & Technology, vol. 1, 2012.

[43] P. D. Chung, "Comparison of Steady-State Characteristics between DFIG and SCIG in Wind Turbine," International Journal of Advanced Science and Technology, vol. 51, 2013.

[44] Z. B. A. B. Habib Benbouhenni, "Using Three-Level Fuzzy Space Vector Modulation Method to Improve Indirect Vector Control Strategy of a DFIG Based Wind Energy Conversion Systems," International Journal of Smart Grid, vol. 2, 2018.

[45] M. M. Milkias Berhanu Tuka, "Performance Analysis of Grid Coupled Doubly Fed Induction Generator in a Wind Power System," WSEAS Transactions on Power Systems, vol. 12, 2017.

[46] D. Z. a. z. R. Song Le-Peng, "VAriable Structure Fuzzy- PID conrol for DFIG system," Advanced material research, Vols. 204-210, 2011.

[47] D.-H. K. J.-H. H. a. I. L. Young-Hwan Chang, "Online Phase Tracking of Interferometric Optical Fiber Sensors for Vibration Control," Journal of Intelligent Material Systems and structures, vol. 18, 2007.

[48] M. S. A. A.-D. S. M. M. A. Reznik, "LCL Filter Design and Performance Analysis for Grid Interconnected Systems," IEEE Transactions on Industry Applications , vol. 50, 2014.

[49] M. K. D. Mustafa DURSUN, "LCL Filter Design for Grid Connected Three-Phase Inverter," IEEE, 2018.

[50] F. B. a. S. H. Marco Liserre, "Design and Control of an LCL-Filter-Based Three-Phase Active Rectifier," IEEE Transactions on Industry Applications, vol. 41, 2005.

[51] T. R. J. M. Ramesh, "Control of RSC in DFIG based WECS using Cascade Feedback Linearization Controller," IEEE, 2018.

[52] Z. A. Reta, "Modeling and Control of Dual Converters on a Grid Connected Wind Power Energy Conversion System with Doubly-Fed Induction Generator in the Case of Adama II Wind Farm," ASTU, Adama, 2020.

APPENDIX

Table A1: 2MW DFIG specifications

Stator frequency (Hz)	f=50
Rated stator power (W)	Ps=2*10^6
Rated rotor speed (RPM)	N=1500
Rated stator voltage (V)	Vs=690
Rated stator current (A)	Is= 1760
Rated torque (N.m)	Tem=12732
Pole pairs	p= 2
Stator resistance (ohm)	Rs=2.6×10−3
Leakage inductance (H)	Rs=2.6×10−3
Magnetizing inductance (L)	Lm=2.5×10−3
Rotor resistance referred to stator (ohm)	Rr=2.9×10−3
Stator inductance (H)	Ls=Lm + Lsi
Rotor inductance (H)	Lr=Lm+ Lsi
DC bus voltage (V)	1200

Appendix A: Matlab Simulink Model

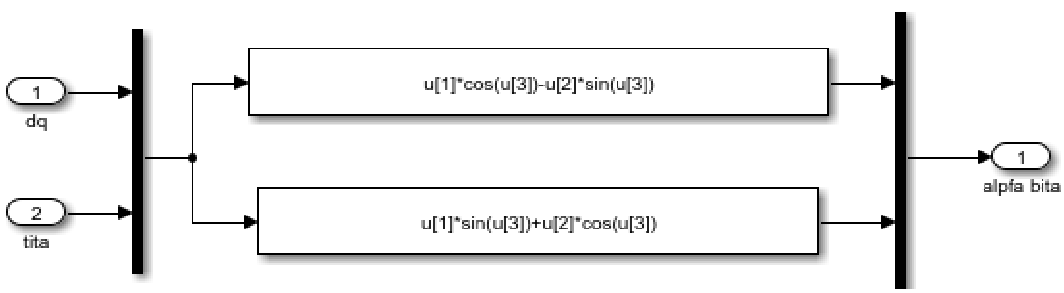

Figure A1: Park Transformation

Figure A2: Clark Transformation

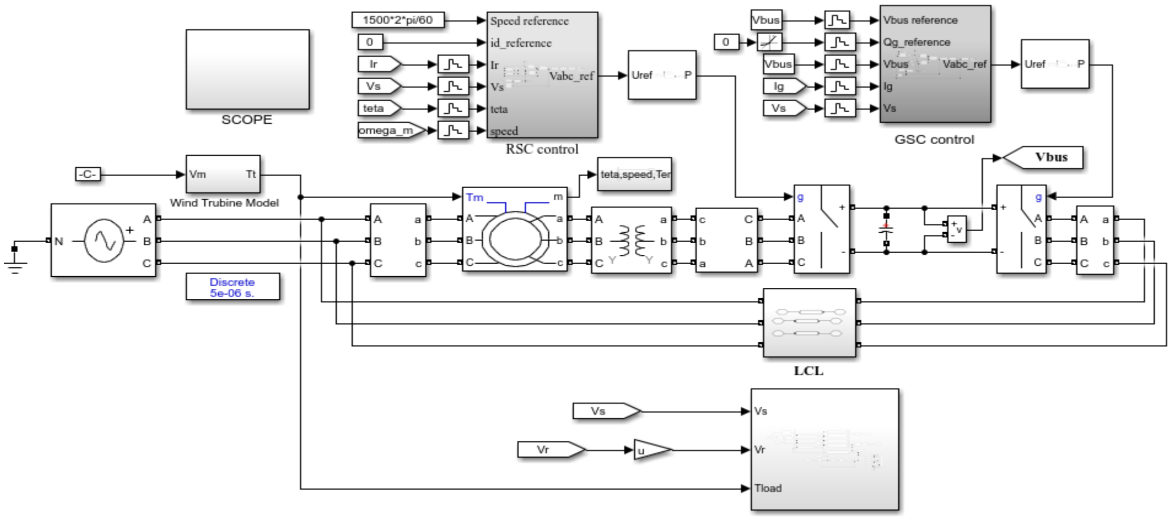

Figure A3: DFIG Simulink Mode

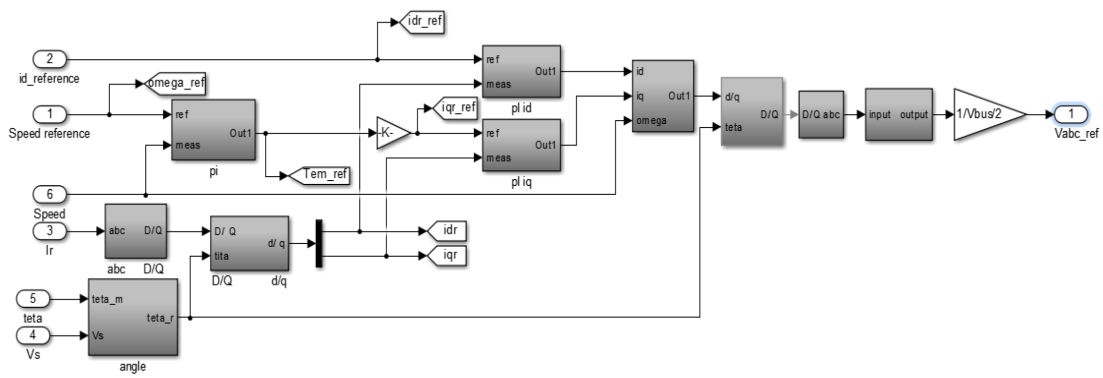

Figure A4: RSC simulink model

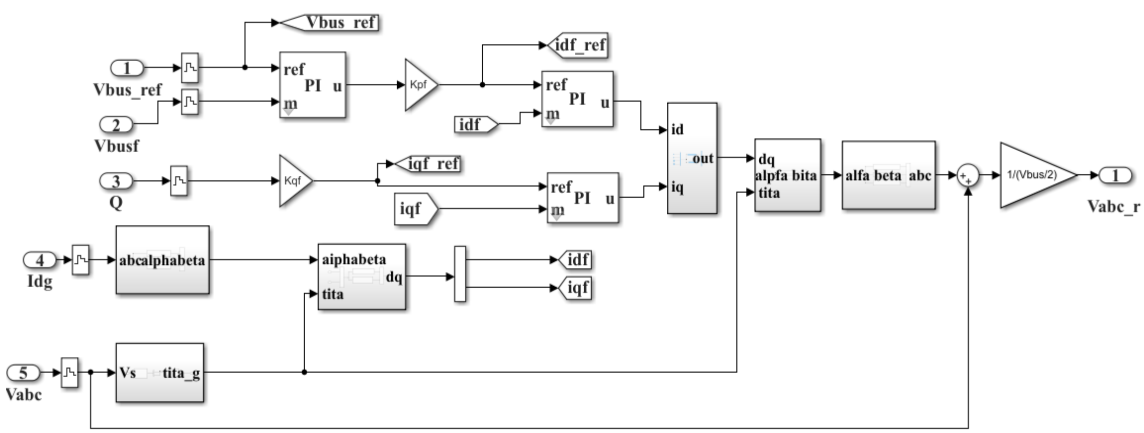

Figure A5: GSC Simulink model

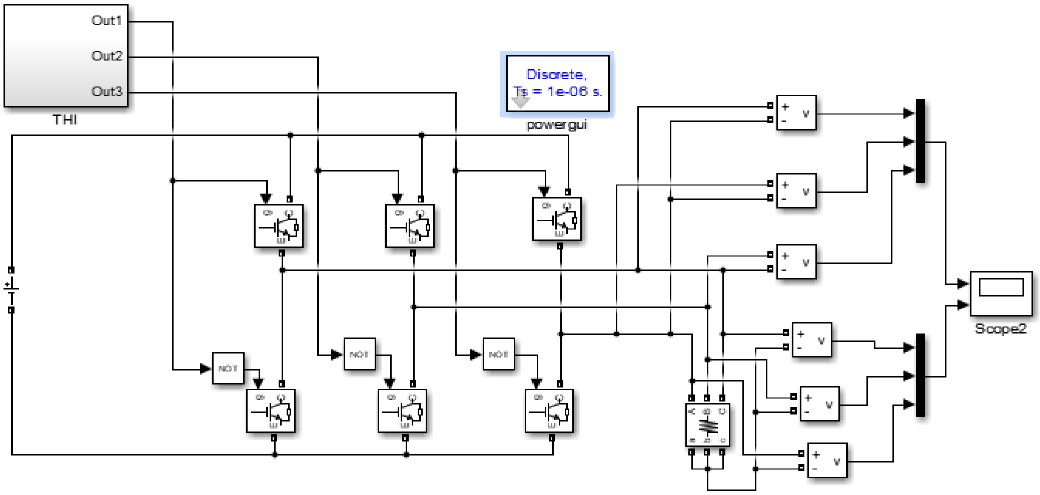

Figure A6: Third harmonic injection with SPWM

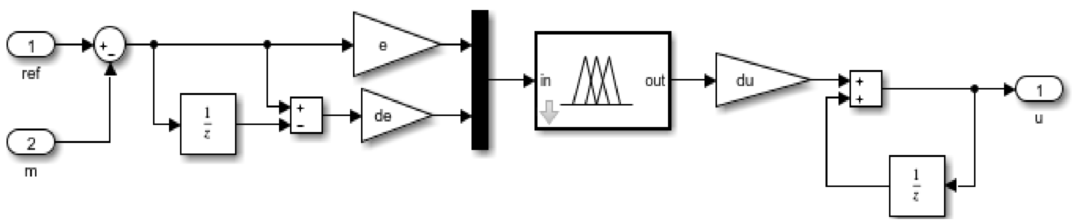

Figure A7: Sub system of FLC block

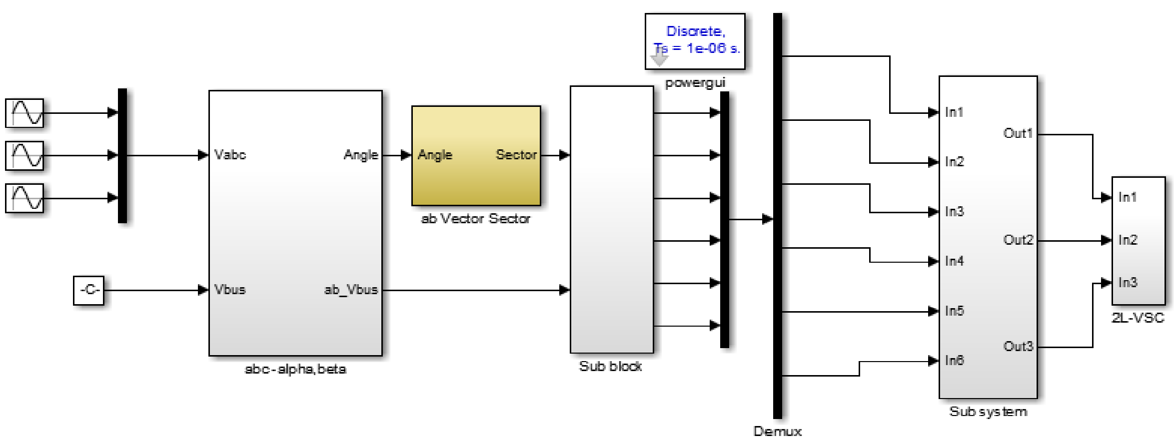

Figure A8: SVPWM of 2L-VSC

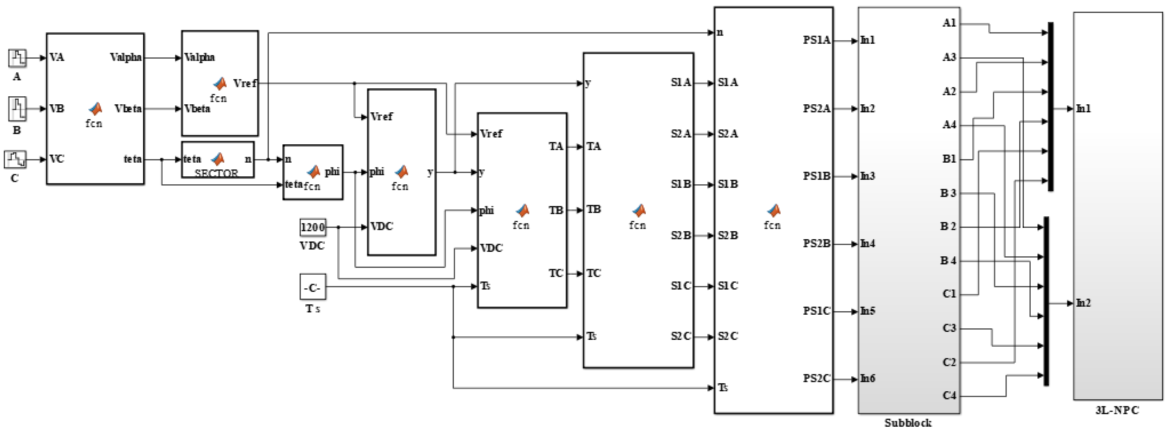

Figure A9: SVPWM of 3L-NPC

Table A2: PI Regulator

RSC (Current Loop)	Kp	Ki	Cbuc(F)
	0.5771	491.599	0.08
DC bus voltage	1000	30000	